ID N. AIDR01/16890

UNIVERSITÀ CAMPUS BIO-MEDICO DI ROMA

DEPARTMENT OF ENGINEERING

UNIVERSITÀ DEGLI STUDI DI TORINO

DEPARTMENT OF MEDICAL SCIENCES

Italian National Ph.D. in Artificial Intelligence
Health and Life Sciences
XXXVII Cycle

Artificial Intelligence in Arrhythmology

Supervisors

Prof. Gaetano Maria De Ferrari, Prof. Francesca Cordero,
Prof. Luca Console, Prof. Marco Aldinucci

Candidate

Andrea Saglietto

May, 2025

To Elena and Umberto,
for being the sunshine that brightens up my days.

Acknowledgements

I would like to express my gratitude to my supervisor Prof. Gaetano Maria De Ferrari, for allowing me to pursue my Ph.D. and for his invaluable guidance, support, and patience throughout this journey. I would like to thank to my co-supervisors, Prof. Francesca Cordero, Prof. Luca Console and Prof. Marco Aldinucci, for their support. I would also like to thank Prof. Matteo Anselmino, who has always been a mentor to me, since the last days of Medical School until now.

I also extend my thanks to Prof. Eugenio Guglielmelli and Prof. Paolo Soda for their excellent coordination of the Ph.D. program, the first of its kind in Italy. I express my sincere gratitude also to my fellow PhD colleagues for their stimulating collaboration, and the shared moments that have greatly enriched this journey, particularly during the summer schools held in Rome.

I am deeply grateful to my mother, my father and my sister for their unconditional love, patience, and encouragement, which have been a constant source of strength.

Finally, thanks to my wife Elena and to my little boy Umberto: every single day, you remind me that building our family is the most beautiful and meaningful journey of all. Your love and presence give purpose to everything I do.

Publications during PhD

The following is the list of publications on indexed journals achieved during the PhD (updated 31 May 2025):

1. Palermi S, Vecchiato M, Ng FS, Attia Z, Cho Y, Anselmino M, De Ferrari GM, **Saglietto A**; International AI-ECG Working Group. Artificial intelligence and the electrocardiogram: A modern renaissance. Eur J Intern Med. 2025 May 20:S0953-6205(25)00178-5. doi: 10.1016/j.ejim.2025.04.036. Epub ahead of print. PMID: 40413058. [77]

2. Pastore MC, Vigna M, **Saglietto A**, Iuliano MA, Mandoli GE, Stefanini A, Carrucola C, Fusini L, Cavigli L, D'ascenzi F, Focardi M, Valente S, Cameli M. Prognostic value of left atrial strain in acute and chronic heart failure: A meta-analysis. ESC Heart Fail. 2025 Apr 20. doi: 10.1002/ehf2.15302. Epub ahead of print. PMID: 40254742. [79]

3. Filiberti G, Antonelli G, Falasconi G, Villaschi A, Figliozzi S, Ruffo MM, Taormina A, Del Monaco G, Latini AC, Carli S, Stankowski K, Valcher S, Cesani N, Amata F, Giaj Levra A, Giunti F, Carella G, Soto-Iglesias D, Turturiello D, Landra F, **Saglietto A**, Curti E, Francia P, Martí-Almor J, Penela D, Berruezo A. The use of cardiac imaging in patients undergoing atrial fibrillation ablation. J Interv Card Electrophysiol. 2025 Apr 7. doi: 10.1007/s10840-025-02035-6. Epub ahead of print. PMID: 40195230. [37]

4. Penela D, Falasconi G, Soto-Iglesias D, Fernández-Armenta J, Zucchelli G, Bisbal F, Zaraket F, Silva E, Parollo M, Latini AC, Alderete J, Viveros D, Bellido A, Turturiello D, Valeriano C, Franco-Ocaña P, **Saglietto A**, Francia P, Martí-Almor J, Berruezo A. Outcomes of ventricular tachycardia ablation facilitated by pre-procedural cardiac imaging-derived scar characterization: a prospective multi-centre international registry. Europace. 2025 Mar 28;27(4):euaf051. doi: 10.1093/europace/euaf051. PMID: 40085771; PMCID: PMC11983391. [82]

5. Sclafani M, Falasconi G, Tini G, Musumeci B, Penela D, **Saglietto A**, Arcari L, Bucciarelli-Ducci C, Barbato E, Berruezo A, Francia P. Substrates of Sudden Cardiac

Death in Hypertrophic Cardiomyopathy. J Clin Med. 2025 Feb 17;14(4):1331. doi: 10.3390/jcm14041331. PMID: 40004861; PMCID: PMC11857077. [110]

6. **Saglietto A**, Falasconi G, Penela D, Francia P, Viveros D, Berruezo A, Russo V, Brignole M, Aksu T, Anselmino M, De Ferrari GM, Dusi V. Cardioneuroablation: a new treatment for vasovagal syncope. J Cardiovasc Med (Hagerstown). 2025 Mar 1;26(3):131-142. doi: 10.2459/JCM.0000000000001703. Epub 2025 Jan 27. PMID: 39976065. [98]

7. Landra F, **Saglietto A**, Falasconi G, Penela D, Soto-Iglesias D, Curti E, Tonello B, Teresi L, Turturiello D, Franco-Ocaña P, Gigante C, Valeriano C, Capobianco C, Francia P, Alderete J, Viveros D, Bellido AF, Zaraket F, Martí-Almor J, Cameli M, Berruezo A. Left atrial intramyocardial fat at pulmonary vein reconnection sites during atrial fibrillation redo ablation. Europace. 2025 Feb 5;27(2):euaf038. doi: 10.1093/europace/euaf038. PMID: 39973295; PMCID: PMC11878564. [64]

8. Randazzo V, Caligari S, Pasero E, Giustetto C, **Saglietto A**, Bertarello W, Averbuch A, Marcus-Kalish M, Zheludev V, Gaita F. A Vision Transformer Model for the Prediction of Fatal Arrhythmic Events in Patients with Brugada Syndrome. Sensors (Basel). 2025 Jan 30;25(3):824. doi: 10.3390/s25030824. PMID: 39943462; PMCID: PMC11820670. [84]

9. Barca L, Mascia G, Haissaguerre M, Monaco C, Xhakupi H, Carmisciano L, **Saglietto A**, Giustetto C, Di Donna P, Arbelo E, Brugada J, Porto I. Incidence of spontaneous Brugada ECG during follow-up in patients with drug-inducible pattern: A systematic review and meta-analysis. Heart Rhythm. 2025 Jan 28:S1547-5271(25)00099-2. doi: 10.1016/j.hrthm.2025.01.029. Epub ahead of print. PMID: 39884324. [11]

10. Calvelli P, Cerrato N, Giustetto C, **Saglietto A**, Anselmino M, Curcio A. Which Brugada patient deserves continuous ECG monitoring through implantable loop recorder? An evidence update. J Cardiovasc Med (Hagerstown). 2025 Feb 1;26(2):64-71. doi: 10.2459/JCM.0000000000001696. Epub 2024 Dec 27. PMID: 39841911 [16]

11. Francia P, Viveros D, Gigante C, Falasconi G, Penela D, Soto-Iglesias D, Landra F, Teresi L, Marti-Almor J, Alderete J, **Saglietto A**, Bellido AF, Turturiello D, Valeriano C, Franco-Ocaña P, Zaraket F, Matiello M, Fernández-Armenta J, Antonio RS, Berruezo A. Differential and synergistic effects of right and left atrial ganglionated plexi ablation in patients undergoing cardioneuroablation: results from the ELEGANCE multicenter

study. J Interv Card Electrophysiol. 2024 Dec 13. doi: 10.1007/s10840-024-01968-8. Epub ahead of print. PMID: 39671156 [40]

12. De Filippo O, Mineo R, Millesimo M, Wańha W, Proietto Salanitri F, Greco A, Leone AM, Franchin L, Palazzo S, Quadri G, Tuttolomondo D, Fabris E, Campo G, Giachet AT, Bruno F, Iannaccone M, Boccuzzi G, Gaibazzi N, Varbella F, Wojakowski W, Maremmani M, Gallone G, Sinagra G, Capodanno D, Musumeci G, Boretto P, Pawlus P, **Saglietto A**, Burzotta F, Aldinucci M, Giordano D, De Ferrari GM, Spampinato C, D'Ascenzo F. Non-invasive physiological assessment of intermediate coronary stenoses from plain angiography through artificial intelligence: the STARFLOW system. Eur Heart J Qual Care Clin Outcomes. 2024 Oct 9:qcae024. doi: 10.1093/ehjqcco/qcae024. Epub ahead of print. PMID: 39382111 [27]

13. Giannino G, Nocera L, Andolfatto M, Braia V, Giacobbe F, Bruno F, **Saglietto A**, Angelini F, De Filippo O, D'Ascenzo F, De Ferrari GM, Dusi V. Vagal nerve stimulation in myocardial ischemia/reperfusion injury: from bench to bedside. Bioelectron Med. 2024 Sep 13;10(1):22. doi: 10.1186/s42234-024-00153-6. PMID: 39267134; PMCID: PMC11395864 [46]

14. **Saglietto A**, Cavallone E, Spartalis M, Vandenberk B, Anselmino M. Editorial: Artificial intelligence in cardiac rhythmology. Front Cardiovasc Med. 2024 Aug 5;11:1466344. doi: 10.3389/fcvm.2024.1466344. PMID: 39161659; PMCID: PMC11330872 [91]

15. Valcher S, Villaschi A, Falasconi G, Chiarito M, Giunti F, Novelli L, Addeo L, Taormina A, Panico C, Francia P, **Saglietto A**, Del Monaco G, Latini AC, Carli S, Frittella S, Giaj Levra A, Antonelli G, Preda A, Guarracini F, Mazzone P, Berruezo A, Tritto M, Condorelli G, Penela D. Low-Voltage Area Ablation in Addition to Pulmonary Vein Isolation in Patients with Atrial Fibrillation: A Systematic Review and Meta-Analysis. J Clin Med. 2024 Aug 3;13(15):4541. doi: 10.3390/jcm13154541. PMID: 39124807; PMCID: PMC11313645 [114]

16. **Saglietto A**, Falasconi G, Penela D, Francia P, Sau A, Ng FS, Dusi V, Castagno D, Gaita F, Berruezo A, De Ferrari GM, Anselmino M. Glucagon-like peptide-1 receptor agonist semaglutide reduces atrial fibrillation incidence: A systematic review and meta-analysis. Eur J Clin Invest. 2024 Jul 26:e14292. doi: 10.1111/eci.14292. Epub ahead of print. PMID: 39058274. [96]

17. **Saglietto A**, Tripoli F, Zwanenburg J, Biessels GJ, De Ferrari GM, Anselmino M, Ridolfi L, Scarsoglio S. Role of the vessel morphology on the lenticulostriate arteries hemo-

dynamics during atrial fibrillation: A CFD-based multivariate regression analysis. Comput Methods Programs Biomed. 2024 Sep;254:108303. doi: 10.1016/j.cmpb.2024.108303. Epub 2024 Jun 24. PMID: 38943985 [106]

18. Ballatore A, Gatti M, Mella S, Tore D, Xhakupi H, Giorgino F, **Saglietto A**, Carmagnola L, Roagna E, De Ferrari GM, Faletti R, Anselmino M. Epicardial Atrial Fat at Cardiac Magnetic Resonance Imaging and AF Recurrence after Transcatheter Ablation. J Cardiovasc Dev Dis. 2024 Apr 28;11(5):137. doi: 10.3390/jcdd11050137. PMID: 38786958; PMCID: PMC11122251 [10]

19. Canova D, Roatta S, **Saglietto A**, Scarsoglio S, Gianotto NR, Piccotti A, De Ferrari GM, Ridolfi L, Anselmino M. A Quantitative Assessment of Cerebral Hemodynamic Perturbations Associated with Long R-R Intervals in Atrial Fibrillation: A Pilot-Case-Based Experience. Medicina (Kaunas). 2024 Mar 25;60(4):531. doi: 10.3390/medicina60040531. PMID: 38674177; PMCID: PMC11052310 [18]

20. Falasconi G, Penela D, Soto-Iglesias D, Francia P, **Saglietto A**, Turturiello D, Viveros D, Bellido A, Alderete J, Zaraket F, Franco-Ocaña P, Huguet M, Cámara Ó, Vătășescu R, Ortiz-Pérez JT, Martí-Almor J, Berruezo A. Personalized pulmonary vein isolation with very high-power short-duration lesions guided by left atrial wall thickness: the QDOT-by-LAWT randomized trial. Europace. 2024 Mar 30;26(4):euae087. doi: 10.1093/europace/euae087. PMID: 38652090; PMCID: PMC11036893 [36]

21. Bocanegra-Pérez ÁJ, Piella G, Sebastian R, Jimenez-Perez G, Falasconi G, **Saglietto A**, Soto-Iglesias D, Berruezo A, Penela D, Camara O. Automatic and interpretable prediction of the site of origin in outflow tract ventricular arrhythmias: machine learning integrating electrocardiograms and clinical data. Front Cardiovasc Med. 2024 Mar 20;11:1353096. doi: 10.3389/fcvm.2024.1353096. PMID: 38572307; PMCID: PMC10987867 [14]

22. Dusi V, Angelini F, Baldi E, Toscano A, Gravinese C, Frea S, Compagnoni S, Morena A, **Saglietto A**, Balzani E, Giunta M, Costamagna A, Rinaldi M, Trompeo AC, Rordorf R, Anselmino M, Savastano S, De Ferrari GM. Continuous stellate ganglion block for ventricular arrhythmias: case series, systematic review, and differences from thoracic epidural anaesthesia. Europace. 2024 Mar 30;26(4):euae074. doi: 10.1093/europace/euae074. PMID: 38531027; PMCID: PMC11020261 [33]

23. **Saglietto A**, Baccega D, Esposito R, Anselmino M, Dusi V, Fiandrotti A, De Ferrari GM. Convolutional neural network (CNN)-enabled electrocardiogram (ECG) analysis:

a comparison between standard twelve-lead and single-lead setups. Front Cardiovasc Med. 2024 Feb 15;11:1327179. doi: 10.3389/fcvm.2024.1327179. Erratum in: Front Cardiovasc Med. 2024 Mar 14;11:1396396. doi: 10.3389/fcvm.2024.1396396. PMID: 38426118; PMCID: PMC10901971 [85]

24. Giannino G, Braia V, Griffith Brookles C, Giacobbe F, D'Ascenzo F, Angelini F, **Saglietto A**, De Ferrari GM, Dusi V. The Intrinsic Cardiac Nervous System: From Pathophysiology to Therapeutic Implications. Biology (Basel). 2024 Feb 7;13(2):105. doi: 10.3390/biology13020105. PMID: 38392323; PMCID: PMC10887082 [45]

25. Francia P, Falasconi G, Penela D, Viveros D, Alderete J, **Saglietto A**, Bellido AF, Martí-Almor J, Franco-Ocaña P, Soto-Iglesias D, Zaraket F, Turturiello D, Berruezo A. Scar architecture affects the electrophysiological characteristics of induced ventricular arrhythmias in hypertrophic cardiomyopathy. Europace. 2024 Mar 1;26(3):euae050. doi: 10.1093/europace/euae050. PMID: 38375690; PMCID: PMC10914403 [38]

26. **Saglietto A**, Bertello E, Barra M, Ferraro I, Rovera C, Orzan F, De Ferrari GM, Anselmino M. MRI pattern characterization of cerebral cardioembolic lesions following atrial fibrillation ablation. Front Cardiovasc Med. 2024 Jan 24;11:1327567. doi: 10.3389/fcvm.2024.1327567. PMID: 38327489; PMCID: PMC10847299 [90]

27. **Saglietto A**, Falasconi G, Berruezo A, De Ferrari GM, Anselmino M. Posterior Wall Isolation in Persistent AF With Rapid Posterior Wall Activity: The Quest for Evidence. JACC Clin Electrophysiol. 2024 Jan;10(1):139-140. doi: 10.1016/j.jacep.2023.10.036. PMID: 38267167. [95]

28. De Filippo O, Piroli F, Bruno F, Bocchino PP, **Saglietto A**, Franchin L, Angelini F, Gallone G, Rizzello G, Ahmad M, Gasparini M, Chatterjee S, De Ferrari GM, D'Ascenzo F. De-escalation of dual antiplatelet therapy for patients with acute coronary syndrome after percutaneous coronary intervention: a systematic review and network meta-analysis. BMJ Evid Based Med. 2024 May 22;29(3):171-186. doi: 10.1136/bmjebm-2023-112476. PMID: 38242567. [28]

29. Palermi S, Vecchiato M, **Saglietto A**, Niederseer D, Oxborough D, Ortega-Martorell S, Olier I, Castelletti S, Baggish A, Maffessanti F, Biffi A, D'Andrea A, Zorzi A, Cavarretta E, D'Ascenzi F. Unlocking the potential of artificial intelligence in sports cardiology: does it have a role in evaluating athlete's heart? Eur J Prev Cardiol. 2024 Mar 4;31(4):470-482. doi: 10.1093/eurjpc/zwae008. PMID: 38198776 [78]

30. **Saglietto A**, Falasconi G, Soto-Iglesias D, Francia P, Penela D, Alderete J, Viveros D, Bellido AF, Franco-Ocaña P, Zaraket F, Turturiello D, Marti-Almor J, Berruezo A. Assessing left atrial intramyocardial fat infiltration from computerized tomography angiography in patients with atrial fibrillation. Europace. 2023 Dec 6;25(12):euad351. doi: 10.1093/europace/euad351. PMID: 38011712; PMCID: PMC10751854 [99]

31. **Saglietto A**, Ballatore A, Griffith Brookles C, Xhakupi H, De Ferrari GM and Anselmino M. Role of atrial high-rate episodes in stratifying thromboembolic risk: a multiple cut-off diagnostic meta-analysis. Front Cardiovasc Med. 2023 Nov 10:1289372. doi: 10.3389/fcvm.2023.1289372 [86]

32. Boretto P, Patel NH, Patel K, Rana M, **Saglietto A**, Soni M, Ahmad M, Sin Ying Ho J, De Filippo O, Providencia RA, Hyett Bray JJ, D'Ascenzo F. Prognosis prediction in cardiac amyloidosis by cardiac magnetic resonance imaging: a systematic review with meta-analysis. Eur Heart J Open. 2023 Sep 22;3(5):oead092. doi: 10.1093/ehjopen/oead092. PMID: 37840586; PMCID: PMC10575621 [15]

33. Gaita F, Cerrato N, Giustetto C, Martino A, Bergamasco L, Millesimo M, Barbonaglia L, Carvalho P, Caponi D, **Saglietto A**, Bonacchi G, Bianchi F, Silvetti E, Crescenzi C, Canestrelli S, De Maio M, De Ferrari GM, Musumeci G, Rametta F, Scaglione M, Calò L. Asymptomatic Patients With Brugada ECG Pattern: Long-Term Prognosis From a Large Prospective Study. Circulation. 2023 Oct 13. doi: 10.1161/CIRCULATIONAHA.123.064689. Epub ahead of print. PMID: 37830188 [41]

34. **Saglietto A**, Scarsoglio S, Tripoli F, Zwanenburg J, Biessels GJ, De Ferrari GM, Ridolfi L, Anselmino M. Atrial fibrillation hemodynamic effects on lenticulostriate arteries identified at 7-Tesla cerebral magnetic resonance imaging. Clin Transl Med. 2023 Sep;13(9):e1367. doi: 10.1002/ctm2.1367. PMID: 37735820 [105]

35. Falasconi G, Penela D, Soto-Iglesias D, Francia P, **Saglietto A**, Alderete J, Viveros D, Bellido A, Zaraket F, Martí-Almor J, Berruezo A. Cardiac magnetic resonance-aided epicardial ventricular tachycardia ablation in post-myocarditis patient. J Interv Card Electrophysiol. 2023 Sep 18. doi: 10.1007/s10840-023-01647-0. Epub ahead of print. PMID: 37721657 [35]

36. Francia P, Viveros D, Falasconi G, Penela D, Soto-Iglesias D, Marti-Almor J, Alderete J, **Saglietto A**, Bellido AF, Ocaña-Franco P, Zaraket F, Matiello M, Fernández-Armenta J, San Antonio R, Berruezo A. Clinical Impact of Aging on Outcomes of Cardioneuroablation for Reflex Syncope or Functional Bradycardia. Results from the

cardionEuroabLation: patiEnt selection, imaGe integrAtioN and outComEs. The ELEGANCE multicenter study. Heart Rhythm. 2023 Jun 15:S1547-5271(23)02349-4. doi: 10.1016/j.hrthm.2023.06.007. Epub ahead of print. PMID: 37329936 [39]

37. **Saglietto A**, Scarsoglio S, Canova D, De Ferrari GM, Ridolfi L, Anselmino M. Beat-to-beat finger photoplethysmography in atrial fibrillation patients undergoing electrical cardioversion. Sci Rep 13, 6751 (2023). doi: 10.1038/s41598-023-33952-z [104]

38. Falasconi G, Penela D, Soto-Iglesias D, Francia P, Teres C, **Saglietto A**, Jauregui B, Viveros D, Bellido A, Alderete J, Meca-Santamaria J, Franco P, Gaspardone C, San Antonio R, Huguet M, Cámara Ó, Ortiz-Pérez JT, Martí-Almor J, Berruezo A. Personalized pulmonary vein antrum isolation guided by left atrial wall thickness for persistent atrial fibrillation. Europace. 2023 May 1:euad118. doi: 10.1093/europace/euad118. Epub ahead of print. PMID: 37125968 [36]

39. Gaita F, Cerrato N, **Saglietto A**, Caponi D, Calò L, Giustetto G. The Brugada syndrome: risk stratification. European Heart Journal Supplements, Volume 25, Issue Supplement C, May 2023, Pages C27–C31. doi: 10.1093/eurheartjsupp/suad035 [42]

40. **Saglietto A**, Falasconi G, Penela D, Francia P, Soto-Iglesias D, Martí-Almor J, Berruezo A. Cardiac magnetic resonance-aided ventricular tachycardia substrate ablation in corrected tetralogy of Fallot. J Interv Card Electrophysiol. 2023 Mar 25. doi: 10.1007/s10840-023-01527-7. Epub ahead of print. PMID: 36964886 [97]

41. Scarsoglio S, **Saglietto A***, Tripoli F, Zwanenburg JJM, Biessels GJ, De Ferrari GM, Anselmino M, Ridolfi L. Cerebral hemodynamics during atrial fibrillation: Computational fluid dynamics analysis of lenticulostriate arteries using 7 T high-resolution magnetic resonance imaging. Phys Fluids (1994). 2022 Dec;34(12):121909. doi: 10.1063/5.0129899. Epub 2022 Dec 29. PMID: 36776539; PMCID: PMC9907777. [*co-first author] [109]

42. Anselmino M, Scarsoglio S, Ridolfi L, De Ferrari GM, **Saglietto A**. Insights from computational modeling on the potential hemodynamic effects of sinus rhythm versus atrial fibrillation. Front Cardiovasc Med. 2022 Sep 14;9:844275. doi: 10.3389/fcvm.2022.844275 [3]

43. **Saglietto A**, Martinengo E, Cerrato N, Bergamasco L, Castagno D, Gaita F, De Ferrari GM, Giustetto C. Time to positivity of diagnostic provocative pharmacologic testing in Brugada syndrome. Heart Rhythm. 2022 Sep 5:S1547-5271(22)02378-5. doi: 10.1016/j.hrthm.2022.08.031 [103]

44. **Saglietto A**, Gaita F, Blomstrom-Lundqvist C, Arbelo E, Dagres N, Brugada J, Maggioni AP, Tavazzi L, Kautzner J, De Ferrari GM, Anselmino M. AFA-Recur: an ESC EORP AFA-LT registry machine-learning web calculator predicting atrial fibrillation recurrence after ablation. Europace. 2022 Aug 25:euac145. doi: 10.1093/europace/euac145 [101]

45. **Saglietto A**, Ballatore A, Xhakupi H, Rubat Baleuri F, Magnano M, Gaita F, De Ferrari GM, Anselmino M. Evidence-based insights on ideal blanking period duration following atrial fibrillation catheter ablation. Europace. 2022 Aug 2:euac098. doi: 10.1093/europace/euac098 [89]

46. **Saglietto A**, Ballatore A, Xhakupi H, De Ferrari GM, Anselmino M. Association of Catheter Ablation and Reduced Incidence of Dementia among Patients with Atrial Fibrillation during Long-Term Follow-Up: A Systematic Review and Meta-Analysis of Observational Studies. J Cardiovasc Dev Dis. 2022 Apr 30;9(5):140. doi: 10.3390/jcdd9050140 [87]

47. **Saglietto A**, Ballatore A, Xhakupi H, De Ferrari GM, Anselmino M. Atrial Fibrillation and Dementia: Epidemiological Insights on an Undervalued Association. Medicina (Kaunas). 2022 Mar 1;58(3):361. doi: 10.3390/medicina58030361 [88]

48. D'Ascenzo F, De Filippo O, Angelini F, Piroli F, DE Lio G, Bocchino PP, Baldetti L, Melillo F, Chieffo A, **Saglietto A**, Omedè P, Montefusco A, Conrotto F, DE Ferrari GM. Duration and kind of dual antiplatelet therapy for acute coronary syndrome patients: a network meta-analysis. Minerva Cardiol Angiol. 2022 Mar 25. doi: 10.23736/S2724-5683.22.06038-0 [23]

49. **Saglietto A**, De Ferrari GM, Anselmino M. Commentary: Differential Risk of Dementia Between Patients With Atrial Flutter and Atrial Fibrillation: A National Cohort Study. Front Cardiovasc Med. 2022 Feb 17;9:850968. doi: 10.3389/fcvm.2022.850968 [92]

50. Cavarretta E, Sciarra L, Biondi-Zoccai G, Maffessanti F, Nigro A, Sperandii F, Guerra E, Quaranta F, Fossati C, Peruzzi M, Pingitore A, Stasinopoulos DM, Rigby RA, Adorisio R, **Saglietto A**, Calò L, Frati G, Pigozzi F. Age-Related Electrocardiographic Characteristics of Male Junior Soccer Athletes. Front Cardiovasc Med. 2022 Feb 3;8:784170. doi: 10.3389/fcvm.2021.784170 [19]

51. **Saglietto A**, Fois M, Ridolfi L, De Ferrari GM, Anselmino M, Scarsoglio S. A computational analysis of atrial fibrillation effects on coronary perfusion across the different

myocardial layers. Sci Rep. 2022 Jan 17;12(1):841. doi: 10.1038/s41598-022-04897-6 [100]

52. **Saglietto A**, De Ferrari GM, Ferraris F, Anselmino M. Pulmonary vein isolation through trans-jugular approach in a patient with inferior vena cava interruption. J Interv Card Electrophysiol. 2022 Jan 10. doi: 10.1007/s10840-021-01114-8. Epub ahead of print [93]

53. Angelini F, Bocchino PP, Peyracchia M, **Saglietto A**, Magnano M, Patanè N, D'Ascenzo F, Giustetto C, Anselmino M, Gaita F, Toso E. Prevalence and predictors of left atrial thrombosis in atrial fibrillation patients treated with non-vitamin K antagonist oral anticoagulants. Acta Cardiol. 2021 Nov 25:1-8. doi: 10.1080/00015385.2021.2005307 [2]

Abstract

This doctoral thesis explores the integration of artificial intelligence (AI) into the field of clinical arrhythmology and electrophysiology, emphasizing its transformative potential in arrhythmia management. The research is structured around three studies that collectively demonstrate AI's capabilities in prediction, localization, and diagnostic analysis within this broad subspecialty field of cardiology. The first study introduces AFA-Recur, a machine-learning web calculator developed from the ESC EORP AFA-LT registry. This tool predicts atrial fibrillation recurrence post-ablation by analyzing clinical variables, highglighting the potential of AI in personalized patient risk stratification. The second study presents a machine-learning model that integrates electrocardiograms (ECGs) and clinical data to automatically and interpretably predict the site of origin in outflow tract ventricular arrhythmias. This approach enhances the precision of arrhythmia localization, facilitating targeted therapeutic interventions. The third study evaluates the efficacy of convolutional neural networks (CNNs) in ECG analysis, comparing standard twelve-lead and single-lead setups. The findings suggest that CNN-enabled analysis can maintain diagnostic accuracy even with reduced lead configurations, indicating potential for scalable and accessible arrhythmia detection. Collectively, these studies underscore AI's emerging role in clinical arrhyhtmology and electrophysiology. The integration of AI into clinical practice holds promise for advancing patient care in this field.

Contents

List of Figures

List of Tables

Chapter 1

Introduction

Artificial Intelligence (AI) has emerged as a transformative force across various fields of medicine, including cardiovascular medicine. AI refers to the development of computer systems capable of performing tasks that typically require human intelligence, such as learning, reasoning, problem-solving, perception, and language understanding. Within medicine, AI often relies on machine learning (ML) algorithms and deep learning (DL) frameworks, which can process vast and complex datasets to extract patterns, generate insights, and assist in decision-making [51, 69].

The application of AI in medicine is driven by the increasing availability of large-scale healthcare data, advances in computational power, and the need for more precise and efficient healthcare delivery. Specifically, in cardiovascular medicine, AI has been instrumental in improving diagnostics, prognostics, and treatment personalization. For example, AI models can integrate data from imaging modalities, electrocardiograms (ECGs), laboratory results, and wearable devices, enabling enhanced disease phenotyping, risk stratification, and therapeutic guidance (Figure 1.1) [47].

1.1 Machine Learning and Deep Learning

Artificial Intelligence encompasses a range of methodologies, with machine learning (ML) and deep learning (DL) being two of its most prominent branches [49, 13]. While both approaches aim to enable computers to learn from data, they differ significantly in their underlying mechanisms and requirements.

Machine learning relies on algorithms that use engineered features derived from the input data [72]. In other words, domain experts must predefine and extract relevant features for the ML model to analyze. This approach is computationally efficient and works well with

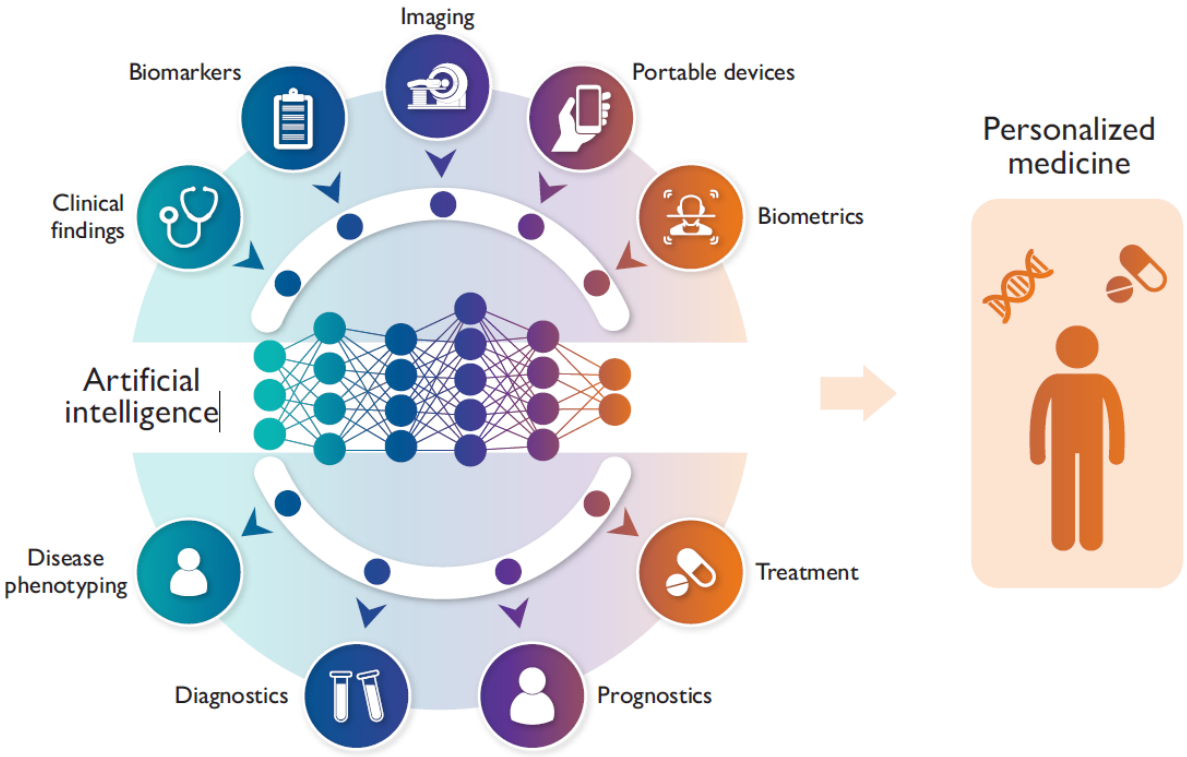

Figure 1.1: Potential uses of AI in cardiovascular medicine. Image from [69]

smaller datasets, but its accuracy heavily depends on the quality of the predefined features and the expertise involved in their selection.

Deep learning, a subset of ML, utilizes neural networks with multiple layers (hence the term ”deep”) to automatically extract features directly from raw data [65]. Unlike traditional ML, DL does not require manual feature engineering, as the model learns hierarchical representations of the data during training (Figure 1.2). This self-learning capability allows DL models to achieve higher accuracy, particularly in complex tasks such as image recognition and natural language processing. However, this enhanced performance comes with the need for significantly larger datasets to train the model effectively and greater computational resources [49].

In cardiovascular medicine, both ML and DL are widely applied. ML is commonly used in tasks where structured data, such as clinical parameters, are involved, while DL is often employed in analyzing unstructured data, such as imaging and ECG waveforms. Understanding these differences is crucial for selecting the most appropriate AI methodology for specific applications.

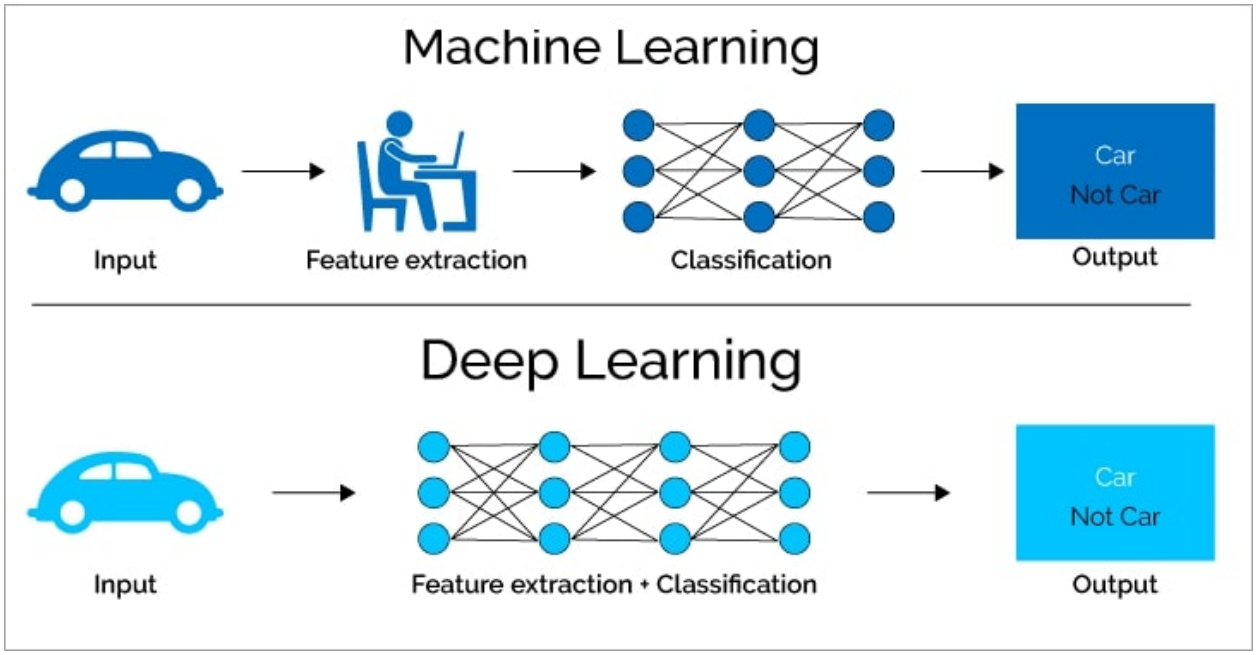

Figure 1.2: Difference between machine learning and deep learning. While ML requires human-based feature extraction before the AI task, DL is able to perform both feature extraction and the subsequent AI task from the raw input. Image from www.levity.ai/blog/difference-machine-learning-deep-learning

1.2 AI applications in Cardiovascular Medicine

AI applications in cardiovascular medicine can be categorized into several domains:

- Imaging Analysis: Deep learning models have demonstrated remarkable accuracy in interpreting imaging studies, such as echocardiography, computed tomography (CT), and cardiac magnetic resonance imaging (MRI). These tools not only automate image segmentation and feature extraction but also identify pathologies, such as left ventricular dysfunction and coronary artery disease, with precision comparable to expert clinicians [121, 5].

- Electrocardiogram Interpretation: The use of AI in ECG analysis has been transformative. AI algorithms can detect subtle abnormalities, predict conditions like atrial fibrillation (AF) from sinus rhythm ECGs, and even estimate patient characteristics such as biological age and sex based on ECG patterns. These advancements have the potential to improve early detection of cardiac diseases [112, 8, 75].

- Predictive Analytics: AI excels in predicting clinical outcomes, such as the likelihood of adverse cardiovascular events, by analyzing complex interactions among clinical variables. Tools like the Global Registry of Acute Coronary Events (GRACE) 3.0 score

leverage machine learning to provide highly accurate risk predictions, accounting for nonlinear relationships and patient-specific factors [120, 26].

- Wearable Devices and Remote Monitoring: The integration of AI with wearable technology enables continuous monitoring of cardiac health. For instance, AI algorithms analyze data from smartwatches and fitness trackers to detect arrhythmias, monitor heart rate variability, and provide actionable insights for both patients and clinicians [66].

1.3 Arrhythmology and Electrophysiology

Within the broader field of cardiovascular medicine, arrhythmology—the study and management of heart rhythm disorders—represents a critical area of focus. Arrhythmias, such as atrial fibrillation (AF), ventricular tachycardia (VT), and bradyarrhythmias, pose significant challenges due to their prevalence and potential to cause severe complications, including stroke and sudden cardiac death. Interventional electrophysiology has become a cornerstone of arrhythmia management, employing minimally invasive techniques to diagnose and treat these disorders [74].

AI's integration into arrhythmology has revolutionized the approach to rhythm disorders. For example, AI-enhanced ECGs enable the detection of subtle patterns indicative of arrhythmias, even when traditional diagnostic methods fall short. Machine learning algorithms have been developed to classify arrhythmias with near-expert accuracy, facilitating earlier and more accurate diagnoses [50]. Furthermore, predictive models assist clinicians in identifying patients at risk of arrhythmia recurrence or complications, enabling more proactive care [101].

In interventional electrophysiology, AI is enhancing procedural planning and execution. Advanced imaging and mapping technologies, combined with AI-driven analytics, allow for precise localization of arrhythmogenic foci, optimizing ablation strategies and improving outcomes. These innovations reduce procedural time, enhance safety, and increase the likelihood of long-term success [57].

The integration of AI into cardiovascular medicine, and specifically into arrhythmology and interventional electrophysiology, marks a paradigm shift in how heart rhythm disorders are diagnosed and managed. By augmenting human expertise with computational intelligence, AI has the potential to improve patient outcomes, streamline workflows, and personalize treatment strategies.

1.4 Organization of the PhD Thesis

The subsequent chapters of this thesis will systematically present the contributions made during the course of my PhD, offering a detailed exploration of the specific advancements and applications developed in the interdisciplinary field of AI-driven arrhythmology and interventional electrophysiology (Figure 1.3). These chapters aim to provide an in-depth analysis of the methodologies employed, the innovations introduced, and the challenges addressed in applying artificial intelligence to clinical cardiology, with a particular focus on the detection, prediction, and management of cardiac arrhythmias. By organizing and consolidating the findings from a series of three different contributions, this thesis will demonstrate the progression from theoretical models and algorithmic development to practical implementations and clinical validations. Emphasis will be placed on how these contributions have enhanced our understanding of cardiac electrophysiology, improved diagnostic and therapeutic workflows. Furthermore, the real-world implications of these innovations, including their potential to transform interventional strategies and optimize healthcare delivery in arrhythmology, will be critically discussed to underscore their broader significance.

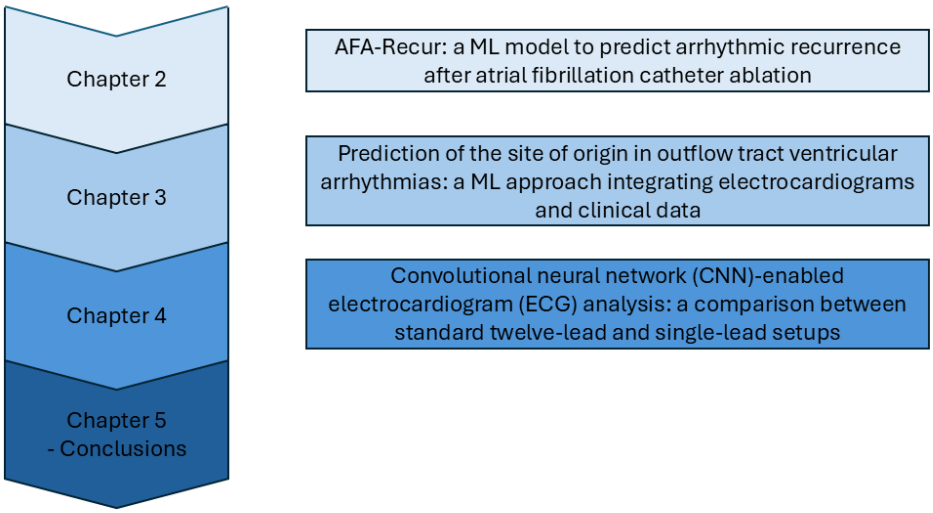

Figure 1.3: Roadmap of the following chapters, which will explore three different contributions in the field of AI and arrhythmology made during the PhD

Chapter 2

AFA Recur

2.1 Background

Atrial fibrillation (AF) is the most prevalent arrhythmia encountered in clinical practice, with its current estimated prevalence in the adult population ranging from 2 to 4%. The burden of mortality and morbidity associated with AF is expected to increase in the coming years, as recent epidemiological projections predict that the prevalence will double by 2050 [116].

A rhythm-control strategy is recommended to improve symptoms and quality of life, and, as shown in the EAST-AFNET 4 trial [60], it may also help reduce adverse cardiovascular outcomes, particularly when the arrhythmia has been present for less than 12 months. In this context, catheter ablation is a well-established option, offering superior efficacy in maintaining sinus rhythm compared to antiarrhythmic drugs [76] and is increasingly considered a first-line treatment [102].

However, recurrent AF following catheter ablation is still relatively common, often necessitating multiple procedures [44, 43]. Achieving freedom from recurrent AF enhances the benefits of catheter ablation in terms of symptom relief and possibly reduces the risk of serious adverse events, given the well-documented association between sinus rhythm maintenance and survival [54]. This highlights the importance of better patient selection. Various scoring systems have been proposed to predict recurrent AF after catheter ablation [31], but the discriminatory power of these models remains largely inadequate, with most studies lacking proper calibration.

The field of machine learning (ML) is expanding, and numerous examples show that ML-derived scores can outperform traditional risk scores in predicting cardiovascular outcomes [107, 25]. This study aims to develop an ML algorithm using pre-procedural, easily accessible clinical variables from the prospective, multicenter, multinational European Society of Cardiology

(ESC)-EHRA Atrial Fibrillation Ablation Long-Term Registry (AFA-LT) to predict the risk of AF recurrence within one year following catheter ablation, as part of a structured management approach aligned with the recently published AF guidelines [116].

2.2 Methods

2.2.1 Atrial Fibrillation Ablation Long-Term Registry

The ESC-EHRA AFA-LT is a prospective, multicenter, observational registry of consecutive patients undergoing AF ablation across 104 centers in 27 countries within European Society of Cardiology (ESC). Centers involved in the study enrolled consecutive patients scheduled for AF ablation from April 2012 to April 2015, with follow-up for one year. AF was categorized as either paroxysmal or persistent, based on the 2010 ESC Guidelines [17]. Written informed consent was obtained from all patients prior to enrollment. Additional details regarding the registry can be found in the original publication [4].

2.2.2 Outcome Assessment

The primary outcome was the 1-year atrial tachyarrhythmia recurrence, defined as an electrocardiographically documented episode of AF or atrial flutter/tachycardia lasting at least 30 seconds after a 3-month blanking period following the ablation. According to the original AFA-LT registry publication, 1-year follow-up (median 12.4 months, interquartile range 11.9–13.4 months) was completed through in-person visits (52.8%), telephone contact (44.2%), or contact with the patient's general practitioner (3.0%). During the registry period, strategies for detecting arrhythmia recurrence included periodic clinical visits with EKG (78.4%) and 24-hour Holter monitoring (64.5%), based on the physician's discretion. In 3.4% of cases, trans-telephonic monitoring and implanted monitoring systems were used. Overall, 86% of patients had at least one EKG, and 82% underwent at least one physical evaluation during the 12-month follow-up.

2.2.3 Study Inclusion Criteria

Patients were included in the study if they met the following criteria: (i) underwent ablation, (ii) had a clearly defined AF type (paroxysmal or persistent), and (iii) had available 1-year follow-up data on arrhythmic recurrences.

2.2.4 Candidate Predictors and Data Preprocessing

The following pre-procedural and easily accessible variables, derived from clinical history, personal data, and echocardiographic assessments, were considered as potential predictors for the ML model training: age, gender, body mass index (BMI), estimated glomerular filtration rate (CKD-EPI formula), smoking status (active, former, never), hypertension, diabetes, dyslipidemia, history of heart failure, coronary artery disease, structural heart disease (valvular heart disease, dilated cardiomyopathy, hypertrophic cardiomyopathy), prior stroke/transient ischemic attack, presence of a cardiac rhythm device (pacemaker, implantable cardioverter defibrillator, or cardiac resynchronization therapy), hyperthyroidism, peripheral artery disease, chronic obstructive pulmonary disease, obstructive sleep apnea, CHA2DS2-VASc score, AF type (paroxysmal or persistent), history of atrial flutter, prior failed antiarrhythmic therapy, pre-procedural sinus rhythm, abnormal EKG findings (e.g., atrioventricular block, bundle branch block, Q waves, ST-T abnormalities, corrected QT >460 ms), procedure type (first ablation or re-do), left ventricular ejection fraction (LVEF), left atrial anteroposterior diameter (LA), and left ventricular end-diastolic volume (LVEDV). Categorical variables are presented as numbers and percentages, while continuous variables are represented as means and standard deviations. Missing data were imputed using the k-nearest neighbor (kNN) technique with k = 5.

2.2.5 Model Derivation and Validation

The original dataset was randomly split into a training set (80%) and a testing set (20%). A preliminary backward stepwise logistic regression model was first applied to the training cohort and tested on the testing cohort with poor outcome (Figure 2.1).

Subsequently, four supervised ML classifiers were trained on the training cohort: decision tree (DT), random forest (RF), AdaBoost (ADA), and k-nearest neighbor (kNN). Model hyperparameters were optimized using 10-fold cross-validation, and the final model was selected based on the set of tuning parameters that maximized the mean area under the curve (AUC). The model's discriminatory performance (AUC) was assessed in the testing cohort. The model with the best AUC was chosen for further analysis, while the others were discarded. The importance of each variable was determined for the chosen ML classifier using a filter-based method. AUC was then assessed as the number of predictors was reduced according to the variable importance ranking. To ensure adequate discrimination and limit model complexity, the model offering the best trade-off between AUC and predictor number was selected. The final model's discriminatory ability in the testing cohort was compared to the widely used APPLE score [62]. Calibration was assessed through a reliability diagram and

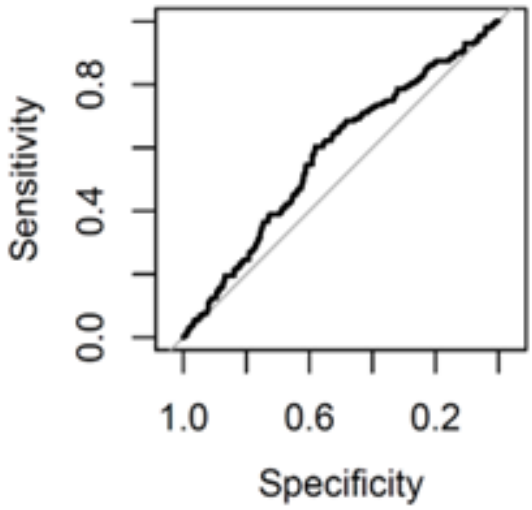

Figure 2.1: ROC curve for standard stepwise backward logistic regression model applied on the testing cohort, yielding an AUC of 0.578 (95% CI 0.527-0.629). The resulting variables of the model after stepwise backward selection were: age, eGFR (CKD-EPI), heart failure, device, dyslipidemia, hyperthyroidism, LA diameter and abnormal EKG.

the Hosmer–Lemeshow test. Platt scaling was applied to re-calibrate the model's predictions. The distribution of re-calibrated probabilities and quintile analysis were also examined, with the first two quintiles considered "low risk," the third and fourth "intermediate risk," and the final quintile "high risk" in terms of recurrence probability. A web-based risk calculator was then developed using the final calibrated ML model.

All analyses were performed independently at our center using R software version 4.0.0 (R Foundation for Statistical Computing, Vienna, Austria). The caret package (https://cran.r-project.org/web/packages/caret/caret.pdf) was used for model training and hyperparameter optimization, and the shiny package (https://shiny.rstudio.com/) was used to build the web calculator. A p-value < 0.05 was considered statistically significant.

2.3 Results

A total of 3,128 patients from the ESC-EHRA AFA-LT registry met the inclusion criteria and were analyzed. Table 2.1 presents the main clinical characteristics. The mean age was 58 ± 10 years, with 68.7% being male. The mean CHA_2DS_2-VASc score was 1.58 ± 1.32, and 20.6% had a history of heart failure. Persistent atrial fibrillation was observed in 31.9% of patients. The majority of ablation procedures (83%) were performed using radiofrequency as the energy source.

During the 1-year follow-up, 797 patients (25.8%) experienced at least one arrhythmic

recurrence, including 23.9% of those with paroxysmal atrial fibrillation (AF). Baseline clinical variables, stratified by the presence of recurrence during follow-up, are presented in Table 2.1. Patients who experienced arrhythmic recurrence were more likely to have persistent AF, a history of heart failure, impaired renal function, and exhibited higher CHA_2DS_2-VASc scores and body mass index (BMI) compared to those without recurrence. Additionally, patients with recurrence showed a larger left atrial (LA) anteroposterior diameter and a lower left ventricular ejection fraction (LVEF) than those without recurrence.

Table 2.1: Baseline clinical features of the original population, stratified by recurrence status

Variables	**Total (n = 3128)**	**No recurrence (n = 2331)**	**Recurrence (n = 797)**	**P-value**
Age (years)	58.09 (10.28)	57.99 (10.27)	58.38 (10.30)	0.361
Male gender (%)	2148 (68.7)	1604 (68.8)	544 (68.3)	0.804
BMI (kg/m2)	28.40 (4.46)	28.29 (4.45)	28.74 (4.45)	0.017
eGFR (mL/min/1.73m2)	80.80 (18.47)	81.62 (18.30)	78.47 (18.77)	< 0.001
Heart failure (%)	431 (20.6)	298 (19.5)	133 (23.6)	0.046
CAD (%)	367 (17.9)	264 (17.6)	103 (18.4)	0.730
Structural heart disease (%)	535 (25.5)	379 (24.8)	156 (27.5)	0.230
Stroke/TIA (%)	96 (3.1)	68 (2.9)	28 (3.5)	0.476
Device carrier (%)	138 (4.4)	87 (3.7)	51 (6.4)	0.002
Smoker status (%)				0.066
Former ($\geq$ 1 month)	588 (19.7)	417 (18.8)	171 (22.4)	
No	2082 (69.9)	1573 (71.0)	509 (66.7)	
Yes	309 (10.4)	226 (10.2)	83 (10.9)	
Diabetes (%)	301 (9.7)	220 (9.5)	81 (10.2)	0.599
Hypertension (%)	1680 (53.9)	1221 (52.7)	459 (57.6)	0.019
Dyslipidaemia (%)	988 (32.2)	739 (32.4)	249 (31.8)	0.809
Hyperthyroidism (%)	72 (2.3)	45 (2.0)	27 (3.5)	0.026
PAD (%)	55 (1.8)	42 (1.8)	13 (1.6)	0.751
COPD (%)	69 (2.3)	49 (2.2)	20 (2.5)	0.616
Obstructive sleep apnoea (%)	105 (3.6)	80 (3.7)	25 (3.4)	0.762
CHA2DS2-VASc score	1.58 (1.32)	1.55 (1.32)	1.66 (1.33)	0.043
AF type (%)				0.005
Paroxysmal AF	2130 (68.1)	1620 (69.5)	510 (64.0)	
Persistent AF	998 (31.9)	711 (30.5)	287 (36.0)	
AFL (%)	724 (24.1)	529 (23.6)	195 (25.7)	0.264
Previous failed AAD (%)	2782 (89.7)	2064 (89.3)	718 (90.8)	0.273
Baseline LVEF (%)	59.81 (8.54)	60.01 (8.49)	59.20 (8.65)	0.045
Baseline LVEDV (mL)	112.47 (30.62)	112.84 (30.17)	111.57 (31.74)	0.543
Baseline LA diameter (mm)	42.63 (6.67)	42.22 (6.64)	43.81 (6.61)	< 0.001
Baseline sinus rhythm (%)	1968 (62.9)	1514 (65.0)	454 (57.0)	< 0.001
Abnormal ECG (%)	1885 (60.3)	1362 (58.4)	523 (65.6)	< 0.001
Re-do procedure (%)	674 (21.5)	490 (21.0)	184 (23.1)	0.240

Four different supervised machine learning (ML) classifiers—decision tree (DT), random forest (RF), adaptive boosting (ADA), and k-nearest neighbors (kNN)—were trained and optimized using the training cohort. Table 2.2 reports full details of the 10-fold cross-validation for the optimally tuned models, showing that the best performer was the RF model, achieving an area under the curve (AUC) of 0.722 (interquartile range: 0.691–0.739).

Receiver operating characteristic (ROC) curves and corresponding AUC values for the testing cohort across different models are shown in Figure 2.2, with the RF model demonstrating the best discriminative performance [AUC = 0.718, 95% confidence interval (CI): 0.674–0.761], making it the model of interest.

Table 2.2: AUC summary statistics obtained by 10-fold cross-validation on the training cohort of the optimally tuned models.

Model	Min.	1st Quartile	Median	Mean	3rd Quartile	Max.
Decision Tree	0.5396	0.5832	0.6073	0.5977	0.6155	0.6425
Random Forest	0.6412	0.6908	0.7218	0.7102	0.7386	0.7544
Adaboost	0.6301	0.6884	0.7162	0.7053	0.7320	0.7584
kNN	0.5162	0.5569	0.5882	0.5860	0.6271	0.6422

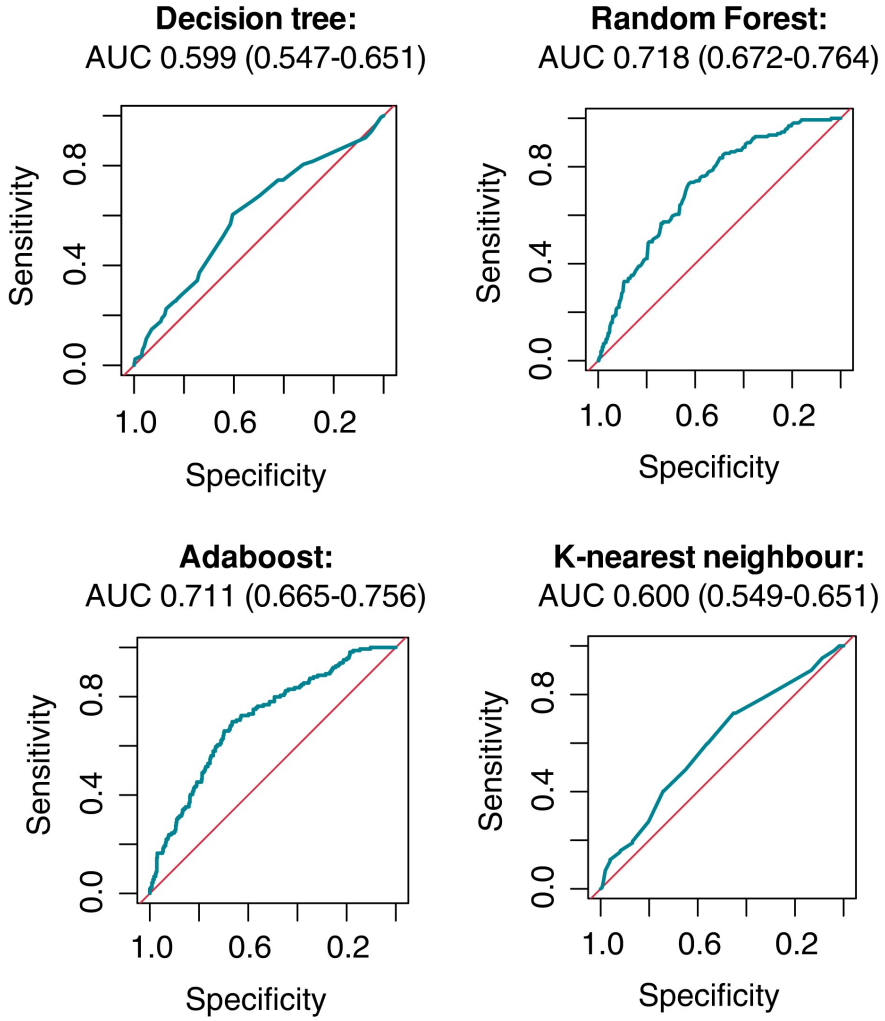

Figure 2.2: Receiver operator curve curves and corresponding AUC of the four evaluated machine-learning classifiers. AUC, area under the receiver operator curve.

Figure 2.3A, presents the variable ranking in the RF model. To ensure effective discrimination while minimizing model complexity, the change in AUC in the testing cohort was assessed by progressively reducing the number of predictors, starting with the lowest-ranked variables. Simplified RF models were fitted using K features, with K ranging from 1 to 27, and the resulting AUC values were plotted against the number of included variables (Figure 2.3B). As model discrimination plateaued after 19 variables, a 19-variable RF model

was selected as the final ML classifier (Figure 2.3C; Table 2.3).

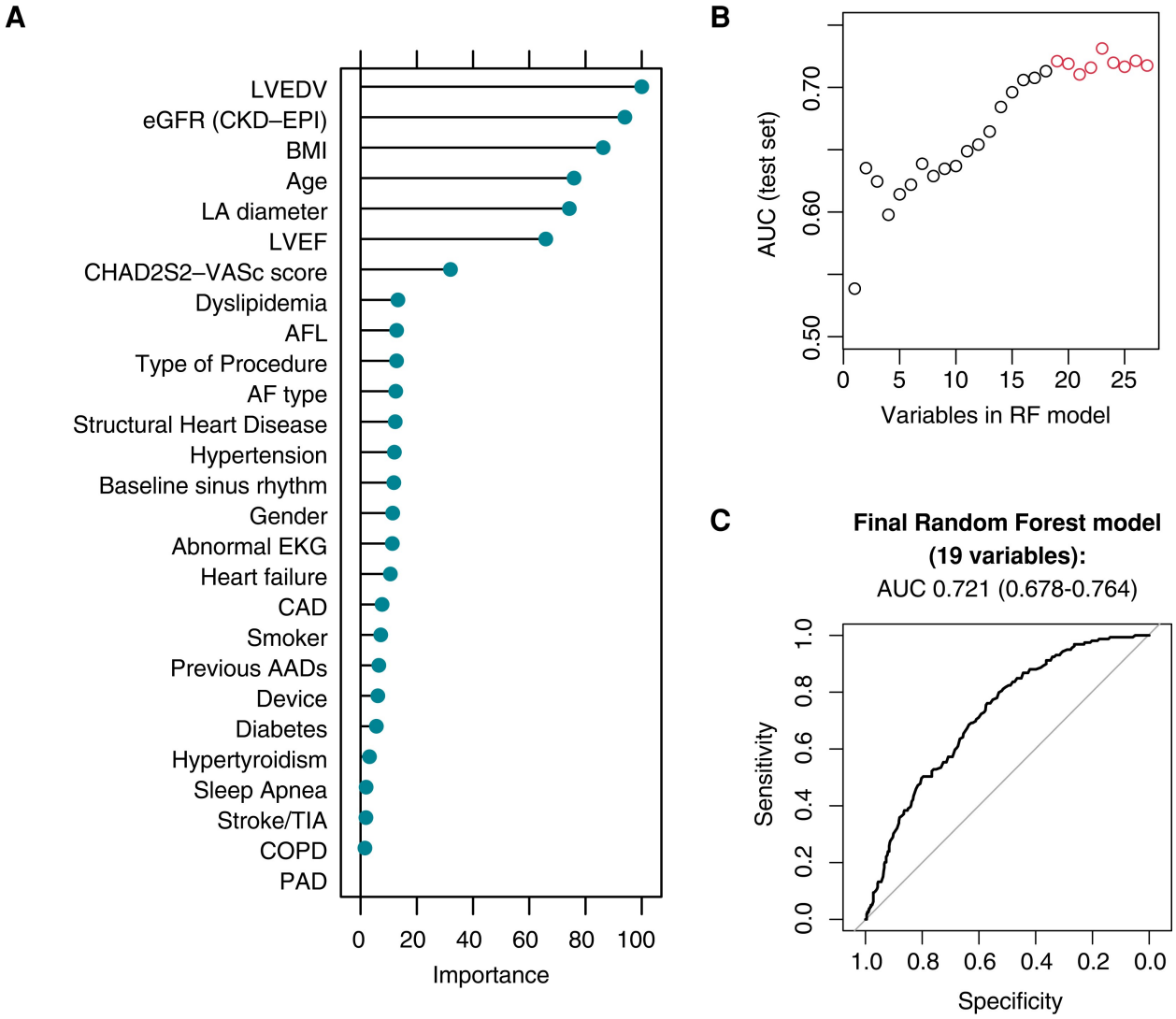

Figure 2.3: Random forest model selection. (A) Variable ranking for the 27 original predictors; (B) the number of included variables strengthens the model AUC reaching a plateau at 19; (C) ROC curve and corresponding AUC of the final 19-variable random forest model. AAD, antiarrhythmic drug; AFL, atrial flutter; AUC, area under the receiver operator curve; AFL, atrial flutter; BMI, body mass index; CAD, coronary artery disease; COPD, chronic obstructive pulmonary disease; LA, left atrium; LVEDV, left ventricular end-diastolic volume; LVEF: left ventricular ejection fraction; PAD, peripheral artery disease; RF: random forest; ROC: receiver operator curve.

The area under the curve (AUC) of the final model in the testing cohort was 0.721 (95% CI: 0.680–0.764), demonstrating superior performance compared to the APPLE score for outcome prediction in the same cohort (AUC = 0.557, 95% CI: 0.506–0.607; Figure 2.4).

Due to uncalibrated predictions of the model, as indicated by the Hosmer–Lemeshow test ($P = 0.005$), over-forecasting was observed in the lower left quadrant of the reliability plot (Figure 2.5, panel A). To address this, calibration was successfully performed using Platt scaling (Figure 2.5, panel B), resulting in an improved Hosmer–Lemeshow test outcome

Table 2.3: Included variables in the final model.

Included Variables
LVEDV
Estimated glomerular filtration rate (CKD-EPI formula)
BMI
Age
LA anteroposterior diameter
LVEF
CHA_2DS_2-VASc score
Dyslipidaemia
AFL
Type of procedure (first procedure or re-do)
Atrial fibrillation type (paroxysmal or persistent)
Structural heart disease
Hypertension
Baseline sinus rhythm
Gender
Abnormal ECG
Heart failure
CAD
Smoker

($P = 0.063$). The frequency distribution of predicted probabilities after re-calibration is shown in Figure 2.6A.

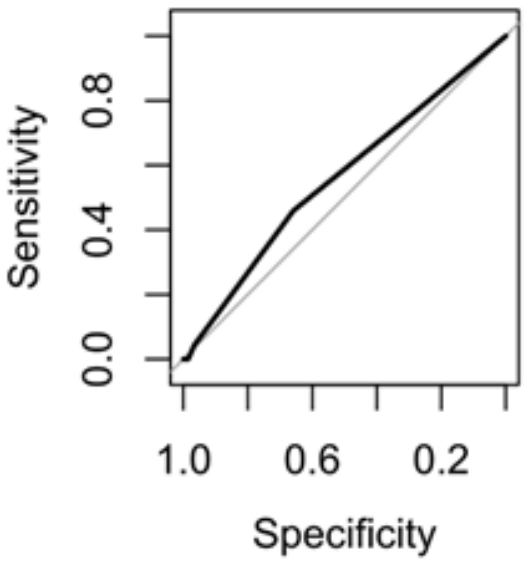

Figure 2.4: ROC curve for APPLE score applied on the testing cohort, yielding an AUC of 0.557 (95% CI 0.506-0.607).

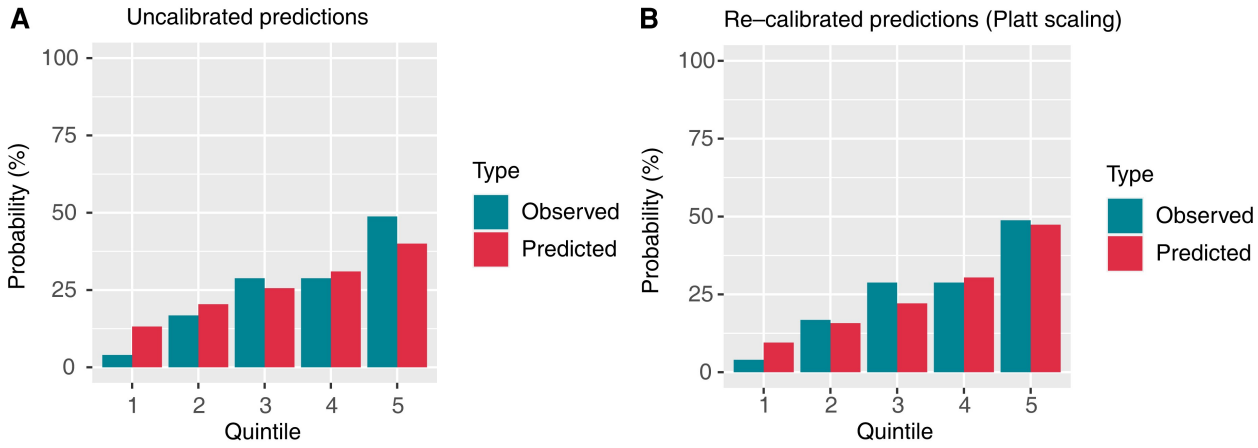

Figure 2.5: Random forest model calibration on the testing cohort. (A) Calibration plot before Platt scaling, showing uncalibrated predictions. (B) Calibration plot after Platt scaling, yielding improved calibration.

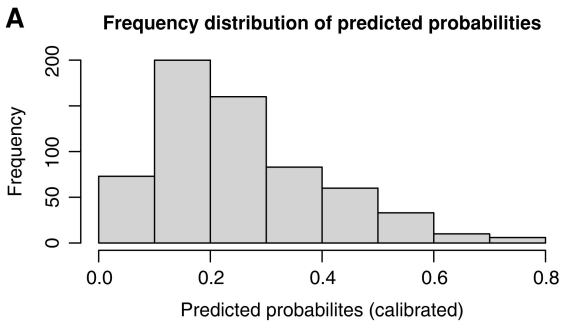

B

Quantile	Median	Minimum	Maximum
1st	0.095	0.044	0.126
2nd	0.158	0.126	0.187
3rd	0.221	0.190	0.259
4th	0.304	0.259	0.376
5th	0.474	0.380	0.764

Figure 2.6: Predicted probability distribution and quantile analysis on the testing cohort. (A) Frequency distribution of the predicted probabilities of AF recurrence (after re-calibration with Platt scaling). (B) Quintile analysis of the predicted probability distribution; the first two quintiles are considered 'low risk' (green), the third and the fourth 'intermediate-risk' (yellow), while the last quintile represent 'high risk' (red) for AF recurrence after catheter ablation.

A quintile-based analysis (Figure 2.6B) identified three distinct risk categories for recurrence. The first two quintiles were classified as the 'low-risk' group (predicted probability range: 0.04–0.19), the third and fourth quintiles as the 'intermediate-risk' group (predicted probability range: 0.19–0.38), and the highest quintile as the 'high-risk' group (predicted probability range: 0.38–0.76).

The final re-calibrated RF model was ultimately implemented in a web calculator, freely available at http://afarec.hpc4ai.unito.it/, allowing the user to input predictor values to obtain the probability output of 1-year AF recurrence for a specific patient, as well as its associated risk class (Figure 2.7).

2.4 Discussion

Catheter ablation has emerged as a well-established and safe approach for rhythm control in patients with symptomatic AF [116]. Although the recent Catheter Ablation vs. An-

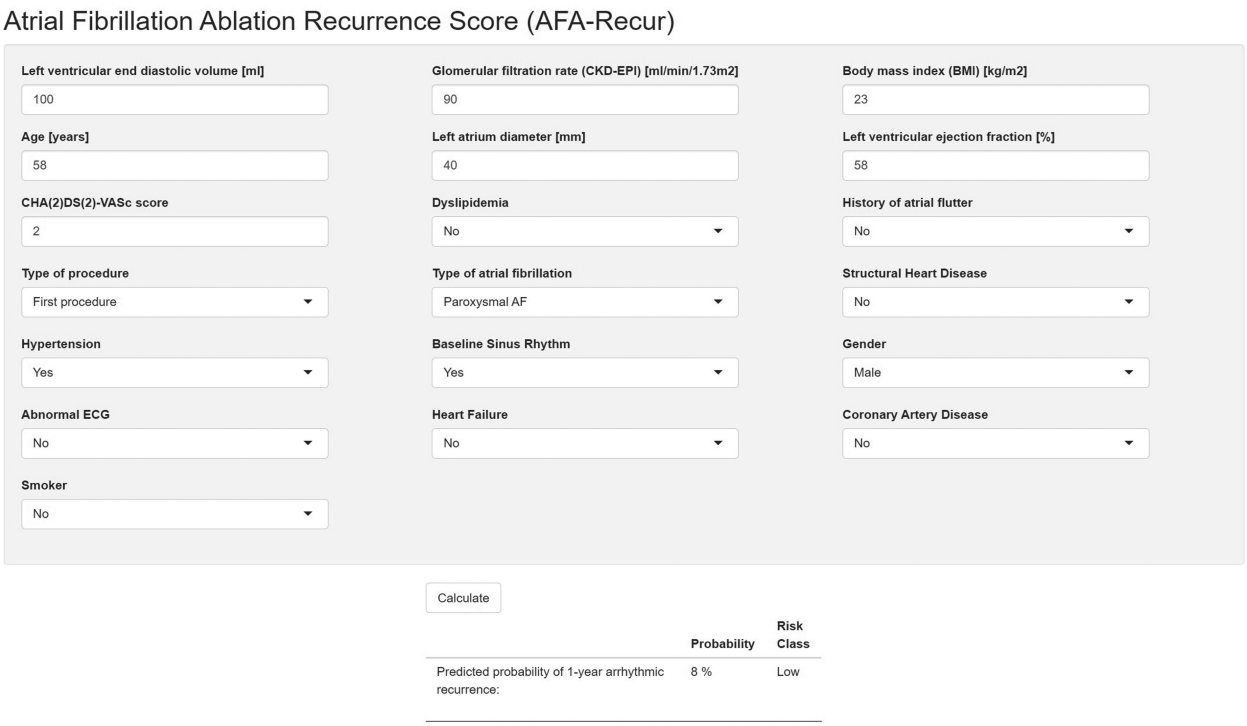

Figure 2.7: Freely available web calculator http://afarec.hpc4ai.unito.it/, which allows the user to input predictor values to obtain a probability output of 1-year AF recurrence, as well as the associated risk class, for a specific patient.

tiarrhythmic Drug Therapy for Atrial Fibrillation (CABANA) trial did not achieve formal statistical significance in its composite primary outcome, it demonstrated that catheter ablation reduces mortality and cardiovascular hospitalization, as observed in its secondary endpoint [76]. Moreover, clinical trials involving patients with concurrent heart failure, along with real-world observational evidence, suggest that catheter ablation may offer superior cardiovascular outcomes compared to medical therapy [71, 94].

However, the efficacy of AF catheter ablation remains a challenge, with recurrence rates after a single procedure ranging from 20% to 45% [44, 43]. One contributing factor is the insufficient durability of ablation lesions, which may be improved through technological advancements. Another key issue is the presence of a complex myocardial substrate, influenced by various clinical risk factors and comorbidities. To optimize treatment outcomes and avoid ineffective interventions, appropriate patient selection is crucial. Established risk factors for arrhythmia recurrence include persistent AF, left atrial enlargement, and underlying structural heart disease [9, 24]. Several prognostic models incorporating different predictive variables have been proposed to address this concern. However, a recent meta-analysis assessing 13 prognostic models found that their predictive accuracy was suboptimal, with none consistently demonstrating strong performance in forecasting rhythm outcomes [31]. Additionally, none of these models underwent internal validation, leading to an overly optimistic estimation of

their predictive capabilities in untested populations. Furthermore, only two out of the 13 models included calibration assessment, a crucial step in refining predictive models that was missing in most cases.

In this study, we developed and evaluated the first machine learning (ML)-based probability score (AFA-Recur) to estimate the risk of recurrent arrhythmic events in patients undergoing AF catheter ablation. This model is derived from the largest available prospective, multicenter, multinational, observational registry of the European Society of Cardiology (ESC-EHRA AFA-LT). ML is an advancing field with increasing applications in cardiovascular medicine [111], leveraging data-driven algorithms to uncover hidden but clinically relevant associations without predefined assumptions about variable interactions. Unlike traditional statistical methods such as logistic regression, ML models consider multiple, complex, and non-linear interactions between patient characteristics and comorbidities. Recent studies have demonstrated that ML-based cardiovascular predictive models outperform conventional risk scores [107, 117] and have been evaluated across various clinical scenarios [22]. Our findings further support this perspective, as the AFA-Recur model demonstrated superior performance in predicting 1-year arrhythmia recurrence after catheter ablation compared to the widely used APPLE score [62].

A key strength of our score is its derivation from a diverse patient cohort across 104 centers in 27 countries within the ESC. Unlike previous risk scores developed in highly selected patient populations, the ESC-EHRA AFA-LT registry allows for the inclusion of broader patient heterogeneity, capturing differences in patient selection and procedural characteristics across centers and countries. This enhances its applicability to real-world clinical practice. Additionally, the prospective nature of the registry ensures that patient selection was not influenced by the availability of predictors or outcome data.

2.4.1 Limitations

Some limitations of this study should be acknowledged. First, because only a subset of patients received loop recorders post-procedure, brief asymptomatic arrhythmia recurrences may have been missed in the outcome assessment. However, prior research suggests that only a small proportion of patients clinically classified as arrhythmia-free after catheter ablation would meet the criteria for ablation failure (defined as recurrent arrhythmia lasting >30 seconds) when monitored with long-term electrocardiographic recordings [122]. Moreover, given that symptom relief is the primary goal of AF ablation, short, asymptomatic arrhythmic episodes may not necessarily indicate procedural failure.

Additionally, the ESC-EHRA AFA-LT registry classified AF as either paroxysmal or

persistent based on the 2010 ESC Guidelines [17]. Subsequent updates to the guidelines have altered these definitions, leading to a significant shift in classification from persistent to paroxysmal AF. Nonetheless, a recent study suggests that the original definition may be a better predictor of rhythm outcomes following AF ablation [119].

Finally, since only a minority of patients (16%) in this study underwent cryoballoon ablation, the AFA-Recur score may primarily apply to patients treated with radiofrequency ablation. While cryoballoon and radiofrequency ablation have comparable success rates [63], predictors of arrhythmia recurrence may differ between these techniques. The predominance of radiofrequency ablation in our study population limited our ability to perform subgroup analyses to explore potential differences in recurrence predictors between energy sources and ablation technologies.

2.4.2 Conclusion

Based on data from the largest available prospective, multicenter, multinational observational registry of AF patients undergoing catheter ablation (ESC-EHRA AFA-LT registry), we developed and validated an ML-based probability score (AFA-Recur) to estimate the 1-year risk of arrhythmia recurrence post-ablation.

The freely accessible online calculator (http://afarec.hpc4ai.unito.it/) enables clinicians to input easily obtainable pre-procedural clinical variables to estimate patient-specific risks of AF recurrence after ablation. The strong predictive performance of this model supports its potential role in guiding personalized therapeutic decision-making.

Chapter 3

ML-based site of origin prediction of outflow tract arrhythmias

3.1 Background

Ventricular tachycardia (VT) is a critical cardiac arrhythmia that can result in sudden cardiac death (SCD). Among VT subtypes, idiopathic ventricular arrhythmias (IVAs) present a particular diagnostic challenge, as their underlying mechanisms remain largely unclear. A prevalent category within IVAs is outflow tract ventricular arrhythmias (OTVAs), which originate from the ventricular outflow tracts—the anatomical regions linking the ventricles to major arteries. The structural and functional complexity of these areas complicates both diagnosis and treatment planning for OTVAs.

Currently, treatment options for OTVAs include antiarrhythmic medications and radiofrequency ablation (RFA) [67]. However, RFA's effectiveness has been limited, with high recurrence rates frequently reported. To enhance the success rate of RFA, accurate pre-procedural planning is crucial. This involves determining the optimal ablation site, also referred to as the ectopic foci or site of origin (SOO) of the OTVA, prior to the procedure.

The electrocardiogram (ECG) serves as a fundamental tool for identifying the SOO in OTVAs, as its morphological variations are distinguishable in affected individuals [67]. Initial estimations of the SOO, differentiating between right ventricular outflow tract (RVOT) and left ventricular outflow tract (LVOT) origins, are commonly made through visual ECG analysis.

Numerous methods have been developed to analyze ECG characteristics for distinguishing LVOT from RVOT origins, as reviewed comprehensively in [1, 55, 70]. Some algorithms assess the proximity of the origin to specific ECG lead patterns, associating left bundle branch block

(LBBB) patterns with origins near lead V1 and right bundle branch block (RBBB) patterns with origins further from the anterior chest. However, complexity arises as LVOT origins can exhibit either LBBB or RBBB patterns, depending on the specific SOO. A crucial component in these algorithms is the precordial transition, defined as the first precordial lead displaying a dominant R wave. This measure establishes criteria for determining the transition zone or analyzing the R/S wave ratio (i.e., the amplitude of the R wave divided by the amplitude of the S wave in the QRS complex) in specific leads. Despite reported accuracies often exceeding 85%, many of these methods are derived from single-center datasets, rely on visually assessed ECG features, and incorporate highly specific thresholds, thereby limiting their general applicability. Alternative methods analyze the precordial transition in both sinus rhythm and premature ventricular contractions (PVCs), which are frequently observed in OTVA cases [12, 34].

Nonetheless, dependence on clinician expertise for visually interpreting these ECG features introduces potential inconsistencies in the analysis. Additionally, variability in precordial lead placement and heart orientation complicates the standardization of diagnostic criteria. Sole reliance on visual ECG analysis may lead to misdiagnosis and suboptimal treatment strategies, ultimately prolonging procedural time and elevating recurrence risks.

Recent advancements have aimed to enhance SOO prediction accuracy beyond visual inspection. These approaches integrate ECG morphological analysis with patient data to improve classification performance. For example, Penela et al. [81] introduced a hybrid algorithm incorporating clinical parameters such as sex, hypertension, and age alongside ECG analysis based on the precordial R/S transition and lead V3 amplitude. However, this method depends on manually set thresholds for age and V3 amplitude and partially relies on clinician expertise in determining the R/S transition.

While these approaches improve upon visual analysis alone, they remain constrained by accuracy and interpretability issues. Doste et al. [29] proposed a machine learning (ML)-based classification model utilizing both real and simulated signals to predict OTVA origins. However, this approach lacks patient-specific data integration, potentially restricting its applicability in real-world clinical settings.

To overcome these challenges, our study proposes a comprehensive ML framework that integrates signal analysis from both simulated and real ECG data, incorporates patient-specific information, and systematically identifies the most relevant predictive features. This integrated strategy enhances classification accuracy while also improving interpretability, providing clinicians with insights into key factors influencing treatment decisions. Furthermore, our approach extends beyond classification by employing unsupervised algorithms to identify specific ectopic foci locations, enabling cluster analysis based on ECG characteristics

and patient demographics. This holistic methodology aims to advance the precision and effectiveness of OTVA treatment planning significantly.

3.2 Methods

The study employed a comprehensive methodology to examine the identification of OTVA's SOO, integrating multiple databases and advanced analytical techniques. The primary objective was to distinguish between LVOT and RVOT origins using a supervised ML approach. Additionally, an unsupervised ML approach was employed to explore the identification of the specific SOO. Four distinct databases were utilized: two containing QRS complexes, one with simulated QRS complexes, and another incorporating both QRS complexes and clinical patient data.

During the supervised training phase, models were developed separately using QRS complexes and patient data. Various combinations of QRS data and patient information from different databases were explored to assess their impact on model performance. Moreover, an innovative strategy was introduced, wherein models were trained independently, and the inference from one was used as input for the other to enhance predictive performance.

Furthermore, an algorithm was designed to automate the identification of the R/S transition from PVC and sinus rhythm beats, thereby improving model precision. Additionally, all predefined thresholds from the original approach proposed by Penela et al. [81] were eliminated.

Feature relevance analysis was performed using SHAP (SHapley Additive exPlanations) [68] and Gini's coefficient metric [20] on the QRS-based models. Insights from this analysis guided the incorporation of additional features into the patient data models, enhancing predictive accuracy.

Finally, an unsupervised hierarchical clustering model was applied to explore structural patterns within the data. Unlike other models that primarily focus on distinguishing between right (RVOT) and left (LVOT) ventricular origins, this model was specifically designed to identify the precise SOO within the ventricular structure. This novel approach enhances the understanding of OTVA and refines targeted treatment strategies.

The following sections detail the databases used, the supervised training models, feature and model analysis, the unsupervised training methodology for specific SOO identification, and the various experiments conducted. The overall pipeline is illustrated in Figure 3.1.

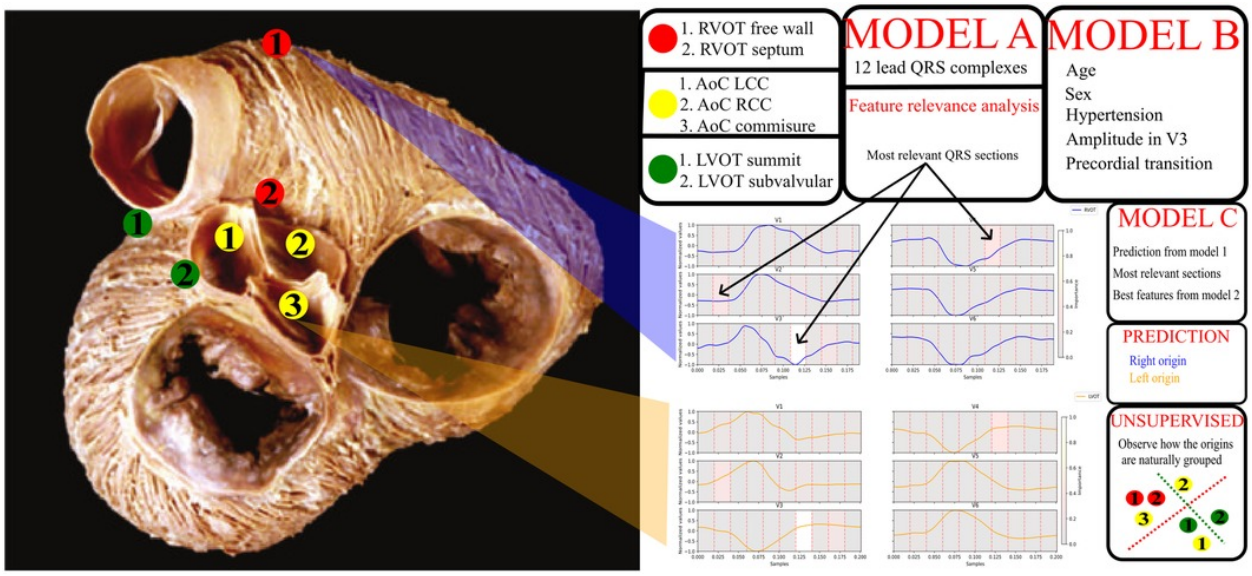

Figure 3.1: Study pipeline. On the left, an adapted image of the outflow tracts from Sánchez-Quintana et al. [108] is displayed, where the specific sites of origin (SOO) are marked. The red points indicate RVOT origins, the green points correspond to LVOT origins, and the yellow points represent aortic cusp (AoC) origins, which form a subgroup within the LVOT origins. On the right, a legend is provided for the origins, along with two example signals representing RVOT (blue) and LVOT (orange) origins. Additionally, a schematic representation of the models obtained from various experiments is shown. **Model A** utilizes 12-lead QRS complexes. **Model B** incorporates patient data along with basic ECG features, as listed in the figure. **Model C** is developed using the best QRS segments identified through feature relevance analysis from Model A, the optimal feature configuration from Model B, and the prediction output from Model A. Finally, unsupervised clustering was conducted to explore the natural distribution of the specific SOO using the most relevant set of features.

3.2.1 Databases

For our study, we utilized four multi-centric ECG databases, each contributing a distinct yet complementary role:

- **DS-2496**: Consisting of 2469 simulated 12-lead ECG signals (RVOT: 1040, LVOT: 1456), this dataset was generated using the pipeline proposed by Doste et al. [30] to simulate OTVA patients.
- **DS-31**: Containing 31 cases (RVOT: 17, LVOT: 14) of 12-lead ECG recordings from Hospital Clínic, Barcelona.
- **DS-334**: An open-source database comprising 334 12-lead ECG signals (RVOT: 234, LVOT: 100) as published by Zheng et al. [123].
- **DS-114**: Comprising 114 cases (RVOT: 79, LVOT: 35) obtained from Hospital Teknon, Barcelona. This dataset, partially employed in Penela et al. [81], includes 12-lead ECG signals, multiple beats per patient, premature ventricular contractions (PVCs), and relevant clinical data.

Ethical considerations were rigorously followed, with written informed consent obtained from all patients. To address the variations across databases, we designed two distinct models. The first model integrated all four datasets to develop a classifier based on QRS complex morphology, while the second model exclusively utilized clinical data from DS-114 for training. Furthermore, a third hybrid model combining both approaches was explored.

The dataset was partitioned into training (80%) and testing (20%) subsets using a stratified split to preserve the RVOT and LVOT proportions [1]. Each database was individually divided before merging subsets according to the training model. A 5-fold cross-validation approach was employed, along with a grid search for hyperparameter tuning, ensuring a rigorous and reliable training process.

3.2.2 Supervised Models

The model based on QRS complexes was trained according to the methodology described in Doste et al. [29]. Each lead's QRS complexes were resampled into ten evenly spaced points, concatenating them into a vector where each entry represented a 10% segment of the complex. Unlike previous studies that focused on select leads, this approach incorporated all 12 leads to ensure a comprehensive assessment of QRS morphology.

For clinical data modeling, we adopted a weighted hybrid algorithm inspired by Penela et al. [81]. Age and V3 amplitude were originally binarized at thresholds of 50 years and 1 mV, respectively. To improve generalizability and reduce overfitting, age was normalized by dividing by 100, ensuring a consistent range across features. Additionally, the raw V3 amplitude was included instead of its binarized counterpart. To automate precordial transition detection, we developed an algorithm that calculates the R/S ratio for each lead, identifying where the R wave starts to dominate.

Considering that precordial transition depends on the horizontal cardiac axis and patient-specific clinical factors [70], we standardized the R/S transition based on sinus rhythm. This involved computing the transition for both beats and combining them into a unified feature by subtracting one from the other.

ECG signal delineation was performed using the convolutional neural network proposed by Jimenez-Perez et al.[56]. Subsequently, cardiac cycles were segmented to extract premature ventricular contraction (PVC) beats alongside their preceding beats. For each case, the QRS complexes were analyzed, and the R/S ratios were computed across the precordial leads.

A range of machine learning algorithms were tested, including Support Vector Machines (SVM) with the NuSVC implementation from scikit-learn [80], multilayer perceptron (MLP), Extra Trees (ET), Random Forest (RF), and XGBoost[21]. Hyperparameter tuning was

conducted through grid search, optimizing parameters for each model (Table 3.1 reports the tuned parameters for each model).

Model	**Parameter**	**Range**	**Step**
SVM	Nu value	[0.4, 0.6]	0.1
	Kernel	{rbf, linear, poly}	-
	Degree*	[1,5]	1
	Gamma	{scale, auto}	-
	Coef0*	[0,1]	0.5
MLP	Solver	{lbfgs, adam}	-
	Alpha	{1e-4, 1e-5, 1e-6}	-
	Hidden layers size	{10, 50, 100}	-
	Activation function	{identity, logistic, tanh, relu}	-
RF	Estimators	[100, 500]	100
	Minimum samples to split	[0.1, 1]	0.1
	Minimum samples per leaf	[0.1, 1]	0.1
ET	Estimators	[100, 500]	100
	Minimum samples to split	[0.1, 1]	0.1
	Minimum samples per leaf	[0.1, 1]	0.1
XGBoost	Maximum depth	[1, 10]	1
	Minimum child weight	[1, 6]	0.5
	Gamma	[0, 0.5]	0.1
	Subsample	[0.6, 1]	0.01
	Column sample by tree	[0.6, 1]	0.1
	Regulation alpha	{1e-5, 1e-2, 0.1, 1, 100}	-

Table 3.1: Hyperparameters tuned per model. *Only for 'poly' kernel.

The models were evaluated using two primary metrics: accuracy and macro-average sensitivity. The latter was particularly relevant due to the class imbalance, ensuring that both LVOT and RVOT classifications were given equal weight. The macro-average sensitivity was computed as:

$$MA = \frac{1}{2}\left(\frac{TP}{TP+FN} + \frac{TN}{TN+FP}\right) \tag{3.1}$$

where TP and TN represent true positives and true negatives, while FP and FN denote false positives and false negatives, respectively.

All reported results were obtained using DS-114 as the test set to ensure comparability, given that it is the only dataset containing both QRS complexes and clinical data. To refine classification performance, SHAP analysis [68] and Gini's coefficient [20] were used to identify the most relevant features, which were subsequently integrated into the clinical model.

3.2.3 Unsupervised Models

Hierarchical clustering was employed to analyze the natural grouping of SOO labels provided by clinicians. This method was chosen due to its ability to flexibly organize samples based on similarity, making it well-suited for the complex nature of ventricular SOOs.

To simplify the classification task, the original 56 clinical SOO labels were consolidated into seven primary categories, following the methodology of Penela et al. [81]: right coronary cusp (RCC), left coronary cusp (LCC), RCC/LCC commissure, LVOT sub-valvular region, LV summit, RVOT septum, and RVOT free wall.

Hierarchical clustering was performed using Ward's variance minimization method [73], which optimally merges clusters by minimizing intra-cluster variance. A key advantage of this approach is its ability to determine the natural number of clusters without requiring predefined constraints, making it ideal for this study.

3.2.4 Experiments

A structured set of experiments was conducted to assess the effectiveness of the proposed models. Experiments A, B, and C were designed to evaluate supervised learning approaches, while Experiment D explored unsupervised clustering of SOOs. A summary of these experiments is provided in Table 3.2.

Experiment A: Training on QRS Morphology

This experiment focused exclusively on training models using QRS complex features. Two scenarios were considered:

- **Scenario A.1:** Training and testing on DS-114 alone.
- **Scenario A.2:** Training on all datasets, with DS-114 used for final evaluation.

Experiment B: Training on Clinical Variables and ECG Features

In this experiment, clinically annotated precordial transitions were compared with automatically computed transitions. Transition vectors were generated for each patient, with elements set to zero except for the transition point, which was marked as one. Differences between manual and automatic transitions were quantified using vector shifting techniques.

Models were trained using various combinations of clinical data and computed transitions, leading to multiple scenarios:

- **Scenario B.1:** Using only clinical variables as per Penela et al. [81].

Experiment	Scenario	Input
A	1	QRS complexes from DS-114
	2	QRS complexes from all databases
B	1	BinAge, sex, HTA, BinV3 and PTR
	2	BinAge, sex, HTA, BinV3 and PTC
	3	NormAge, sex, HTA, AmpV3 and PTR
	4	NormAge, sex, HTA, AmpV3 and vPTC
	5	NormAge, sex, HTA, AmpV3 and vPTCPs
	6	NormAge, sex, HTA, AmpV3 and vPTCVal
	7	NormAge, sex, HTA, AmpV3 and vPTCPsVal
C	1	Binary prediction of best model in Experiment A Best features from best model in Experiment B
	2	Probability per class of best model in Experiment A Best features from best model in Experiment B
	3	Best features from best model in Experiment A Best features from best model in Experiment B
	4	Binary prediction of best model in Experiment A Best features from best model in Experiment B
	5	Probability per class of best model in Experiment A Best features from best model in Experiment B

Table 3.2: Summary of experiments and their input features. BinAge: Binarized age with threshold >50; NormAge: Normalized age; HTA: Hypertension; BinV3: Binarized amplitude in V3 with threshold >1 mV; NormV3: Amplitude in V3; PTR: Precordial transition reported by clinicians; PTC: Precordial transition calculated; vPTC: Precordial transition calculated in vector form; vPTCVal: R/S values of the precordial transition calculated in vector form; vPTCPs: Precordial transition calculated considering sinus rhythm and PVC beats in vector form; vPTCPsVal: R/S values of the precordial transition calculated considering sinus rhythm and PVC beats in vector form.

- **Scenario B.2:** Replacing manually annotated precordial transitions with computed ones.
- **Scenario B.3:** Removing binarization thresholds.
- **Scenario B.4:** Using computed PVC transition without thresholds.
- **Scenario B.5-B.7:** Incorporating sinus rhythm features and refined transition metrics.

Experiment C: Combining QRS Morphology and Clinical Data

This experiment aimed to integrate QRS complex features from Experiment A with clinical data from Experiment B. Five scenarios were tested, incorporating different combinations of features, probability outputs, and selected amplitudes.

Experiment D: Unsupervised Clustering of SOOs

To explore natural distributions within SOOs, hierarchical clustering was applied to the best feature set. A grid search was used to determine the optimal cluster threshold based on silhouette scores. Results were visualized using heatmaps, grouping SOOs into three primary anatomical regions: aortic cusp (AoC), RVOT, and LVOT.

3.3 Results

3.3.1 Experiment A: Training on QRS Morphology

The results from Experiment A (Figure 3.2) indicate that Scenario A.1 achieved the highest accuracy across the RF, MLP, and ET models. However, the macro-average sensitivity was relatively lower. Upon analyzing the performance of individual classes, Scenario A.1 showed 68% accuracy and 41% macro-average sensitivity, with perfect classification for RVOT but 0% for LVOT. In contrast, Scenario A.2, where the XGB model was used, produced similar accuracy results (66%) and a higher macro-average sensitivity. This suggests that using multiple databases for training reduces the likelihood of overfitting, as evidenced by Figure 3.3, which presents the confusion matrix for the XGB model, showing improved performance for LVOT cases.

The XGB model was determined to be the most effective in Experiment A. When evaluating the Gini's coefficient for the model, it was found that the most influential leads were V3, V4, and V2, contributing to approximately 51% of the total cumulative score. These were followed by aVR (9.7%) and V1 (8%). A closer inspection of the signal revealed that the most critical segments of the QRS complex were in V3, between 60%-70% of the cardiac cycle, corresponding to the transition from the R to the S wave, followed by V4 in the same section of the QRS complex. V2 was most significant in the 10%-20% range, which corresponds to the start of the Q wave. Figure 3.4 shows the distribution of relevance across sections for the most influential leads.

These key segments, identified using Gini's coefficient, align closely with those found in the SHAP analysis, as illustrated in Figure 3.5. The beeswarm plot visually displays the most significant features, with the X-axis representing their impact. The amplitude of the SHAP values reflects each feature's relevance, with the sign indicating its direction—negative values correspond to LVOT, and positive values to RVOT. Warm colors signify higher voltages, while cool colors indicate lower voltages.

Leads V2, V3, and V4 remain the most influential, followed by V1 and aVR. The beeswarm plot emphasizes the relationship between low voltage values (blue in Figure 3.5) in the R/S

Figure 3.2: Model score comparison. RF, Random Forest; SVM, Support Vector Machine; MLP, Multilayer Perceptron; ET, Extra Trees; XGB, XGBoost. (A) Models accuracy: * indicates the highest scores, 68% for RF, MLP, and ET in Experiment A, Scenario 1 (A.1). (B) Models macro-average sensitivity comparison: * shows the highest score, 54% for XGB in Experiment A, Scenario 2 (A.2). Using all databases (Scenario 2) achieves better results than using only DS-114 (Scenario 1).

transition section of the QRS complexes in V1, V2, V3, and V4 (50%-80% of the QRS complex) and the initial part of the QRS complex in V2, associated with RVOT origin. In contrast, elevated voltages (orange in Figure 3.4) in these sections are connected to LVOT origin. These trends are also apparent in Figure 3.4, where differences between LVOT and RVOT origin signals are shown. Specifically, in the R/S transition of V1, V2, V3, and V4, LVOT exhibits higher average normalized voltage, as does the initial segment of V2, just before the discernible slope of the R wave.

3.3.2 Experiment B: Training on Clinical Variables and ECG Features

When compared to clinician annotations, the automatic ones matched the same precordial lead only 23.5% of the time. The average shift between leads was 1.37, with an interquartile

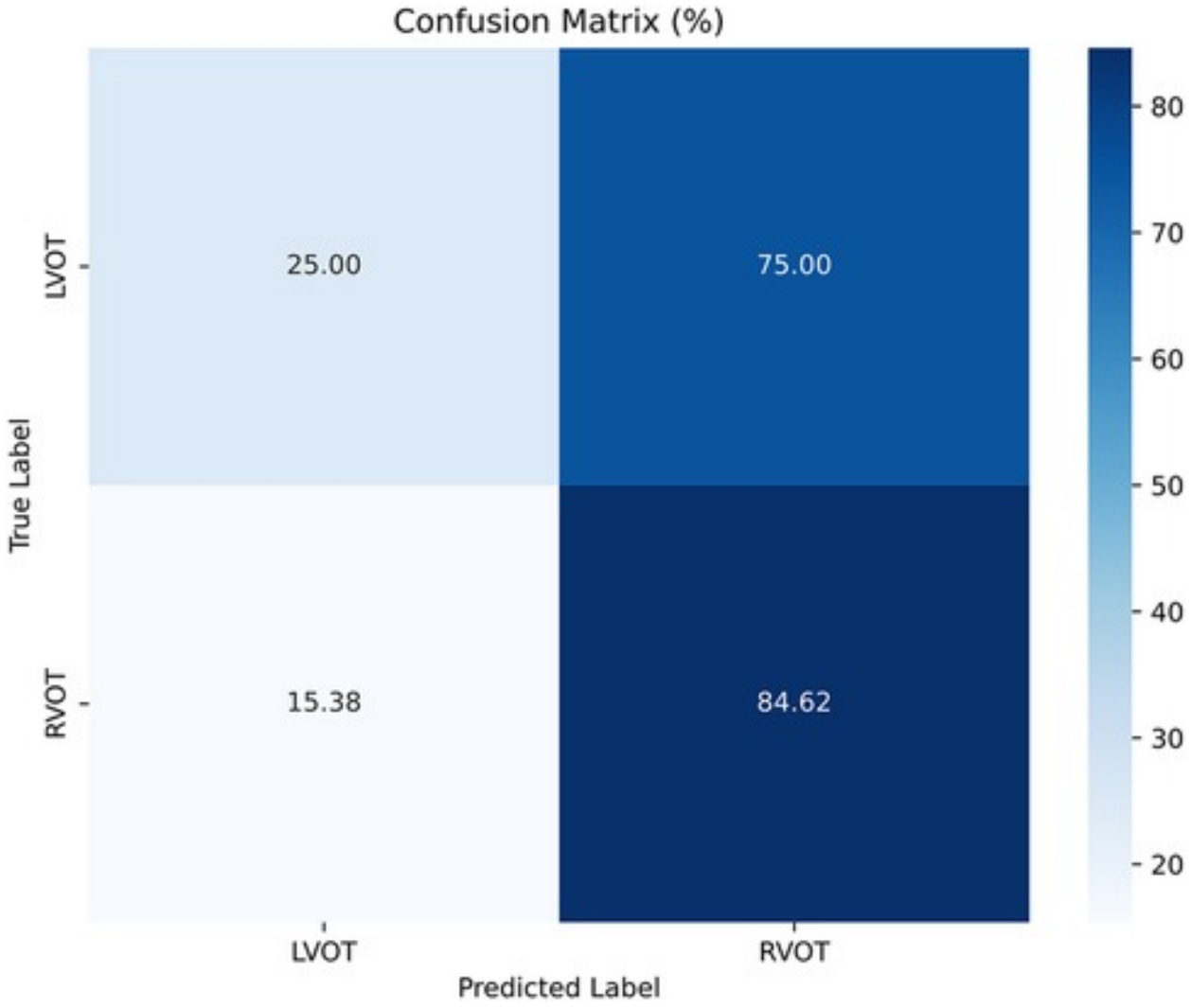

Figure 3.3: Confusion matrix of the model from Experiment A.2 with XGBoost.

range of 1.5 and a median of 1, indicating a typical shift of around one lead (e.g., from V2 to V3 or from V3 to V4), with some instances showing larger deviations. The impact of these shifts is reflected in the model training results.

In contrast to the findings shown in Figure 3.2, the results of the models trained with clinical variables (Figure 3.6) revealed that the top-performing scenario remained the same for both accuracy and macro-average sensitivity metrics. Scenario B.4, which included automatic precordial transition in vector form, sex, hypertension, V3 lead amplitude, and normalized age, achieved an impressive 89% accuracy and 86% macro-average sensitivity (see Figure 3.6). Using Scenario B.1 as a baseline, which only uses the clinical features from Penela et al. [81], performance decreased with the inclusion of the computed transition (Scenario B.2). Furthermore, normalizing age and including V3 lead amplitude (Scenario B.3) did not improve performance. Adding R/S ratio values per lead (Scenarios B.6 and B.7) also

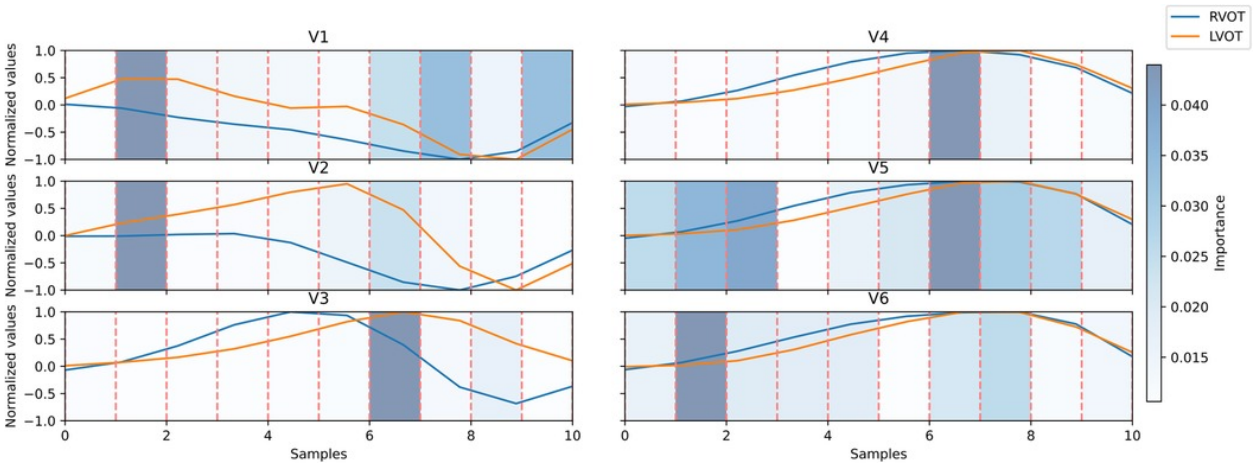

Figure 3.4: Signal comparison between the average QRS complex of RVOT (blue) and LVOT (orange) cases in the precordial leads. The distribution of relevance per section; in blue, scaled in the background, amplitudes normalized per lead. Red dashed lines mark 10% segments of the original signal.

failed to enhance the model's performance. Notably, only Scenarios B.4 (89% accuracy and 86% macro-average sensitivity) and B.5 (87% accuracy and 82% macro-average sensitivity) outperformed B.1 (86% accuracy and 81% macro-average sensitivity). The key distinction between these scenarios is the inclusion of the sinus rhythm transition in B.5. While features from B.1 generally outperform other configurations across all models, models that use the precordial transition for both sinus rhythm and PVC, as well as PVC alone, outperform Scenario B.1.

3.3.3 Experiment C: Training on a Combination of QRS Morphology and Clinical Data

The results of the third set of experiments are presented in Figure 3.7. Notably, the best results mirrored the optimal outcomes from Experiment B, achieving 89% accuracy and 86% macro-average sensitivity. A detailed analysis of the feature relevance in the best model from Experiment C (C.1, which combines the prediction from the best model in Experiment A.2 and the features from the best model in Experiment B.4, including normalized age, sex, hypertension, V3 amplitude, and calculated precordial transition in vector form) using the Gini's coefficient revealed that age and V3 amplitude were the most crucial features. These were closely followed by the prediction from Experiment A.2, with sex ranked further behind. Interestingly, the SHAP analysis (Figure 3.8) suggests that age and sex were the most significant features, followed by the prediction from the QRS model and V3 amplitude.

The similarity in results between Experiment C and Experiment B suggests possible redundancy in the features used by the model. Specifically, there seems to be overlap between

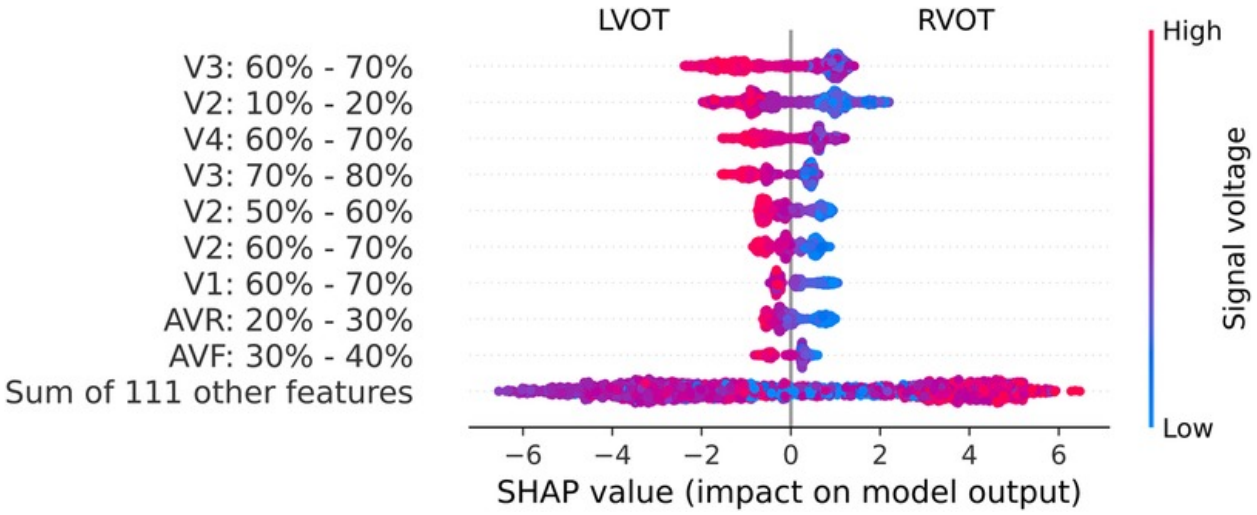

Figure 3.5: Beeswarm plot from SHAP values. The SHAP values (horizontal axis) show how each feature (left column) contributes to the negative (LVOT) or positive (RVOT) outcomes. The color represents the original value of a feature, in this case, mean voltage per QRS complex section (each feature corresponds to 10% sections of the QRS complex per lead). Each dot corresponds to one patient.

the prediction from the best model in Experiment A.2 and the precordial transition vector. To investigate this, we tested a model excluding both features and compared it to two other models that included each feature separately.

We found that adding both features separately resulted in an increase in performance by approximately 4.5 percentage points. This suggests that both the model prediction from Experiment A.2 and the precordial transition vector contribute similarly to the model's performance.

Moreover, when comparing the model without both features to the model from Experiment C, we observed a 4.5 percentage point decrease in classification performance. This further supports the conclusion that both features have a comparable impact on the model.

These findings highlight the importance of accounting for feature redundancy in model development and suggest potential areas for optimization in future iterations.

3.3.4 Experiment D: Unsupervised Clustering of the Site of Origin

The silhouette score identified 25 clusters as the optimal number, revealing the underlying data distribution of DS-114. Figure 3.9 shows the clustering results with refined labels, color-coded based on major region classification (AoC, LVOT, and RVOT). Clusters with similar numbers are closely grouped in the dendrogram, indicating that origins in cluster 20 are nearer to those in cluster 25 than those in cluster 1. The labels were simplified into three categories: top (1-8), mid (9-17), and bottom (18-25). The top category showed few LVOT cases, with most RVOT cases originating from the free wall. The mid category displayed an

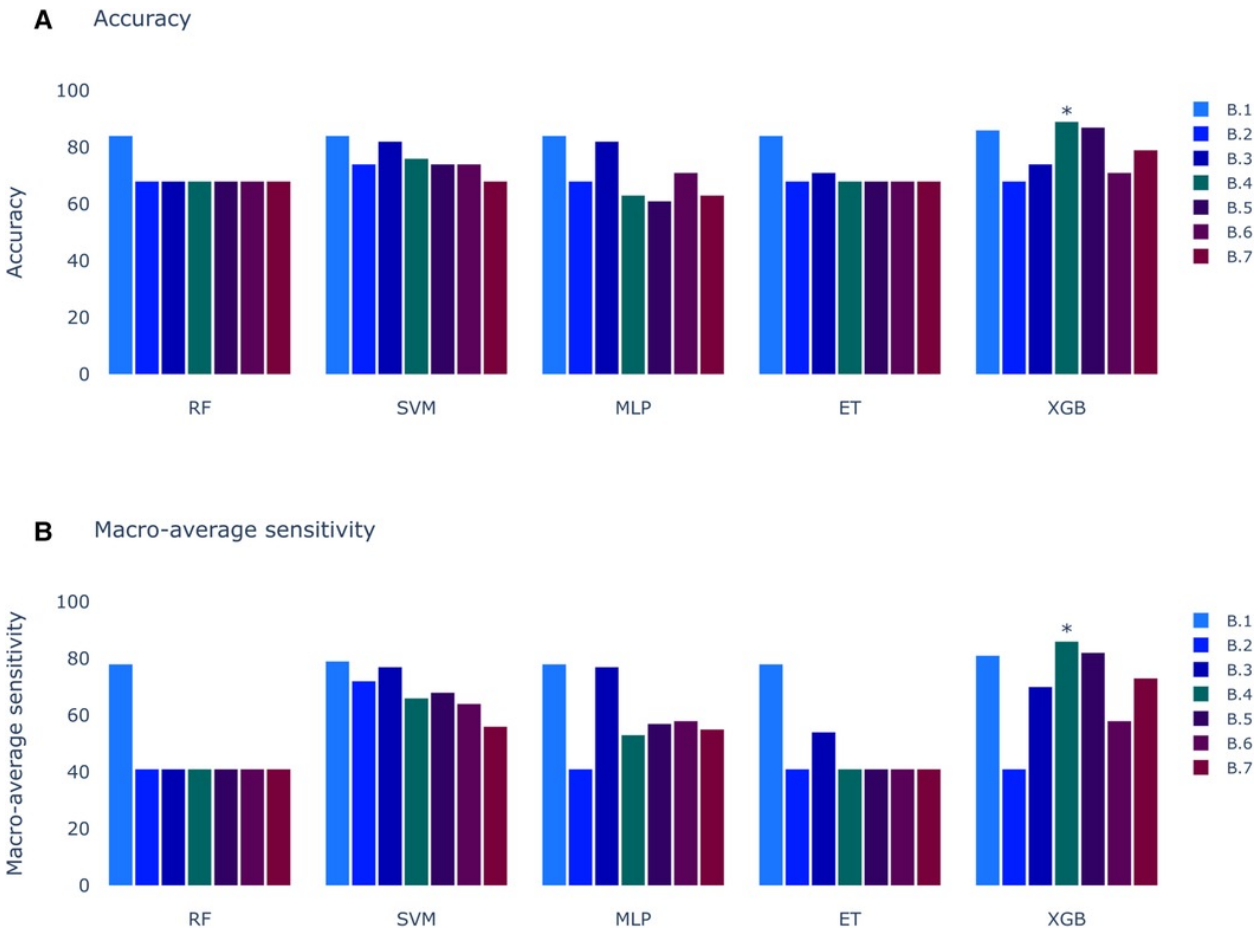

Figure 3.6: Models score comparison. RF, Random Forest; SVM, Support Vector Machine; MLP, Multilayer Perceptron; ET, Extra Trees; XGB, XGBoost. (A) Models accuracy. * indicates the highest scores at 89% in XGB for Experiment B, Scenario 4 (B.4). (B) Models macro-average sensitivity comparison. * shows the highest score at 86% for XGB in Experiment B, Scenario 4 (B.4).

even distribution of RVOT origins from the septum and free wall, with a higher prevalence of aortic cusp cases in clusters with more RVOT septum origins. The bottom section of the heatmap revealed more RVOT septum cases and a decrease in RCC cases, indicating that RCC origins tend to cluster more than other AoC origins, and AoC sites closely align with septal origins. The density distribution of RVOT free wall and septum origins showed greater clustering, with peak densities in certain clusters (1 and 8 for the free wall and 9 and 21 for the septum).

3.4 Discussion

Radiofrequency ablation procedures have become a widely used technique for treating outflow tract ventricular arrhythmias (OTVAs). However, their effectiveness still presents room for improvement, as recurrence rates remain high. A crucial factor in enhancing this procedure

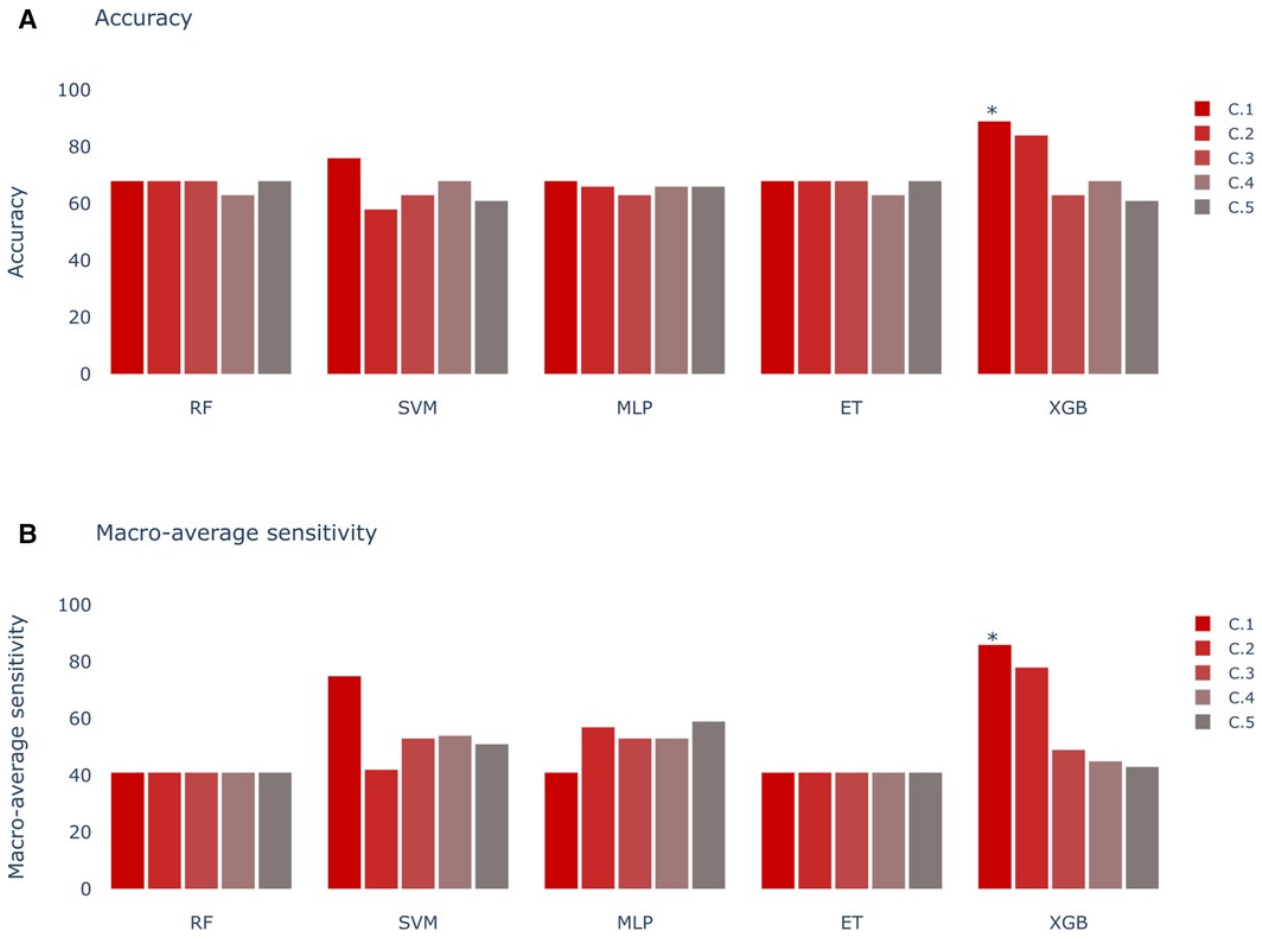

Figure 3.7: Models score comparison. RF, Random Forest; SVM, Support Vector Machine; MLP, Multilayer Perceptron; ET, Extra Trees; XGB, XGBoost. (A) Models accuracy. * indicates the highest scores at 89% in XGB for Experiment C, Scenario 1 (C.1). (B) Models macro-average sensitivity comparison. * shows the highest score at 86% for XGB in Experiment C, Scenario 1 (C.1).

lies in careful planning, particularly the identification of the site of origin (SOO) before the intervention. Several methods exist for SOO determination, including morphological ECG analysis, clinical data assessment, and signal analysis via machine learning (ML).

In clinical practice, optimizing SOO identification significantly enhances efficiency. By reducing the time required for clinicians to locate the SOO, the proposed approach has the potential to streamline patient care and lower procedural risks. Additionally, by integrating multi-center data and considering patient-specific variables such as age and sex, this methodology aims to reduce biases present in current diagnostic criteria, ultimately enabling more personalized treatment strategies. This comprehensive approach not only provides clinicians with actionable insights but also represents a step toward standardizing OTVA diagnosis and treatment across diverse patient populations.

The present study introduces a decision system designed to differentiate between right ventricular outflow tract (RVOT) and left ventricular outflow tract (LVOT) origins, expanding

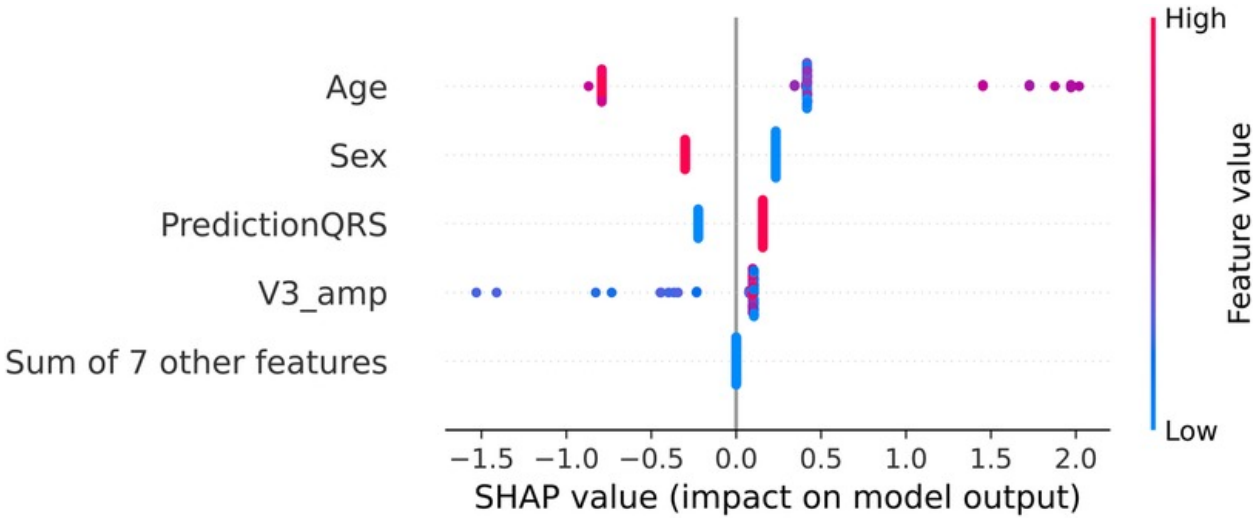

Figure 3.8: SHAP values for the best model in Experiment C (C.1 with XGBoost). The SHAP values (horizontal axis) show how each feature (left column) contributes to the negative (LVOT) or positive (RVOT) outputs. Color is employed to represent the original value of a feature. Each dot corresponds to one patient. Age: age of the patient, red indicates an older patient. Sex: sex of the patient, red indicates male patients. PredictionQRS: Binary prediction from the best model of Experiment A.2, red indicates LVOT prediction. V3_Amp: Amplitude in lead V3, red indicates a higher peak voltage in V3.

upon previous research by Penela et al. [81] and Doste et al. [29]. Their earlier studies leveraged clinical data with visual ECG analysis and simulated multi-center ECG signals, respectively. Our work proposes three approaches utilizing distinct input features.

The first approach (Experiment A), inspired by Doste et al. [29], relies solely on QRS complexes. This method not only facilitates SOO classification but also provides insights into the significance of different QRS complex segments, aiding in understanding the model's decision-making process. Results from Experiment A achieved a peak accuracy of approximately 68%. However, a more detailed analysis, including macro-average sensitivity, highlighted a major limitation: the model predominantly classified all samples as RVOT origin. While this resulted in high accuracy due to the greater prevalence of RVOT cases, it introduced a bias stemming from class imbalance. The best-performing model, XGBoost trained with all databases, attained 61% accuracy and 41% macro-average sensitivity. This discrepancy underscores the importance of macro-average sensitivity as a metric, as models with higher accuracy (e.g., RF, ET, SVM, and MLP) exhibited lower macro-average sensitivity than the top-performing model.

Although our results fall short of the 84%–86% accuracy reported by Doste et al.[29], differences in preprocessing, particularly signal alignment, may account for the variation. Additionally, inconsistencies in data acquisition across databases present standardization challenges. Applying uniformization techniques may help improve accuracy.

SHAP analysis indicated that leads V1–V4 are crucial in the R/S transition segment. Higher voltages in these regions correlated with LVOT origins, likely due to early R/S

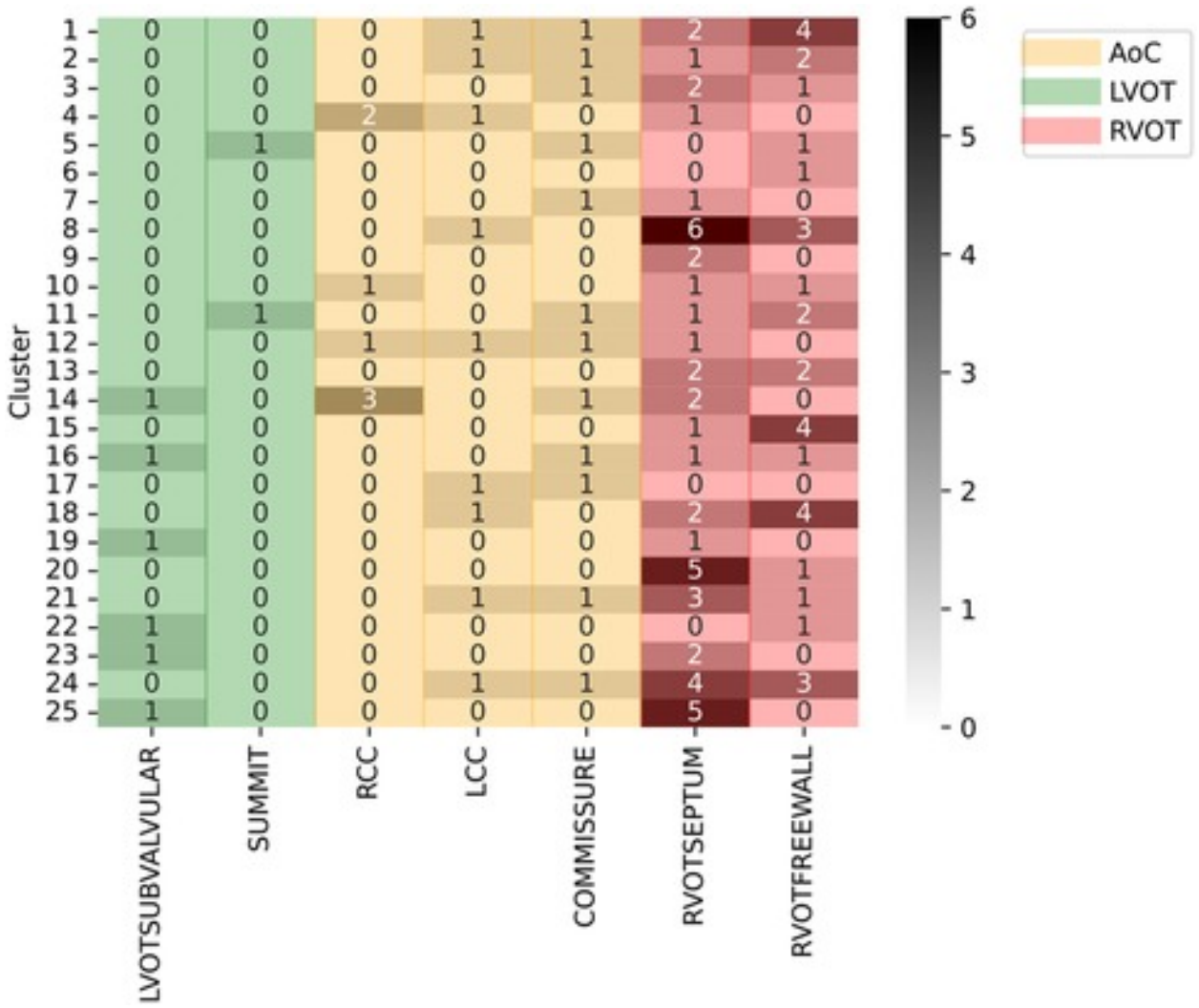

Figure 3.9: Clustering results using 25 clusters. Colors represent major region classification (AoC, LVOT, and RVOT). The dendrogram shows the similarity between clusters with similar numbers.

transitions, where elevated voltages signify a less negative S-wave peak. This aligns with Anderson et al. [1], who identified early precordial transitions as indicative of LVOT origin.

The second approach (Experiment B) integrated clinical variables with select ECG features, as proposed by Penela et al.[81]. To enhance generalization and mitigate overfitting, this approach removed clinician-dependent thresholds and labels. Furthermore, it introduced an algorithm to determine precordial transition based on R/S amplitudes, assigning a unique transition value to each lead. The highest accuracy (89%) and macro-average sensitivity (86%) were observed when binarizing these values and converting them into a zero vector, with a one at the calculated transition point. Comparison with clinician-determined transitions showed agreement in only 23.5% of cases, though discrepancies were often confined to a single lead, suggesting variability in signal selection contributed to the mismatch.

Despite achieving slightly lower accuracy than Penela et al. [81] (89% vs. 94%), our approach eliminates reliance on manual thresholds and subjective decisions, enhancing its robustness across different clinical settings.

The third approach (Experiment C) introduced a novel strategy combining the inference of Experiment A's best model with the most influential features from Experiment B. This iterative process aimed to refine the integration of QRS complex data and clinical variables, enhancing system robustness.

However, Experiment C did not outperform Experiment B, indicating that adding raw QRS complexes did not significantly improve classification. This highlights the complexity of XGBoost, where hyperparameter tuning may inadvertently increase tree complexity, reducing the impact of additional features. SHAP analysis (Figure 3.8) revealed that predictions from Experiment A's best model ranked among the top three most influential features in Experiment C, reinforcing its contribution.

Interestingly, precordial transition and V3 amplitude may be sufficient to differentiate LVOT from RVOT origins. Feature analysis identified age, sex, and binary predictions from Experiment A.2 as the most critical features, with V3 amplitude also playing a key role. The precordial transition vector had reduced importance in this approach, possibly due to redundancy with Experiment A.2's best model. Further testing by removing these features confirmed a similar impact on performance.

Comparison with Penela et al.'s [81] weighted hybrid score showed consistent trends: older male patients with high V3 amplitude were more likely to have LVOT origins. However, SHAP analysis indicated minimal influence from precordial transition, while the Gini coefficient highlighted age and V3 amplitude as the most relevant features. Discrepancies in feature rankings between SHAP and Gini analyses may stem from differences in sample selection—Gini uses training samples, whereas SHAP considers the entire dataset.

An unsupervised approach was employed for specific SOO analysis due to challenges in supervised classification, such as class imbalance and limited cases (e.g., only two summit LVOT cases). This method identified natural clustering patterns, aiding in decomposing the problem into specific SOO classifications. Results suggest that aortic cusp (AoC) origins cluster with septal origins, while right coronary cusp (RCC) origins cluster more consistently than left coronary cusp (LCC) origins, which exhibited greater dispersion.

Free wall and septal origins displayed clearer distinctions, facilitating classification. Although LVOT origins (excluding AoC) lacked clear clustering due to sample limitations, this preliminary analysis suggests a tiered classification approach—first identifying AoC and RVOT, then refining classifications accordingly.

While promising, the developed system has limitations. Preprocessing of QRS complexes

eliminates high-frequency features, restricting pattern identification. Additionally, the dataset exhibits an LVOT underrepresentation, which, despite signal simulations, remains a challenge. Addressing these limitations requires tools capable of processing higher-frequency signals and strategies to counteract data imbalance.

3.5 Conclusions

The proposed method effectively classifies LVOT and RVOT origins by combining signal analysis and clinical data while removing subjective thresholds and manual assessments. This enhances consistency in diagnosis while maintaining interpretability. Future work should focus on expanding feature sets and increasing case numbers to improve generalization. Preliminary findings in SOO classification suggest discernible patterns, paving the way for a refined system capable of identifying specific SOOs with greater precision.

Chapter 4

AI-enabled ECG: single vs 12-lead approach

4.1 Introduction

The 12-lead electrocardiogram (ECG) is an essential tool for diagnosing cardiac abnormalities. Traditionally, its interpretation is performed by trained medical professionals. However, recent advancements in artificial intelligence (AI), particularly deep neural networks [65], have facilitated the accurate analysis of ECGs [112, 52]. In the context of rhythm disorder diagnosis, these AI-driven approaches have demonstrated superior diagnostic accuracy compared to expert cardiologists [53]. Additionally, AI has shown the capability to identify specific patterns and waveform abnormalities in ECGs that may not be visible to the human eye. For instance, it can detect a high likelihood of cardiac contractile dysfunction or past and potential future episodes of atrial fibrillation from an ECG that appears normal and in sinus rhythm [8, 7]. Consequently, AI-driven analysis of the 12-lead ECG holds promise for the rapid and precise identification of ECG abnormalities and the early diagnosis of various cardiac diseases.

The increasing adoption of wearable devices capable of recording single-lead ECGs [58, 61, 32, 115] has created new opportunities for diagnosing cardiac conditions, such as atrial fibrillation. Notably, a precordial smartwatch has been reported to detect signs of myocardial ischemia through a 12-lead ECG and record an episode of ventricular fibrillation [83]. AI-based algorithms have also demonstrated the ability to detect cardiac abnormalities from single-lead ECG recordings. For example, Attia et al. [6] showed that an AI-driven analysis of a smartwatch's single-lead ECG, worn by approximately 2,500 patients, successfully identified a left ventricular ejection fraction (LVEF) of less than 40% in 16 individuals. However, to the best of our knowledge, no comprehensive studies have systematically evaluated the

performance of AI-based algorithms using single-lead ECGs across various cardiac diagnoses.

Moreover, the computational capabilities of battery-powered wearable devices are often constrained, making large deep neural networks impractical for such platforms. This necessitates the development of tailored algorithms for ECG analysis. This study aims to address these challenges through a twofold contribution. First, we introduce a specialized method for detecting cardiac abnormalities using a lightweight convolutional neural network (CNN), in contrast to the complex architectures typically employed for this task. Second, we train our CNN to recognize more than 20 distinct cardiac conditions from the single-lead D1 (and in combination with D2), which are conventionally diagnosed using standard 12-lead ECGs with significantly more complex models. Our findings indicate that for several ECG abnormalities—such as AV block, complete left or right bundle branch block, and lateral myocardial infarction (LMI)—our single-lead lightweight CNN achieves performance levels comparable to those of more sophisticated architectures utilizing full 12-lead ECGs. These results highlight the potential for integrating AI-driven algorithms into wearable devices, enabling large-scale population screening for cardiac diseases, as discussed in the concluding section of this article.

4.2 Methods

4.2.1 The PTB-XL ECG Dataset

The PTB-XL ECG dataset [118, 48] is a publicly available resource comprising 21,837 clinical 12-lead ECG recordings, each 10 seconds long, collected from 18,885 patients (52% male, 48% female, median age: 62 years, interquartile range: 22 years, range: 0–95 years). These ECGs were recorded using the Wilson lead system at a sampling frequency of 500 Hz.

Prediction was formulated as a multi-label classification task [118], based on 20 diagnostic classes illustrated in Figure 4.1. The five macro classes were included only for completeness and were not considered in this study.

The dataset was partitioned into 10 folds. Following Wagner et al. [118], the ninth fold, containing ECGs validated by at least one cardiologist and considered to have the highest label quality, was designated as the validation set, while the tenth fold was used as the test set. The remaining eight folds comprised the training set.

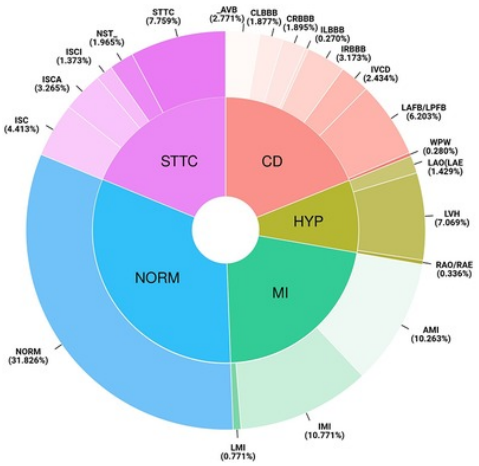

NORM - Normal ECG
ISC_ - Non-specific ischemic
ISCA - Ischemic in anterior leads
ISCI - Ischemic in inferior leads
NST_ - Non-specific ST changes
STTC - ST-T changes
_AVB - AV block
CLBBB - Complete left bundle branch block
CRBBB - Complete right bundle branch block
ILBBB - Incomplete left bundle branch block
IRBBB - Incomplete right bundle branch block
IVCD - Non-specific intraventricular conduction disturbance (block)
LFB/LPFB - Left anterior/left posterior fascicular block
WPW - Wolff-Parkinson-White syndrome
LAO/LAE - Left atrial overload/enlargement
LVH - Left ventricular hypertrophy
RAO/RAE - Right atrial overload/enlargement
AMI - Anterior myocardial infarction
IMI - Inferior myocardial infarction
LMI - Lateral myocardial infarction

Figure 4.1: Distribution of PTB-XL ECG diagnoses, grouped into 20 diagnostic classes and 5 superclasses.

4.2.2 Data Preprocessing

As per existing literature, ECG signals were downsampled to 100 Hz (yielding 1,000 samples per lead per ECG). ECGs were filtered based on the following criteria:

- Conflicting labels (classified both as normal (NORM) and as another diagnostic class).
- Unclassified ECGs (not assigned to any diagnostic class).
- Diagnostic statements with a likelihood of 0%.

This filtering resulted in a final dataset of 21,008 ECGs, with 17,598 used for training, 1,708 for validation, and 1,702 for testing. Each lead was independently normalized using the mean and standard deviation computed from the training set.

Each ECG was structured as a matrix with L rows (representing the number of leads, from 1 to 12) and W columns (length of the ECG, up to 1,000 samples at 100 Hz). The actual number of samples input to the CNN depended on the network's receptive field.

4.2.3 Convolutional Network Architecture

While Strodthoff et al. [113] identified a deep ResNet with 101 layers as the best-performing model, we opted for a simpler CNN with eight convolutional layers to assess performance across varying numbers of input leads (Figure 4.2).

The architecture consists of:

- A preliminary 1×1 convolutional layer for linear transformation over L input leads.

- Six convolution-normalization-pooling blocks, with MaxPooling (1×2) applied along the temporal axis W. The number of feature maps per block was: 16, 16, 32, 32, 64, and 64, with filter sizes of 1×5, 1×5, 1×5, 1×3, 1×3, and 1×3, respectively.
- A final convolutional layer (128 filters, size 1×1) to project features onto a higher-dimensional space.
- An output layer consisting of 20 sigmoid-activated neurons, corresponding to the 20 diagnostic classes.

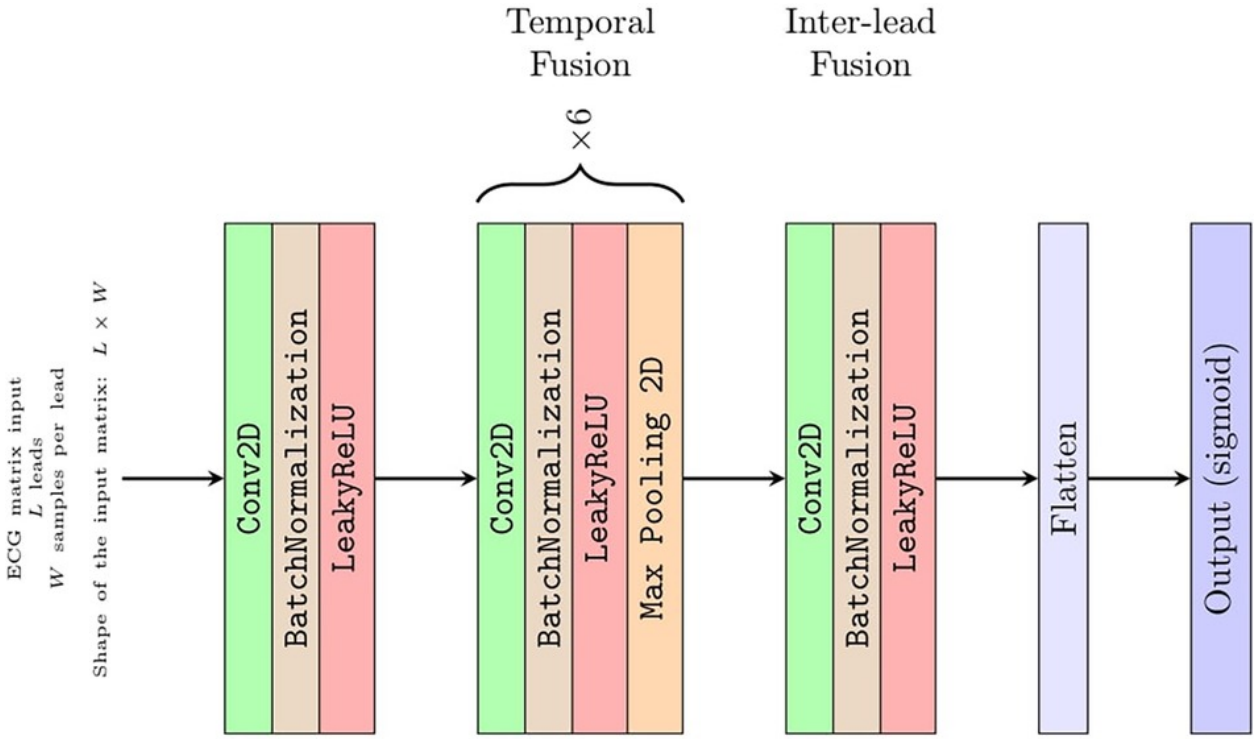

Figure 4.2: Detailed CNN architecture.

The CNN's parameter count depends on the number of input leads (L), ranging from 36,000 parameters for $L = 1$ to 96,000 for $L = 12$.

4.2.4 Data Augmentation

To enhance generalization, training samples were augmented with the following transformations:

- **Gaussian noise**: Added from a zero-mean Gaussian distribution with a standard deviation uniformly drawn from [0.01, 0.1].

- **Time scaling**: ECGs were randomly stretched or compressed by a factor from [0.8, 1.2].
- **Amplitude scaling**: Signals were multiplied by a random factor from [0.7, 1.3].
- **Temporal cropping**: Random 344-sample windows were extracted per ECG, corresponding to the CNN receptive field.

Temporal cropping was applied to both training and test sets, whereas the other augmentations were applied only to training data.

4.2.5 Input Setups

The CNN was designed to accept input matrices of size $L \times W$, where L could be 1 to 12 leads. The network produced a 20-value output vector $y \in (0, 1)$, corresponding to diagnostic classes. We evaluated four input configurations:

- **12-lead ECG**: 12×344 matrix (12 leads, 344 samples each, equivalent to 3.4s at 100 Hz).
- **8 independent leads**: 8×344 matrix (excluding leads derived as linear combinations of others).
- **Single-lead ECG (D1)**: 1×344 matrix.
- **Two-lead ECG (D1 + another lead)**: 2×344 matrix, pairing D1 with another lead.

4.2.6 Training Procedure and Performance Assessment

The CNN was trained to minimize the sum of binary cross-entropies over 20 outputs, using the Adam optimizer [59]. The learning rate linearly decayed from 10^{-2} to 10^{-4} over 200 epochs with a batch size of 32.

Following Wagner et al. [118], results were reported using macro-averaged, threshold-free metrics, particularly the area under the curve (AUC). Sensitivity and specificity were also evaluated using the best threshold from receiver-operating characteristic (ROC) analysis.

To validate model consistency, we additionally tested a fine-tuned version the trained network on the publicly available Georgia and China datasets[48].

4.3 Results

Figure 4.3 provides a summary of the AUC with a 95% confidence interval (CI) (over 50 runs) for the PTB-XL ECG test set, categorized by diagnostic class and inter-class average, for each investigated diagnostic scenario. As a state-of-the-art reference, the table also includes results obtained using the architecture (deep ResNet with 101 layers) proposed by Strodthoff et al. [113].

Classes	D1	D1 + D2	D1 + V1	D1 + V2	D1 + V3	D1 + V4	D1 + V5	D1 + V6	8 leads	12 leads	12 w/o aug	Ref
NORM	89.76 [89.69, 89.83]	93.95 [93.91, 93.99]	92.00 [91.94, 92.06]	91.91 [91.84, 91.98]	92.23 [92.17, 92.29]	92.90 [92.86, 92.94]	93.07 [93.01, 93.13]	92.79 [92.75, 92.83]	96.06 [96.02, 96.10]	**96.07** [96.03, 96.11]	96.06 [95.96, 96.16]	95.2
ISC_	90.73 [90.64, 90.82]	92.96 [92.88, 93.04]	91.81 [91.72, 91.90]	91.68 [91.58, 91.78]	91.64 [91.54, 91.74]	93.46 [93.38, 93.54]	95.18 [95.10, 95.26]	95.57 [95.50, 95.64]	95.28 [95.19, 95.37]	95.40 [95.31, 95.49]	95.10 [94.96, 95.24]	**96.5**
ISCA	87.94 [87.81, 88.07]	87.77 [87.65, 87.89]	89.11 [88.98, 89.24]	88.76 [88.62, 88.90]	89.68 [89.53, 89.83]	89.74 [89.60, 89.88]	89.44 [89.29, 89.59]	88.47 [88.34, 88.60]	91.85 [91.70, 92.00]	91.97 [91.80, 92.14]	90.38 [90.00, 90.76]	**93.4**
ISCI	72.01 [71.37, 72.65]	91.68 [91.40, 91.96]	71.75 [71.17, 72.33]	77.32 [76.75, 77.89]	76.59 [76.04, 77.14]	79.16 [78.64, 79.68]	81.60 [81.16, 82.04]	81.90 [81.42, 82.38]	92.68 [92.40, 92.96]	**93.85** [93.48, 94.22]	90.72 [90.16, 91.28]	91.5
NST_	84.86 [84.59, 85.13]	87.11 [86.86, 87.36]	85.09 [84.82, 85.36]	84.60 [84.29, 84.91]	84.86 [84.64, 85.08]	84.97 [84.71, 85.23]	87.32 [87.07, 87.57]	86.57 [86.30, 86.84]	**88.24** [88.03, 88.45]	88.23 [87.96, 88.50]	86.92 [86.45, 87.39]	86.7
STTC	80.73 [80.58, 80.88]	84.81 [84.69, 84.93]	81.97 [81.84, 82.10]	84.52 [84.38, 84.66]	85.87 [85.76, 85.98]	87.53 [87.42, 87.64]	88.29 [88.19, 88.39]	86.53 [86.43, 86.63]	90.11 [90.00, 90.22]	90.58 [90.48, 90.68]	89.60 [89.45, 89.75]	**91.1**
_AVB	92.50 [92.21, 92.79]	95.20 [95.09, 95.31]	93.27 [93.09, 93.45]	92.97 [92.79, 93.15]	93.21 [93.06, 93.36]	93.18 [92.97, 93.39]	93.59 [93.48, 93.70]	93.60 [93.38, 93.82]	94.24 [94.09, 94.39]	93.73 [93.58, 93.88]	93.75 [93.55, 93.95]	**96.9**
CLBBB	99.56 [99.52, 99.60]	99.67 [99.65, 99.69]	99.75 [99.72, 99.78]	99.76 [99.74, 99.78]	99.68 [99.66, 99.70]	99.65 [99.62, 99.68]	99.72 [99.71, 99.73]	99.71 [99.69, 99.73]	99.56 [99.51, 99.61]	99.52 [99.46, 99.58]	99.20 [99.08, 99.32]	**99.9**
CRBBB	98.94 [98.84, 99.04]	99.34 [99.31, 99.37]	99.69 [99.68, 99.70]	99.58 [99.56, 99.60]	99.22 [99.14, 99.30]	99.16 [99.10, 99.22]	99.24 [99.20, 99.28]	99.16 [99.11, 99.21]	99.58 [99.56, 99.60]	99.56 [99.54, 99.58]	99.60 [99.58, 99.62]	**99.8**
ILBBB	90.48 [89.92, 91.04]	90.74 [90.26, 91.22]	92.07 [91.70, 92.44]	93.07 [92.71, 93.43]	91.18 [90.55, 91.81]	93.39 [92.89, 93.89]	**93.72** [93.22, 94.22]	92.87 [92.13, 93.61]	92.32 [91.73, 92.91]	91.47 [90.87, 92.07]	87.43 [86.34, 88.52]	91.9
IRBBB	73.86 [73.48, 74.24]	79.14 [78.82, 79.46]	96.17 [96.09, 96.25]	91.41 [91.25, 91.57]	76.17 [75.91, 76.43]	75.33 [75.03, 75.63]	76.07 [75.77, 76.37]	79.75 [79.46, 80.04]	95.90 [95.78, 96.02]	96.16 [96.03, 96.29]	95.02 [94.79, 95.25]	**98.0**
IVCD	68.41 [68.10, 68.72]	73.86 [73.57, 74.15]	71.46 [71.17, 71.75]	72.52 [72.24, 72.80]	71.41 [71.14, 71.68]	69.89 [69.62, 70.16]	68.94 [68.60, 69.28]	70.82 [70.51, 71.13]	75.47 [75.23, 75.71]	76.40 [76.03, 76.77]	**78.52** [78.14, 78.90]	74.4
LAFB/ LPFB	79.01 [78.78, 79.24]	97.57 [97.51, 97.63]	83.56 [83.40, 83.72]	80.94 [80.72, 81.16]	81.72 [81.55, 81.89]	85.87 [85.71, 86.03]	89.58 [89.48, 89.68]	90.86 [90.74, 90.98]	97.83 [97.76, 97.90]	**98.20** [98.15, 98.25]	97.67 [97.59, 97.75]	97.5
WPW	86.55 [85.44, 87.66]	84.40 [83.16, 85.64]	90.70 [89.56, 91.84]	84.33 [82.85, 85.81]	85.12 [83.96, 86.28]	84.68 [83.69, 85.67]	83.07 [81.55, 84.59]	83.02 [81.31, 84.73]	92.38 [91.40, 93.36]	**93.36** [92.22, 94.50]	90.26 [88.81, 91.71]	85.5
LAO/LAE	80.60 [80.19, 81.01]	**86.93** [86.57, 87.29]	83.52 [83.08, 83.96]	80.27 [79.74, 80.80]	79.92 [79.55, 80.29]	81.30 [80.83, 81.77]	82.16 [81.70, 82.62]	81.90 [81.44, 82.36]	81.22 [80.59, 81.85]	82.43 [81.75, 83.11]	80.37 [79.64, 81.10]	78.2
LVH	87.97 [87.85, 88.09]	90.77 [90.62, 90.92]	91.42 [91.27, 91.57]	90.92 [90.76, 91.08]	90.98 [90.84, 91.12]	92.06 [91.92, 92.20]	93.23 [93.10, 93.36]	94.08 [93.98, 94.18]	94.44 [94.33, 94.55]	94.24 [94.11, 94.37]	95.10 [94.95, 95.25]	**95.3**
RAO/ RAE	84.93 [84.14, 85.72]	**97.11** [96.83, 97.39]	87.60 [86.83, 88.37]	84.21 [83.34, 85.08]	80.86 [79.63, 82.09]	88.83 [87.83, 89.83]	89.35 [88.56, 90.14]	89.41 [88.62, 90.20]	93.81 [93.15, 94.47]	92.55 [91.83, 93.27]	92.02 [91.01, 93.03]	95.9
AMI	83.18 [83.03, 83.33]	85.67 [85.57, 85.77]	90.29 [90.18, 90.40]	94.94 [94.87, 95.01]	94.16 [94.09, 94.23]	90.17 [90.04, 90.30]	86.26 [86.16, 86.36]	86.35 [86.21, 86.49]	96.70 [96.64, 96.76]	96.72 [96.64, 96.80]	96.21 [96.06, 96.36]	**96.9**
IMI	71.59 [71.23, 71.95]	93.28 [93.16, 93.40]	75.18 [74.96, 75.40]	74.34 [74.06, 74.62]	75.40 [75.18, 75.62]	77.05 [76.78, 77.32]	80.26 [80.04, 80.48]	83.05 [82.84, 83.26]	93.05 [92.93, 93.17]	**95.16** [95.08, 95.24]	95.11 [94.97, 95.25]	94.6
LMI	98.81 [98.58, 99.04]	**99.59** [99.51, 99.67]	98.61 [98.40, 98.82]	99.17 [99.01, 99.33]	99.29 [99.10, 99.48]	99.36 [99.26, 99.46]	99.36 [99.27, 99.45]	99.58 [99.51, 99.65]	98.25 [97.62, 98.88]	99.08 [98.86, 99.30]	95.88 [94.72, 97.04]	91.4
Avg	85.12 [85.00, 85.24]	90.58 [90.50, 90.66]	88.25 [88.16, 88.34]	87.86 [87.76, 87.96]	86.96 [86.86, 87.06]	87.88 [87.80, 87.96]	88.47 [88.36, 88.58]	88.80 [88.68, 88.92]	92.95 [92.85, 93.05]	**93.23** [93.15, 93.31]	92.25 [92.08, 92.42]	93.10

The last column represents the results of the best architecture proposed by Strodthoff et al. (15). The AUCs are reported as percentages. The bold numbers correspond to the best performer for each class. The underlined numbers correspond to the competitive results.

Figure 4.3: Summary of average AUC with 95% CI (over 50 runs) for the considered scenarios. The last column represents the results of the best architecture proposed by Strodthoff et al.[113]. The AUCs are reported as percentages. The bold numbers correspond to the best performer for each class. The underlined numbers correspond to the competitive results.

Table 4.1 and Table 4.2 reports sensitivity and specificity were also evaluated using the best threshold from receiver-operating characteristic (ROC) analysis.

Table 4.1: Average sensitivity computed on the test set of the PTB-XL dataset (over 50 runs).

Classes	D1	D1+D2	D1+V1	D1+V2	D1+V3	D1+V4	D1+V5	D1+V6	8 leads	12 leads	12 w/o aug
NORM	90.37	93.79	90.31	90.28	91.77	92.81	92.22	91.98	93.55	93.74	93.25
STTC	78.34	83.75	78.42	82.25	83.80	83.10	85.35	85.43	84.40	86.32	85.52
AMI	80.96	81.03	86.36	90.88	88.34	83.92	84.71	84.98	92.91	93.06	91.82
IMI	70.97	88.61	76.85	73.87	73.79	74.79	76.74	76.21	88.71	90.95	91.15
LAFB/LPFB	70.44	94.94	78.63	73.59	75.94	79.01	81.18	82.21	95.26	95.30	93.99
IRBBB	62.91	70.76	92.21	86.19	68.14	69.07	69.50	75.32	91.61	91.83	90.16
LVH	82.46	84.02	84.55	84.53	83.45	83.92	87.58	88.73	89.78	88.73	91.19
CLBBB	95.89	96.04	96.52	96.59	97.04	96.74	97.04	96.19	96.11	95.70	96.00
NST_	87.22	88.47	88.04	88.75	86.12	84.75	83.41	84.67	87.69	88.35	87.29
ISCA	86.80	86.08	87.15	90.61	91.84	91.15	85.87	83.68	92.00	91.01	88.75
CRBBB	95.59	96.59	98.15	97.30	95.63	96.11	96.56	96.22	98.00	98.00	97.70
IVCD	60.12	64.51	58.15	64.42	59.01	59.43	58.06	57.91	61.82	59.85	69.70
ISC_	81.17	87.95	84.92	85.24	86.04	89.08	90.99	91.06	90.04	90.30	90.14
_AVB	91.37	93.12	90.76	92.37	91.98	92.02	93.00	93.22	93.17	92.34	90.83
ISCI	78.96	88.59	74.52	76.15	81.11	79.56	71.19	73.78	88.37	89.33	83.70
WPW	69.43	65.71	69.43	61.43	65.71	68.00	65.14	64.00	73.71	76.00	73.43
LAO/LAE	81.26	89.63	85.19	82.81	83.56	83.63	80.81	80.37	78.74	81.33	75.33
ILBBB	75.00	75.00	74.50	75.25	70.75	75.75	76.00	75.50	75.00	73.75	69.50
RAO/RAE	69.25	85.50	77.75	73.00	63.75	73.50	73.75	75.25	80.75	74.00	78.50
LMI	66.67	66.67	66.67	66.67	66.67	66.67	66.67	66.67	66.67	66.67	66.00
Average	78.76	84.04	81.95	81.61	80.22	81.15	80.79	81.17	85.91	85.83	85.20

Table 4.2: Average specificity computed on the test set of the PTB-XL dataset (over 50 runs).

Classes	D1	D1+D2	D1+V1	D1+V2	D1+V3	D1+V4	D1+V5	D1+V6	8 leads	12 leads	12 w/o aug
NORM	76.37	82.18	79.97	80.30	80.30	80.48	81.05	80.90	87.17	87.69	87.22
STTC	70.58	71.06	71.60	72.74	72.87	77.22	76.56	73.51	80.55	79.11	78.51
AMI	73.36	77.36	80.31	86.63	88.08	81.92	73.00	75.09	87.93	88.18	88.11
IMI	63.59	85.12	63.23	65.02	67.40	68.41	71.38	75.61	84.27	86.90	86.37
LAFB/LPFB	75.09	92.33	74.72	75.00	73.14	78.15	82.98	85.82	92.40	91.55	91.34
IRBBB	74.94	73.66	89.90	81.35	72.15	71.10	70.79	70.74	90.79	90.30	88.74
LVH	82.83	81.39	85.30	83.03	85.42	87.13	84.64	86.56	85.50	86.50	86.38
CLBBB	97.24	98.60	98.58	98.32	97.06	97.17	97.40	98.79	98.95	98.58	98.21
NST_	70.17	73.02	68.59	69.48	70.34	71.69	77.37	75.09	76.84	76.24	75.90
ISCA	77.75	79.54	78.38	75.75	77.27	77.84	79.49	79.45	80.15	81.55	79.52
CRBBB	96.20	97.31	98.55	97.52	97.12	96.65	96.53	97.04	98.28	98.20	98.03
IVCD	68.76	74.01	79.48	73.90	75.03	72.55	73.22	75.78	81.25	83.48	74.82
ISC_	87.24	85.45	85.86	83.77	83.49	85.79	88.39	89.08	89.23	88.77	88.52
_AVB	81.19	85.31	82.84	81.54	81.92	82.12	82.50	82.05	83.09	82.52	83.58
ISCI	56.93	79.74	62.43	66.53	64.70	68.14	79.64	74.53	82.46	85.05	83.70
WPW	93.32	91.06	91.26	91.21	92.60	90.68	90.96	88.52	88.91	89.55	86.87
LAO/LAE	70.46	71.81	70.54	66.70	65.70	69.38	72.73	70.93	71.19	71.33	73.16
ILBBB	94.51	94.70	93.68	93.50	91.37	93.42	93.41	91.18	89.27	90.19	85.20
RAO/RAE	81.96	90.22	79.09	79.16	85.75	86.29	86.03	82.37	86.07	89.48	85.39
LMI	97.54	99.23	97.41	98.40	98.53	98.74	98.78	99.18	96.23	98.08	91.88
Average	79.50	84.15	81.59	80.99	81.01	81.74	82.84	82.61	86.53	87.16	85.57

4.3.1 Standard (12-lead) Setup

The standard 12-lead setup achieved an average AUC of 93.2% across 20 diagnostic classes. When the data augmentation strategy was excluded during CNN training, performance declined by 1.1%.

4.3.2 Independent (Eight-lead) Setup

The eight-lead setup (leads D1, D2, V1, V2, V3, V4, V5, and V6) did not result in a significant performance loss compared to the 12-lead setup. The average percentage difference across the 20 diagnostic classes was -0.3%. Since the four omitted leads (D3, aVR, aVL, aVF) are linear combinations of D1 and D2, this result suggests that they provide redundant information, while also contributing to computational overhead (96,000 vs. 56,000 parameters in the 12- and 8-lead setups, respectively).

4.3.3 Single-lead (D1) Setup

Using only the D1 lead resulted in an average accuracy reduction of -8.7% compared to the 12-lead setup. Certain diagnostic classes showed a notable performance drop, exceeding 20% for inferior myocardial infarction (IMI), inferior myocardial ischemia (ISCI), and incomplete right bundle branch block (IRBBB). Conversely, several other classes, including non-specific ischemic changes (ISC_), ischemic changes in anterior leads (ISCA), non-specific ST changes (NST_), AV block (_AVB), complete left bundle branch block (CLBBB), complete right bundle branch block (CRBBB), incomplete left bundle branch block (ILBBB), left atrial overload/enlargement (LAO/LAE), and LMI, exhibited a performance decline of less than 5%, with the accuracy reduction being below 1% for CLBBB, CRBBB, and LMI.

The upper panel of Figure 4.4 illustrates the performance comparison between single-lead and standard 12-lead setups.

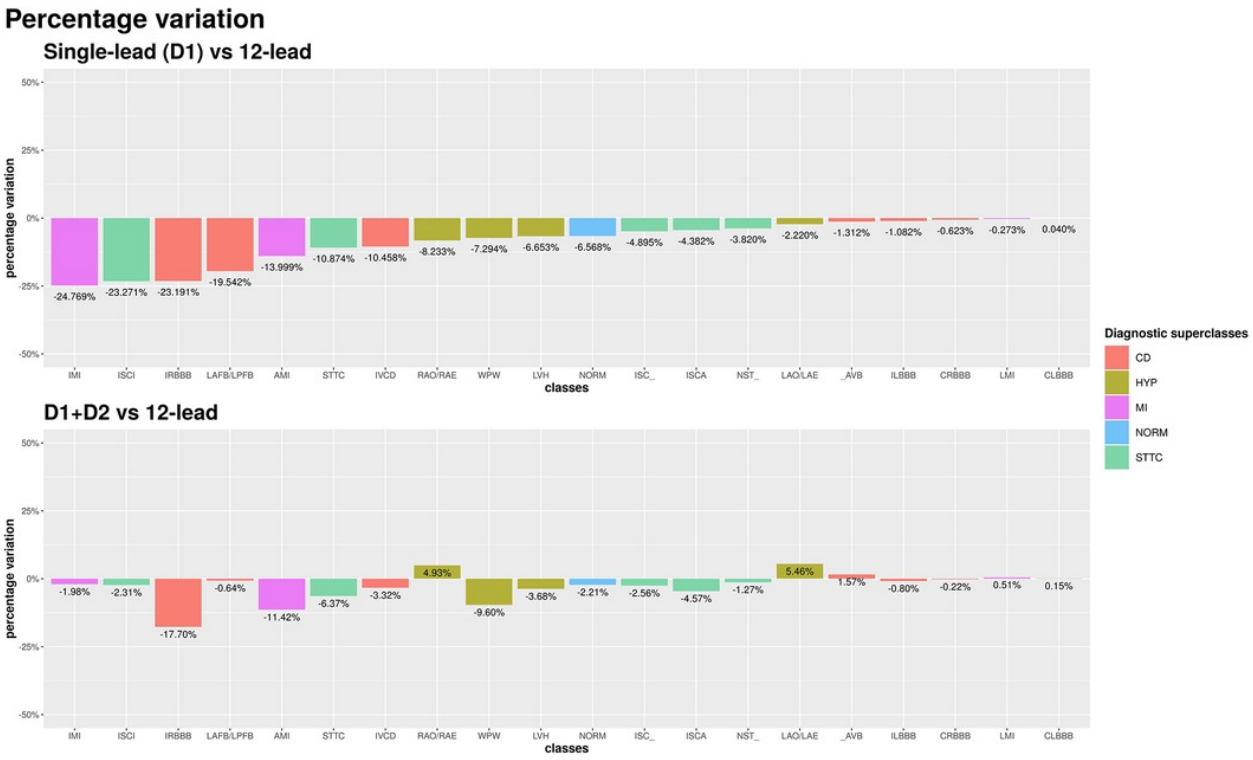

Figure 4.4: AUC percentage variation between single-lead (D1) and 12-lead setups (top), and between D1+D2 and 12-lead setups (bottom). Percentage differences are relative to the 12-lead setup.

4.3.4 Two-lead Setup

Among all leads, D2 yielded the greatest improvement in average AUC when combined with the single D1-lead setup. The two-lead setup achieved an average AUC of 90.6% across 20 diagnostic classes, corresponding to an average percentage difference of -2.8% compared to the standard 12-lead setup (90.6% vs. 93.2%).

Adding a second lead was particularly beneficial for diagnostic classes where the single-lead setup performed poorly. In the IMI and SCI classes, the accuracy loss compared to the standard 12-lead ECG was reduced from over 20% (single-lead) to below 2% (two-lead setup). The lower panel of Figure 4.4 presents a performance comparison of two-lead versus standard 12-lead setups.

Interestingly, for right atrial overload/enlargement (RAO/RAE) and left atrial overload/enlargement (LAO/LAE), the two-lead setup outperformed the 12-lead configuration by +4.9% and +5.5%, respectively. However, for anterior myocardial infarction (excluding anterolateral cases), the two-lead setup resulted in a 10% lower accuracy than the 12-lead setup. The addition of V2, which captures information from a different spatial axis, reduced this diagnostic loss to below 2%.

4.3.5 Validation on an External Dataset

To enhance the robustness of our findings, we fine-tuned the trained network on two external, publicly available datasets—the Georgia and China datasets [48]. The observed drops in average AUC on these test datasets align with our findings on the PTB-XL dataset, as reported in Table 4.3 and in Table 4.4.

Table 4.3: Average AUCs on Georgia test set (over 10 runs). Legend: 1st degree AV Block (IAVB), Atrial Fibrillation (AF), Atrial Flutter (AFL), Complete Right Bundle Branch Block (CRBBB), Incomplete Right Bundle Branch Block (IRBBB), Left Anterior Fascicular Block (LAnFB), Left Axis Deviation (LAD), Left Bundle Branch Block (LBBB), Low QRS Voltages (LQRSV), NonSpecific IntraVentricular Conduction disorder (NSIVCB), Premature Atrial Contraction (PAC), proLonged QT interval (LQT), Qwave Abnormalities (QAb), Right Axis Deviation (RAD), Sinus Arrhythmia (SA), Sinus Bradycardia (SB), SiNus Rhythm (SNR), Sinus Tachycardia (STach), T wave abnormalities (Tab), T wave Inversion (TInv), Ventricular Premature Beats (VPB).

Classes	D1	D1 + D2	12 Leads
IAVB	93.81	95.30	94.84
AF	86.24	89.42	89.35
AFL	81.47	83.09	85.21
CRBBB	95.67	96.34	97.61
IRBBB	81.36	87.15	95.22
LAnFB	74.64	96.82	96.33
LAD	71.17	96.61	96.31
LBBB	98.97	98.83	98.78
LQRSV	79.77	87.97	93.73
NSIVCB	75.58	80.22	87.62
PAC	63.2	64.83	66.46
LQT	77.96	80.02	85.25
QAb	71.60	79.49	86.47
RAD	91.02	92.53	96.17
SA	68.56	71.40	68.48
SB	96.37	96.81	96.96
SNR	87.12	89.66	91.66
STach	97.68	97.66	97.54
TAb	80.92	84.97	88.37
TInv	65.35	68.07	67.85
VPB	76.41	78.33	80.20
Average	81.66	86.45	88.59

Table 4.4: Average AUCs on China test set (over 10 runs). Legend: 1st degree AV Block (IAVB), Atrial Fibrillation (AF), Atrial Flutter (AFL), Complete Right Bundle Branch Block (CRBBB), Incomplete Right Bundle Branch Block (IRBBB), Left Bundle Branch Block (LBBB), Premature Atrial Contraction (PAC), Sinus Arrhythmia (SA), Sinus Bradycardia (SB), SiNus Rhythm (SNR), Sinus Tachycardia (STach), T wave Abnormal (TAb).

Classes	D1	D1 + D2	12 Leads
IAVB	71.79	86.19	91.09
AF	85.74	94.99	95.82
AFL	70.07	60.87	74.94
CRBBB	91.98	95.93	98.32
IRBBB	71.15	80.24	90.40
LBBB	47.63	64.11	61.34
PAC	62.89	62.98	66.66
SA	90.11	79.08	76.86
SB	59.97	74.65	78.57
SNR	79.66	74.03	86.12
STach	91.75	94.21	95.60
TAb	33.99	43.00	60.46
Average	71.39	75.86	81.35

4.4 Discussion

This study analyzed over 20,000 ECGs across 20 different abnormalities, confirming the accuracy of a lightweight deep learning algorithm based on CNN, even with a highly simplified architecture. Additionally, it significantly enhances our understanding of AI-based ECG diagnostics. Figure 4.5 presents a graphical summary of the key findings.

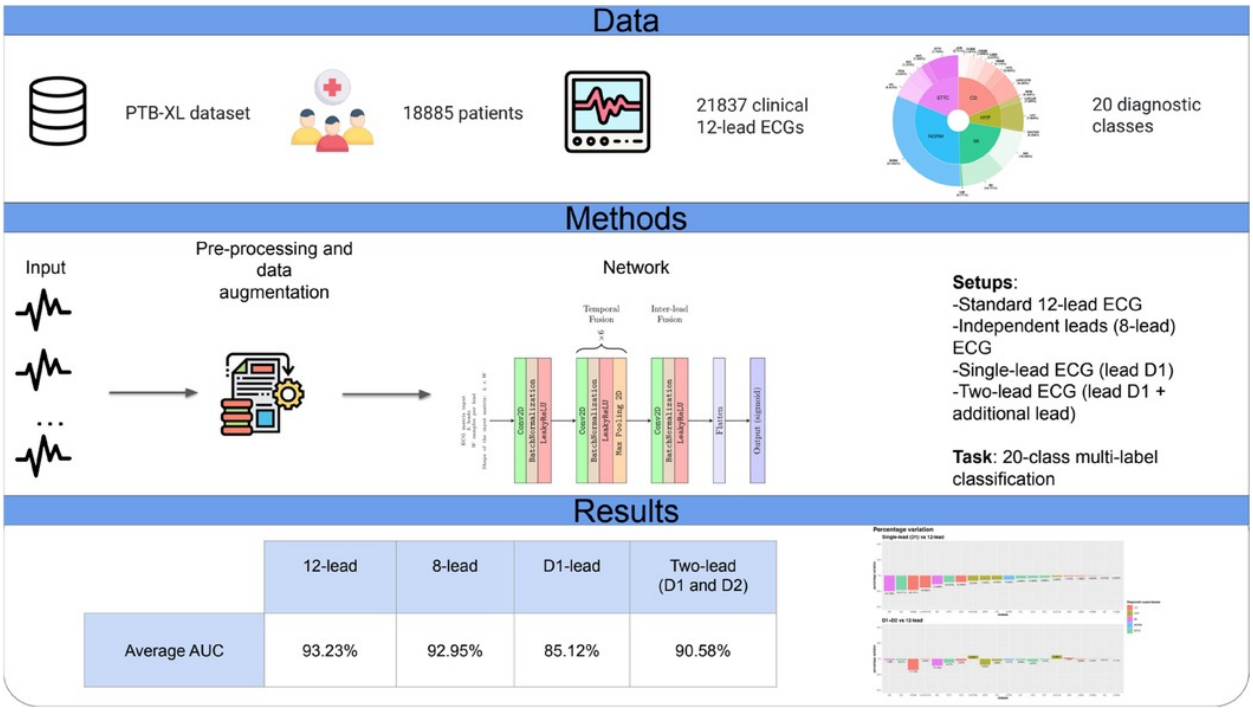

	12-lead	8-lead	D1-lead	Two-lead (D1 and D2)
Average AUC	93.23%	92.95%	85.12%	90.58%

Figure 4.5: Graphical summary of the study.

A key finding of this research is that analyzing the D1 lead using the same CNN approach yielded an accuracy only slightly lower than that of the full 12-lead setup. For several ECG abnormalities, such as AV block, complete left or right bundle branch block, and LMI, the diagnostic performance of the single-lead approach closely matched that of the standard 12-lead configuration.

The inclusion of a second lead (D2) further minimized the performance gap with the 12-lead ECG setup. On average, the highest AUC for a two-lead setup was achieved with the D1+D2 combination. The addition of this second spatial axis in the analysis of cardiac electrical activity reduced the diagnostic gap by 64% (from a relative percentage difference of -7.8% to -2.8%). Notably, this setup significantly improved the accuracy of detecting inferior wall myocardial ischemia and infarction, conditions that are difficult to diagnose with only the D1 lead. Furthermore, in certain cases, such as the detection of right and left atrial enlargement, the two-lead setup outperformed the 12-lead configuration, likely because it prioritized the most informative lead (D2) while avoiding less relevant ones that could introduce noise. Conversely, for the detection of anterior wall myocardial ischemia and infarction, the D1+V2 setup proved superior to D1+D2, as the spatial orientation of V2 better captures abnormalities in these conditions.

From an architectural perspective, the relatively lightweight neural network used in this study (36,000–96,000 trainable parameters) achieved results comparable to those of signifi-

cantly more complex architectures [e.g., Attia et al.[8] with 300,000 parameters; Strodthoff et al.[113] with 3.5 million parameters]. Notably, our CNN model in the 12-lead setup outperformed the more complex ResNet architecture by Strodthoff et al. for the same multi-label classification task (AUC: 0.932 vs. 0.931; see Figure 4.3). This high level of performance is attributed to the tailored neural network design and extensive data augmentation, marking a substantial advancement over previous studies.

4.5 Conclusions

The AI-enabled ECG analysis based on the single D1 lead demonstrated strong predictive performance for cardiac abnormalities, with only a minor reduction in AUC compared to the 12-lead ECG. Incorporating D2 further mitigated this performance gap. These findings suggest that AI-driven single or two-lead ECG analysis could be sufficient for detecting cardiac abnormalities traditionally diagnosed using a 12-lead ECG.

Given the simplicity of this approach, it paves the way for broader applications, particularly in wearable devices. Many smartwatches already record a D1-like lead (via a left wrist placement and right index finger contact), and a D2-like lead can be obtained by moving the watch to the left lower abdomen while maintaining right finger contact. Although precordial leads could also be captured, their recording process is more cumbersome.

Recent work by Attia et al.[6] successfully adapted a deep neural network originally trained on 12-lead ECGs for single-lead wearable ECGs. However, our study is based entirely on standard 12-lead ECG leads rather than wearable-derived single-lead recordings. Translating these findings to wearable devices presents unique challenges, such as increased impedance in dry electrodes, amplified sampling noise, and attenuated signal amplitude when worn on peripheral body locations. Robust noise filtering techniques and computational efficiency considerations will be crucial for successful implementation in wearable technology. Further research is warranted to address these challenges from both medical and engineering perspectives.

Chapter 5

Conclusions

Summary of the Research Journey

This thesis has explored the evolving landscape of Artificial Intelligence (AI) in clinical and interventional electrophysiology, presenting a series of three papers that chronicle a progressive journey from traditional machine learning approaches to advanced deep learning techniques. The first two papers investigated the application of machine learning algorithms in risk stratification and clinical decision support, demonstrating the feasibility and utility of structured data-driven models. The final paper embraced the capabilities of deep learning, focusing on end-to-end neural networks for complex pattern recognition within electrocardiographic signals. This progression underscores the increasing sophistication of AI tools and their transformative potential in electrophysiology.

The Promise of AI in Electrophysiology

AI holds the promise of revolutionizing the field of arrhythmology by enabling more precise diagnostics, personalized therapy, and streamlined clinical workflows. In particular, the ability of AI algorithms to identify subtle patterns within large datasets—such as electrocardiograms (ECGs), imaging data, and clinical parameters—can greatly enhance diagnostic accuracy, risk prediction, and procedural planning. Furthermore, AI can serve as a valuable decision-support tool in interventional settings, augmenting the electrophysiologist's capabilities in real-time and improving patient outcomes.

The research presented in this thesis highlights several domains where AI can make significant contributions: from automated ECG analysis and arrhythmia detection to procedural planning for catheter ablation and device implantation. The deployment of AI-driven tools

in these contexts can promote consistency, reduce operator variability, and optimize the use of healthcare resources.

Current Limitations and Challenges

Despite the promising results, the adoption of AI in electrophysiology is not without challenges. Several barriers must be addressed to ensure the safe, effective, and equitable implementation of these technologies:

- **Regulatory and Ethical Concerns:** The development of AI-based clinical tools must align with stringent regulatory frameworks to ensure patient safety and data integrity. Regulatory agencies are still adapting to the rapid pace of innovation, often resulting in a lag between technological readiness and clinical deployment.
- **Explainability and Trust:** Clinicians need to understand the rationale behind AI-driven recommendations. The "black-box" nature of many AI models, particularly deep learning architectures, can hinder trust and adoption. Enhancing explainability through interpretable AI methods is critical to bridge this gap.
- **External Validation:** Many AI models are developed using data from single centers or homogeneous populations. Generalizability requires rigorous external validation in diverse, multinational cohorts to ensure robustness across different healthcare systems and patient demographics.
- **Data Quality and Availability:** A significant proportion of ECG data is still paper-based and not digitally archived, limiting the availability of large, high-quality datasets required for AI training and validation. Digitization efforts, alongside standardized data formats, are essential to unlock the full potential of AI.

Future Perspectives

The field of AI in clinical electrophysiology is poised for substantial growth. In the coming years, we anticipate a transition from proof-of-concept models to clinically validated tools integrated within electronic health records and procedural platforms. The combination of multimodal data sources—such as ECGs, imaging, genomics, and real-time electrophysiological signals—will enable the development of comprehensive, patient-specific models that support truly personalized arrhythmia management.

Interdisciplinary collaboration will be fundamental in driving these advancements. Clinicians, data scientists, engineers, and regulatory bodies must work in concert to design, evaluate, and implement AI systems that are safe, effective, and ethically sound. The incorporation of federated learning and privacy-preserving techniques may further promote data sharing and model development across institutions without compromising patient confidentiality.

In conclusion, the research presented in this thesis represents a step forward in the integration of AI into clinical and interventional arrhythmology. While challenges remain, the trajectory of innovation is clear. With continued effort, AI has the potential to become an indispensable ally in the fight against cardiac arrhythmias, transforming the landscape of electrophysiology for the benefit of patients and clinicians alike.

Bibliography

[1] Robert D Anderson, Saurabh Kumar, Ramanathan Parameswaran, Geoffrey Wong, Aleksandr Voskoboinik, Hariharan Sugumar, Troy Watts, Paul B Sparks, Joseph B Morton, Alex McLellan, et al. Differentiating right-and left-sided outflow tract ventricular arrhythmias: classical ecg signatures and prediction algorithms. *Circulation: Arrhythmia and Electrophysiology*, 12(6):e007392, 2019.

[2] Filippo Angelini, Pier Paolo Bocchino, Mattia Peyracchia, Andrea Saglietto, Massimo Magnano, Nicolo Patane, Fabrizio D'Ascenzo, Carla Giustetto, Matteo Anselmino, Fiorenzo Gaita, et al. Prevalence and predictors of left atrial thrombosis in atrial fibrillation patients treated with non-vitamin k antagonist oral anticoagulants. *Acta Cardiologica*, 78(3):290–297, 2023.

[3] Matteo Anselmino, Stefania Scarsoglio, Luca Ridolfi, Gaetano Maria De Ferrari, and Andrea Saglietto. Insights from computational modeling on the potential hemodynamic effects of sinus rhythm versus atrial fibrillation. *Frontiers in Cardiovascular Medicine*, 9:844275, 2022.

[4] Elena Arbelo, Josep Brugada, Carina Blomström-Lundqvist, Cecile Laroche, Josef Kautzner, Evgeny Pokushalov, Pekka Raatikainen, Michael Efremidis, Gerhard Hindricks, Alberto Barrera, et al. Contemporary management of patients undergoing atrial fibrillation ablation: in-hospital and 1-year follow-up findings from the esc-ehra atrial fibrillation ablation long-term registry. *European heart journal*, 38(17):1303–1316, 2017.

[5] Federico M Asch, Nicolas Poilvert, Theodore Abraham, Madeline Jankowski, Jayne Cleve, Michael Adams, Nathanael Romano, Ha Hong, Victor Mor-Avi, Randolph P Martin, et al. Automated echocardiographic quantification of left ventricular ejection fraction without volume measurements using a machine learning algorithm mimicking a human expert. *Circulation: Cardiovascular Imaging*, 12(9):e009303, 2019.

[6] Zachi I Attia, David M Harmon, Jennifer Dugan, Lukas Manka, Francisco Lopez-Jimenez, Amir Lerman, Konstantinos C Siontis, Peter A Noseworthy, Xiaoxi Yao,

Eric W Klavetter, et al. Prospective evaluation of smartwatch-enabled detection of left ventricular dysfunction. *Nature medicine*, 28(12):2497–2503, 2022.

[7] Zachi I Attia, Suraj Kapa, Francisco Lopez-Jimenez, Paul M McKie, Dorothy J Ladewig, Gaurav Satam, Patricia A Pellikka, Maurice Enriquez-Sarano, Peter A Noseworthy, Thomas M Munger, et al. Screening for cardiac contractile dysfunction using an artificial intelligence–enabled electrocardiogram. *Nature medicine*, 25(1):70–74, 2019.

[8] Zachi I Attia, Peter A Noseworthy, Francisco Lopez-Jimenez, Samuel J Asirvatham, Abhishek J Deshmukh, Bernard J Gersh, Rickey E Carter, Xiaoxi Yao, Alejandro A Rabinstein, Brad J Erickson, et al. An artificial intelligence-enabled ecg algorithm for the identification of patients with atrial fibrillation during sinus rhythm: a retrospective analysis of outcome prediction. *The Lancet*, 394(10201):861–867, 2019.

[9] Ethan M Balk, Ann C Garlitski, ALAWI A ALSHEIKH-ALI, Teruhiko Terasawa, Mei Chung, and Stanley Ip. Predictors of atrial fibrillation recurrence after radiofrequency catheter ablation: a systematic review. *Journal of cardiovascular electrophysiology*, 21(11):1208–1216, 2010.

[10] Andrea Ballatore, Marco Gatti, Serena Mella, Davide Tore, Henri Xhakupi, Fabio Giorgino, Andrea Saglietto, Ludovica Carmagnola, Edoardo Roagna, Gaetano Maria De Ferrari, et al. Epicardial atrial fat at cardiac magnetic resonance imaging and af recurrence after transcatheter ablation. *Journal of Cardiovascular Development and Disease*, 11(5):137, 2024.

[11] Luca Barca, Giuseppe Mascia, Michel Haissaguerre, Cinzia Monaco, Henri Xhakupi, Luca Carmisciano, Andrea Saglietto, Carla Giustetto, Paolo Di Donna, Elena Arbelo, et al. Incidence of spontaneous brugada ecg during follow-up in patients with drug-inducible pattern: a systematic review and meta-analysis. *Heart Rhythm*, 2025.

[12] Brian P Betensky, Robert E Park, Francis E Marchlinski, Matthew D Hutchinson, Fermin C Garcia, Sanjay Dixit, David J Callans, Joshua M Cooper, Rupa Bala, David Lin, et al. The v2 transition ratio: a new electrocardiographic criterion for distinguishing left from right ventricular outflow tract tachycardia origin. *Journal of the American College of Cardiology*, 57(22):2255–2262, 2011.

[13] Christopher M Bishop and Nasser M Nasrabadi. *Pattern recognition and machine learning*, volume 4. Springer, 2006.

[14] Álvaro J Bocanegra-Pérez, Gemma Piella, Rafael Sebastian, Guillermo Jimenez-Perez, Giulio Falasconi, Andrea Saglietto, David Soto-Iglesias, Antonio Berruezo, Diego Penela, and Oscar Camara. Automatic and interpretable prediction of the site of origin in outflow tract ventricular arrhythmias: machine learning integrating electrocardiograms and clinical data. *Frontiers in Cardiovascular Medicine*, 11:1353096, 2024.

[15] Paolo Boretto, Neal Hitesh Patel, Keval Patel, Mannat Rana, Andrea Saglietto, Manas Soni, Mahmood Ahmad, Jamie Sin Ying Ho, Ovidio De Filippo, Rui Andre Providencia, et al. Prognosis prediction in cardiac amyloidosis by cardiac magnetic resonance imaging: a systematic review with meta-analysis. *European Heart Journal Open*, 3(5):oead092, 2023.

[16] Pierangelo Calvelli, Natascia Cerrato, Carla Giustetto, Andrea Saglietto, Matteo Anselmino, and Antonio Curcio. Which brugada patient deserves continuous ecg monitoring through implantable loop recorder? an evidence update. *Journal of Cardiovascular Medicine*, 26(2):64–71, 2025.

[17] A John Camm, GY Lip, Raffaele De Caterina, Irene Savelieva, Dan Atar, Stefan H Hohnloser, Gerhard Hindricks, and Paulus Kirchhof. 2012 focused update of the esc guidelines for the management of atrial fibrillation. *an update of the 2010 ESC Guidelines for the management of atrial fibrillation–developed with the special contribution of the European Heart Rhythm Association*, 14:1385–1413, 2013.

[18] Daniela Canova, Silvestro Roatta, Andrea Saglietto, Stefania Scarsoglio, Nefer Roberta Gianotto, Alessandro Piccotti, Gaetano Maria De Ferrari, Luca Ridolfi, and Matteo Anselmino. A quantitative assessment of cerebral hemodynamic perturbations associated with long rr intervals in atrial fibrillation: A pilot-case-based experience. *Medicina*, 60(4):531, 2024.

[19] Elena Cavarretta, Luigi Sciarra, Giuseppe Biondi-Zoccai, Francesco Maffessanti, Antonia Nigro, Fabio Sperandii, Emanuele Guerra, Federico Quaranta, Chiara Fossati, Mariangela Peruzzi, et al. Age-related electrocardiographic characteristics of male junior soccer athletes. *Frontiers in cardiovascular medicine*, 8:784170, 2022.

[20] Lidia Ceriani and Paolo Verme. The origins of the gini index: extracts from variabilità e mutabilità (1912) by corrado gini. *The Journal of Economic Inequality*, 10:421–443, 2012.

[21] Tianqi Chen and Carlos Guestrin. Xgboost: A scalable tree boosting system. In *Proceedings of the 22nd acm sigkdd international conference on knowledge discovery and data mining*, pages 785–794, 2016.

[22] Filippo Crea. Prediction of sudden death in the era of personalized medicine. *European Heart Journal*, 42(17):1641–1644, 2021.

[23] Fabrizio D'ascenzo, F Angelini, F Piroli, PP Bocchino, L Baldetti, F Melillo, A Chieffo, A Saglietto, P Omedè, A Montefusco, et al. Duration and kind of dual antiplatelet therapy for acute coronary syndrome patients: a network meta-analysis. *Minerva Cardiology and Angiology*, 71(5):494–503, 2022.

[24] Fabrizio D'Ascenzo, A Corleto, Giuseppe Biondi-Zoccai, Matteo Anselmino, F Ferraris, Luigi di Biase, A Natale, RJ Hunter, RJ Schilling, S Miyazaki, et al. Which are the most reliable predictors of recurrence of atrial fibrillation after transcatheter ablation?: a meta-analysis. *International journal of cardiology*, 167(5):1984–1989, 2013.

[25] Fabrizio D'Ascenzo, Ovidio De Filippo, Guglielmo Gallone, Gianluca Mittone, Marco Agostino Deriu, Mario Iannaccone, Albert Ariza-Solé, Christoph Liebetrau, Sergio Manzano-Fernández, Giorgio Quadri, et al. Machine learning-based prediction of adverse events following an acute coronary syndrome (praise): a modelling study of pooled datasets. *The Lancet*, 397(10270):199–207, 2021.

[26] Ovidio De Filippo, Victoria L Cammann, Corrado Pancotti, Davide Di Vece, Angelo Silverio, Victor Schweiger, David Niederseer, Konrad A Szawan, Michael Würdinger, Iva Koleva, et al. Machine learning-based prediction of in-hospital death for patients with takotsubo syndrome: The intertak-ml model. *European journal of heart failure*, 25(12):2299–2311, 2023.

[27] Ovidio De Filippo, Raffaele Mineo, Michele Millesimo, Wojciech Wańha, Federica Proietto Salanitri, Antonio Greco, Antonio Maria Leone, Luca Franchin, Simone Palazzo, Giorgio Quadri, et al. Non-invasive physiological assessment of intermediate coronary stenoses from plain angiography through artificial intelligence: the starflow system. *European Heart Journal-Quality of Care and Clinical Outcomes*, page qcae024, 2024.

[28] Ovidio De Filippo, Francesco Piroli, Francesco Bruno, Pier Paolo Bocchino, Andrea Saglietto, Luca Franchin, Filippo Angelini, Guglielmo Gallone, Giulia Rizzello, Mahmood Ahmad, et al. De-escalation of dual antiplatelet therapy for patients with acute

coronary syndrome after percutaneous coronary intervention: a systematic review and network meta-analysis. *BMJ Evidence-Based Medicine*, 29(3):171–186, 2024.

[29] Ruben Doste, Miguel Lozano, Guillermo Jimenez-Perez, Lluis Mont, Antonio Berruezo, Diego Penela, Oscar Camara, and Rafael Sebastian. Training machine learning models with synthetic data improves the prediction of ventricular origin in outflow tract ventricular arrhythmias. *Frontiers in Physiology*, 13:909372, 2022.

[30] Ruben Doste, Rafael Sebastian, Juan Francisco Gomez, David Soto-Iglesias, Alejandro Alcaine, Lluis Mont, Antonio Berruezo, Diego Penela, and Oscar Camara. In silico pace-mapping: prediction of left vs. right outflow tract origin in idiopathic ventricular arrhythmias with patient-specific electrophysiological simulations. *EP Europace*, 22(9):1419–1430, 2020.

[31] Janine Dretzke, Naomi Chuchu, Ridhi Agarwal, Clare Herd, Winnie Chua, Larissa Fabritz, Susan Bayliss, Dipak Kotecha, Jonathan J Deeks, Paulus Kirchhof, et al. Predicting recurrent atrial fibrillation after catheter ablation: a systematic review of prognostic models. *EP Europace*, 22(5):748–760, 2020.

[32] David Duncker and Emma Svennberg. wearable devices for cardiac rhythm monitoring, 2022.

[33] Veronica Dusi, Filippo Angelini, Enrico Baldi, Antonio Toscano, Carol Gravinese, Simone Frea, Sara Compagnoni, Arianna Morena, Andrea Saglietto, Eleonora Balzani, et al. Continuous stellate ganglion block for ventricular arrhythmias: case series, systematic review, and differences from thoracic epidural anaesthesia. *Europace*, 26(4):euae074, 2024.

[34] Michael Efremidis, Konstantinos Vlachos, Maria Kyriakopoulou, Panagiotis Mililis, Claire A Martin, George Bazoukis, Stylianos Dragasis, Athanasia Megarisiotou, Philippe Unger, Antonio Frontera, et al. The rv1-v3 transition ratio: A novel electrocardiographic criterion for the differentiation of right versus left outflow tract premature ventricular complexes. *Heart Rhythm O2*, 2(5):521–528, 2021.

[35] Giulio Falasconi, Diego Penela, David Soto-Iglesias, Pietro Francia, Andrea Saglietto, José Alderete, Daniel Viveros, Aldo Bellido, Fatima Zaraket, Julio Martí-Almor, et al. Cardiac magnetic resonance-aided epicardial ventricular tachycardia ablation in post-myocarditis patient. *Journal of Interventional Cardiac Electrophysiology*, 67(2):249–251, 2024.

[36] Giulio Falasconi, Diego Penela, David Soto-Iglesias, Pietro Francia, Cheryl Teres, Andrea Saglietto, Beatriz Jauregui, Daniel Viveros, Aldo Bellido, Jose Alderete, et al. Personalized pulmonary vein antrum isolation guided by left atrial wall thickness for persistent atrial fibrillation. *Europace*, 25(5):euad118, 2023.

[37] Gaia Filiberti, Giulia Antonelli, Giulio Falasconi, Alessandro Villaschi, Stefano Figliozzi, Martina Maria Ruffo, Antonio Taormina, Guido Del Monaco, Alessia Chiara Latini, Sebastiano Carli, et al. The use of cardiac imaging in patients undergoing atrial fibrillation ablation. *Journal of Interventional Cardiac Electrophysiology*, pages 1–20, 2025.

[38] Pietro Francia, Giulio Falasconi, Diego Penela, Daniel Viveros, José Alderete, Andrea Saglietto, Aldo Francisco Bellido, Julio Martí-Almor, Paula Franco-Ocaña, David Soto-Iglesias, et al. Scar architecture affects the electrophysiological characteristics of induced ventricular arrhythmias in hypertrophic cardiomyopathy. *Europace*, 26(3):euae050, 2024.

[39] Pietro Francia, Daniel Viveros, Giulio Falasconi, Diego Penela, David Soto-Iglesias, Julio Martí-Almor, José Alderete, Andrea Saglietto, Aldo Francisco Bellido, Paula Franco-Ocaña, et al. Clinical impact of aging on outcomes of cardioneuroablation for reflex syncope or functional bradycardia: results from the cardioneuroablation: patient selection, image integration and outcomes—the elegance multicenter study. *Heart Rhythm*, 20(9):1279–1286, 2023.

[40] Pietro Francia, Daniel Viveros, Carlo Gigante, Giulio Falasconi, Diego Penela, David Soto-Iglesias, Federico Landra, Lucio Teresi, Julio Marti-Almor, José Alderete, et al. Differential and synergistic effects of right and left atrial ganglionated plexi ablation in patients undergoing cardioneuroablation: results from the elegance multicenter study. *Journal of Interventional Cardiac Electrophysiology*, pages 1–8, 2024.

[41] Fiorenzo Gaita, Natascia Cerrato, Carla Giustetto, Annamaria Martino, Laura Bergamasco, Michele Millesimo, Lorella Barbonaglia, Paula Carvalho, Domenico Caponi, Andrea Saglietto, et al. Asymptomatic patients with brugada ecg pattern: long-term prognosis from a large prospective study. *Circulation*, 148(20):1543–1555, 2023.

[42] Fiorenzo Gaita, Natascia Cerrato, Andrea Saglietto, Domenico Caponi, Leonardo Calò, and Carla Giustetto. The brugada syndrome: risk stratification. *European Heart Journal Supplements*, 25(Supplement_C):C27–C31, 2023.

[43] Fiorenzo Gaita, Marco Scaglione, Alberto Battaglia, Mario Matta, Cristina Gallo, Michela Galata, Domenico Caponi, Paolo Di Donna, and Matteo Anselmino. Very

long-term outcome following transcatheter ablation of atrial fibrillation. are results maintained after 10 years of follow up? *Ep Europace*, 20(3):443–450, 2018.

[44] Anand N Ganesan, Nicholas J Shipp, Anthony G Brooks, Pawel Kuklik, Dennis H Lau, Han S Lim, Thomas Sullivan, Kurt C Roberts-Thomson, and Prashanthan Sanders. Long-term outcomes of catheter ablation of atrial fibrillation: a systematic review and meta-analysis. *Journal of the American Heart Association*, 2(2):e004549, 2013.

[45] Giuseppe Giannino, Valentina Braia, Carola Griffith Brookles, Federico Giacobbe, Fabrizio D'Ascenzo, Filippo Angelini, Andrea Saglietto, Gaetano Maria De Ferrari, and Veronica Dusi. The intrinsic cardiac nervous system: from pathophysiology to therapeutic implications. *Biology*, 13(2):105, 2024.

[46] Giuseppe Giannino, Lorenzo Nocera, Maria Andolfatto, Valentina Braia, Federico Giacobbe, Francesco Bruno, Andrea Saglietto, Filippo Angelini, Ovidio De Filippo, Fabrizio D'Ascenzo, et al. Vagal nerve stimulation in myocardial ischemia/reperfusion injury: from bench to bedside. *Bioelectronic Medicine*, 10(1):22, 2024.

[47] Simrat K Gill, Andreas Karwath, Hae-Won Uh, Victor Roth Cardoso, Zhujie Gu, Andrey Barsky, Luke Slater, Animesh Acharjee, Jinming Duan, Lorenzo Dall'Olio, et al. Artificial intelligence to enhance clinical value across the spectrum of cardiovascular healthcare. *European Heart Journal*, 44(9):713–725, 2023.

[48] Ary L Goldberger, Luis AN Amaral, Leon Glass, Jeffrey M Hausdorff, Plamen Ch Ivanov, Roger G Mark, Joseph E Mietus, George B Moody, Chung-Kang Peng, and H Eugene Stanley. Physiobank, physiotoolkit, and physionet: components of a new research resource for complex physiologic signals. *circulation*, 101(23):e215–e220, 2000.

[49] Ian Goodfellow. *Deep learning*, volume 196. MIT press, 2016.

[50] Awni Y Hannun, Pranav Rajpurkar, Masoumeh Haghpanahi, Geoffrey H Tison, Codie Bourn, Mintu P Turakhia, and Andrew Y Ng. Cardiologist-level arrhythmia detection and classification in ambulatory electrocardiograms using a deep neural network. *Nature medicine*, 25(1):65–69, 2019.

[51] Charlotte J Haug and Jeffrey M Drazen. Artificial intelligence and machine learning in clinical medicine, 2023. *New England Journal of Medicine*, 388(13):1201–1208, 2023.

[52] Shenda Hong, Yuxi Zhou, Junyuan Shang, Cao Xiao, and Jimeng Sun. Opportunities and challenges of deep learning methods for electrocardiogram data: A systematic review. *Computers in biology and medicine*, 122:103801, 2020.

[53] Yu-Chang Huang, Yu-Chun Hsu, Zhi-Yong Liu, Ching-Heng Lin, Richard Tsai, Jung-Sheng Chen, Po-Cheng Chang, Hao-Tien Liu, Wen-Chen Lee, Hung-Ta Wo, et al. Artificial intelligence-enabled electrocardiographic screening for left ventricular systolic dysfunction and mortality risk prediction. *Frontiers in Cardiovascular Medicine*, 10:1070641, 2023.

[54] Affirm Investigators. Relationships between sinus rhythm, treatment, and survival in the atrial fibrillation follow-up investigation of rhythm management (affirm) study. *Circulation*, 109(12):1509–1513, 2004.

[55] ZY Jiao, YB Li, J Mao, XY Liu, XC Yang, C Tan, JM Chu, and XP Liu. Differentiating origins of outflow tract ventricular arrhythmias: a comparison of three different electrocardiographic algorithms. *Brazilian Journal of Medical and Biological Research*, 49(5):e5206, 2016.

[56] Guillermo Jimenez-Perez, Alejandro Alcaine, and Oscar Camara. Delineation of the electrocardiogram with a mixed-quality-annotations dataset using convolutional neural networks. *Scientific reports*, 11(1):863, 2021.

[57] Rajesh Kabra, Sharat Israni, Bharat Vijay, Chaitanya Baru, Raghuveer Mendu, Mark Fellman, Arun Sridhar, Pamela Mason, Jim W Cheung, Luigi DiBiase, et al. Emerging role of artificial intelligence in cardiac electrophysiology. *Cardiovascular Digital Health Journal*, 3(6):263–275, 2022.

[58] Paola Kamga, Rasik Mostafa, and Saba Zafar. The use of wearable ecg devices in the clinical setting: a review. *Current emergency and hospital medicine reports*, 10(3):67–72, 2022.

[59] Diederik P Kingma and Jimmy Ba. Adam: A method for stochastic optimization. *arXiv preprint arXiv:1412.6980*, 2014.

[60] Paulus Kirchhof, A John Camm, Andreas Goette, Axel Brandes, Lars Eckardt, Arif Elvan, Thomas Fetsch, Isabelle C van Gelder, Doreen Haase, Laurent M Haegeli, et al. Early rhythm-control therapy in patients with atrial fibrillation. *New England Journal of Medicine*, 383(14):1305–1316, 2020.

[61] Maarten A Koole, Dirkjan Kauw, Kirsten M Kooiman, Joris R de Groot, Danielle Robbers-Visser, Igor I Tulevski, Barbara J Mulder, Berto J Bouma, and Mark J Schuuring. An implantable loop recorder or smartphone based single-lead electrocardiogram to

detect arrhythmia in adults with congenital heart disease? *Frontiers in cardiovascular medicine*, 9:1099014, 2023.

[62] Jelena Kornej, Gerhard Hindricks, M Benjamin Shoemaker, Daniela Husser, Arash Arya, Philipp Sommer, Sascha Rolf, Pablo Saavedra, Arvindh Kanagasundram, S Patrick Whalen, et al. The apple score: a novel and simple score for the prediction of rhythm outcomes after catheter ablation of atrial fibrillation. *Clinical Research in Cardiology*, 104:871–876, 2015.

[63] Karl-Heinz Kuck, Josep Brugada, Alexander Fürnkranz, Andreas Metzner, Feifan Ouyang, KR Julian Chun, Arif Elvan, Thomas Arentz, Kurt Bestehorn, Stuart J Pocock, et al. Cryoballoon or radiofrequency ablation for paroxysmal atrial fibrillation. *New England Journal of Medicine*, 374(23):2235–2245, 2016.

[64] Federico Landra, Andrea Saglietto, Giulio Falasconi, Diego Penela, David Soto-Iglesias, Emanuele Curti, Bruno Tonello, Lucio Teresi, Dario Turturiello, Paula Franco-Ocaña, et al. Left atrial intramyocardial fat at pulmonary vein reconnection sites during atrial fibrillation redo ablation. *Europace*, 27(2):euaf038, 2025.

[65] Yann LeCun, Yoshua Bengio, and Geoffrey Hinton. Deep learning. *nature*, 521(7553):436–444, 2015.

[66] Solam Lee, Yuseong Chu, Jiseung Ryu, Young Jun Park, Sejung Yang, and Sang Baek Koh. Artificial intelligence for detection of cardiovascular-related diseases from wearable devices: a systematic review and meta-analysis. *Yonsei medical journal*, 63(Suppl):S93, 2022.

[67] Bruce B Lerman. Mechanism, diagnosis, and treatment of outflow tract tachycardia. *Nature Reviews Cardiology*, 12(10):597–608, 2015.

[68] Scott M Lundberg and Su-In Lee. A unified approach to interpreting model predictions. *Advances in neural information processing systems*, 30, 2017.

[69] Thomas F Lüscher, Florian A Wenzl, Fabrizio D'Ascenzo, Paul A Friedman, and Charalambos Antoniades. Artificial intelligence in cardiovascular medicine: clinical applications. *European heart journal*, 45(40):4291–4304, 2024.

[70] Marco V Mariani, Agostino Piro, Domenico G Della Rocca, Giovanni B Forleo, Naga Venkata Pothineni, Jorge Romero, Luigi Di Biase, Francesco Fedele, and Carlo

Lavalle. Electrocardiographic criteria for differentiating left from right idiopathic outflow tract ventricular arrhythmias. *Arrhythmia & Electrophysiology Review*, 10(1):10, 2021.

[71] Nassir F Marrouche, Johannes Brachmann, Dietrich Andresen, Jürgen Siebels, Lucas Boersma, Luc Jordaens, Béla Merkely, Evgeny Pokushalov, Prashanthan Sanders, Jochen Proff, et al. Catheter ablation for atrial fibrillation with heart failure. *New England Journal of Medicine*, 378(5):417–427, 2018.

[72] Tom M Mitchell and Tom M Mitchell. *Machine learning*, volume 1. McGraw-hill New York, 1997.

[73] Daniel Müllner. Modern hierarchical, agglomerative clustering algorithms. *arXiv preprint arXiv:1109.2378*, 2011.

[74] Venkat D Nagarajan, Su-Lin Lee, Jan-Lukas Robertus, Christoph A Nienaber, Natalia A Trayanova, and Sabine Ernst. Artificial intelligence in the diagnosis and management of arrhythmias. *European heart journal*, 42(38):3904–3916, 2021.

[75] Peter A Noseworthy, Zachi I Attia, Emma M Behnken, Rachel E Giblon, Katherine A Bews, Sijia Liu, Tara A Gosse, Zachery D Linn, Yihong Deng, Jun Yin, et al. Artificial intelligence-guided screening for atrial fibrillation using electrocardiogram during sinus rhythm: a prospective non-randomised interventional trial. *The Lancet*, 400(10359):1206–1212, 2022.

[76] Douglas L Packer, Daniel B Mark, Richard A Robb, Kristi H Monahan, Tristram D Bahnson, Jeanne E Poole, Peter A Noseworthy, Yves D Rosenberg, Neal Jeffries, L Brent Mitchell, et al. Effect of catheter ablation vs antiarrhythmic drug therapy on mortality, stroke, bleeding, and cardiac arrest among patients with atrial fibrillation: the cabana randomized clinical trial. *Jama*, 321(13):1261–1274, 2019.

[77] Stefano Palermi, Marco Vecchiato, Fu Siong Ng, Zachi Attia, Youngjin Cho, Matteo Anselmino, Gaetano Maria De Ferrari, Andrea Saglietto, Arunashis Sau, I-Min Chiu, et al. Artificial intelligence and the electrocardiogram: A modern renaissance. *European Journal of Internal Medicine*, 2025.

[78] Stefano Palermi, Marco Vecchiato, Andrea Saglietto, David Niederseer, David Oxborough, Sandra Ortega-Martorell, Ivan Olier, Silvia Castelletti, Aaron Baggish, Francesco Maffessanti, et al. Unlocking the potential of artificial intelligence in sports cardiology:

does it have a role in evaluating athlete's heart? *European Journal of Preventive Cardiology*, 31(4):470–482, 2024.

[79] Maria Concetta Pastore, Mariangela Vigna, Andrea Saglietto, Maria Alma Iuliano, Giulia Elena Mandoli, Andrea Stefanini, Chiara Carrucola, Laura Fusini, Luna Cavigli, Flavio D'ascenzi, et al. Prognostic value of left atrial strain in acute and chronic heart failure: A meta-analysis. *ESC Heart Failure*, 2025.

[80] Fabian Pedregosa, Gaël Varoquaux, Alexandre Gramfort, Vincent Michel, Bertrand Thirion, Olivier Grisel, Mathieu Blondel, Peter Prettenhofer, Ron Weiss, Vincent Dubourg, et al. Scikit-learn: Machine learning in python. *the Journal of machine Learning research*, 12:2825–2830, 2011.

[81] Diego Penela, Giulio Falasconi, Jose Miguel Carreño, David Soto-Iglesias, Juan Fernández-Armenta, Juan Acosta, Julio Martí-Almor, Begoña Benito, Aldo Bellido, Alfredo Chauca, et al. A hybrid clinical and electrocardiographic score to predict the origin of outflow tract ventricular arrhythmias. *Journal of Interventional Cardiac Electrophysiology*, 66(8):1877–1888, 2023.

[82] Diego Penela, Giulio Falasconi, David Soto-Iglesias, Juan Fernández-Armenta, Giulio Zucchelli, Felipe Bisbal, Fatima Zaraket, Etelvino Silva, Matteo Parollo, Alessia Chiara Latini, et al. Outcomes of ventricular tachycardia ablation facilitated by pre-procedural cardiac imaging-derived scar characterization: a prospective multi-centre international registry. *Europace*, 27(4):euaf051, 2025.

[83] Andrés Provencio and Miguel Ángel Cobos Gil. Smartwatch electrocardiogram records st depression, premature ventricular complexes, and ventricular fibrillation. *The Lancet*, 400(10364):e12, 2022.

[84] Vincenzo Randazzo, Silvia Caligari, Eros Pasero, Carla Giustetto, Andrea Saglietto, William Bertarello, Amir Averbuch, Mira Marcus-Kalish, Valery Zheludev, and Fiorenzo Gaita. A vision transformer model for the prediction of fatal arrhythmic events in patients with brugada syndrome. *Sensors*, 25(3):824, 2025.

[85] Andrea Saglietto, Daniele Baccega, Roberto Esposito, Matteo Anselmino, Veronica Dusi, Attilio Fiandrotti, and Gaetano Maria De Ferrari. Convolutional neural network (cnn)-enabled electrocardiogram (ecg) analysis: a comparison between standard twelve-lead and single-lead setups. *Frontiers in Cardiovascular Medicine*, 11:1327179, 2024.

[86] Andrea Saglietto, Andrea Ballatore, Carola Griffith Brookles, Henri Xhakupi, Gaetano Maria De Ferrari, and Matteo Anselmino. Role of atrial high-rate episodes in stratifying thromboembolic risk: a multiple cut-off diagnostic meta-analysis. *Frontiers in Cardiovascular Medicine*, 10:1289372, 2023.

[87] Andrea Saglietto, Andrea Ballatore, Henri Xhakupi, Gaetano Maria De Ferrari, and Matteo Anselmino. Association of catheter ablation and reduced incidence of dementia among patients with atrial fibrillation during long-term follow-up: a systematic review and meta-analysis of observational studies. *Journal of Cardiovascular Development and Disease*, 9(5):140, 2022.

[88] Andrea Saglietto, Andrea Ballatore, Henri Xhakupi, Gaetano Maria De Ferrari, and Matteo Anselmino. Atrial fibrillation and dementia: Epidemiological insights on an undervalued association. *Medicina*, 58(3):361, 2022.

[89] Andrea Saglietto, Andrea Ballatore, Henri Xhakupi, Federico Rubat Baleuri, Massimo Magnano, Fiorenzo Gaita, Gaetano Maria De Ferrari, and Matteo Anselmino. Evidence-based insights on ideal blanking period duration following atrial fibrillation catheter ablation. *Europace*, 24(12):1899–1908, 2022.

[90] Andrea Saglietto, Eleonora Bertello, Marina Barra, Ilenia Ferraro, Chiara Rovera, Fulvio Orzan, Gaetano Maria De Ferrari, and Matteo Anselmino. Mri pattern characterization of cerebral cardioembolic lesions following atrial fibrillation ablation. *Frontiers in Cardiovascular Medicine*, 11:1327567, 2024.

[91] Andrea Saglietto, Elena Cavallone, Michael Spartalis, Bert Vandenberk, and Matteo Anselmino. Artificial intelligence in cardiac rhythmology, 2024.

[92] Andrea Saglietto, Gaetano Maria De Ferrari, and Matteo Anselmino. Commentary: Differential risk of dementia between patients with atrial flutter and atrial fibrillation: A national cohort study. *Frontiers in Cardiovascular Medicine*, 9:850968, 2022.

[93] Andrea Saglietto, Gaetano Maria De Ferrari, Federico Ferraris, and Matteo Anselmino. Pulmonary vein isolation through trans-jugular approach in a patient with inferior vena cava interruption. *Journal of Interventional Cardiac Electrophysiology*, 64(2):267–268, 2022.

[94] Andrea Saglietto, Roberto De Ponti, Luigi Di Biase, Mario Matta, Fiorenzo Gaita, Jorge Romero, Gaetano M De Ferrari, and Matteo Anselmino. Impact of atrial fibrillation

catheter ablation on mortality, stroke, and heart failure hospitalizations: a meta-analysis. *Journal of cardiovascular electrophysiology*, 31(5):1040–1047, 2020.

[95] Andrea Saglietto, Giulio Falasconi, Antonio Berruezo, Gaetano Maria De Ferrari, and Matteo Anselmino. Posterior wall isolation in persistent af with rapid posterior wall activity: The quest for evidence. *Clinical Electrophysiology*, 10(1):139–140, 2024.

[96] Andrea Saglietto, Giulio Falasconi, Diego Penela, Pietro Francia, Arunashis Sau, Fu Siong Ng, Veronica Dusi, Davide Castagno, Fiorenzo Gaita, Antonio Berruezo, et al. Glucagon-like peptide-1 receptor agonist semaglutide reduces atrial fibrillation incidence: A systematic review and meta-analysis. *European Journal of Clinical Investigation*, 54(12):e14292, 2024.

[97] Andrea Saglietto, Giulio Falasconi, Diego Penela, Pietro Francia, David Soto-Iglesias, Julio Martí-Almor, and Antonio Berruezo. Cardiac magnetic resonance–aided ventricular tachycardia substrate ablation in corrected tetralogy of fallot. *Journal of Interventional Cardiac Electrophysiology*, 66(6):1317–1319, 2023.

[98] Andrea Saglietto, Giulio Falasconi, Diego Penela, Pietro Francia, Daniel Viveros, Antonio Berruezo, Vincenzo Russo, Michele Brignole, Tolga Aksu, Matteo Anselmino, et al. Cardioneuroablation: a new treatment for vasovagal syncope. *Journal of Cardiovascular Medicine*, 26(3):131–142, 2025.

[99] Andrea Saglietto, Giulio Falasconi, David Soto-Iglesias, Pietro Francia, Diego Penela, José Alderete, Daniel Viveros, Aldo Francisco Bellido, Paula Franco-Ocaña, Fatima Zaraket, et al. Assessing left atrial intramyocardial fat infiltration from computerized tomography angiography in patients with atrial fibrillation. *Europace*, 25(12):euad351, 2023.

[100] Andrea Saglietto, Matteo Fois, Luca Ridolfi, Gaetano Maria De Ferrari, Matteo Anselmino, and Stefania Scarsoglio. A computational analysis of atrial fibrillation effects on coronary perfusion across the different myocardial layers. *Scientific reports*, 12(1):841, 2022.

[101] Andrea Saglietto, Fiorenzo Gaita, Carina Blomstrom-Lundqvist, Elena Arbelo, Nikolaos Dagres, Josep Brugada, Aldo Pietro Maggioni, Luigi Tavazzi, Josef Kautzner, Gaetano Maria De Ferrari, et al. Afa-recur: an esc eorp afa-lt registry machine-learning web calculator predicting atrial fibrillation recurrence after ablation. *Europace*, 25(1):92–100, 2023.

[102] Andrea Saglietto, Fiorenzo Gaita, Roberto De Ponti, Gaetano Maria De Ferrari, and Matteo Anselmino. Catheter ablation vs. anti-arrhythmic drugs as first-line treatment in symptomatic paroxysmal atrial fibrillation: a systematic review and meta-analysis of randomized clinical trials. *Frontiers in Cardiovascular Medicine*, 8:664647, 2021.

[103] Andrea Saglietto, Eleonora Martinengo, Natascia Cerrato, Laura Bergamasco, Davide Castagno, Fiorenzo Gaita, Gaetano Maria De Ferrari, and Carla Giustetto. Time to positivity of diagnostic provocative pharmacologic testing in brugada syndrome. *Heart Rhythm*, 20(1):144–145, 2023.

[104] Andrea Saglietto, Stefania Scarsoglio, Daniela Canova, Gaetano Maria De Ferrari, Luca Ridolfi, and Matteo Anselmino. Beat-to-beat finger photoplethysmography in atrial fibrillation patients undergoing electrical cardioversion. *Scientific Reports*, 13(1):6751, 2023.

[105] Andrea Saglietto, Stefania Scarsoglio, Francesco Tripoli, Jaco Zwanenburg, Geert Jan Biessels, Gaetano Maria De Ferrari, Luca Ridolfi, and Matteo Anselmino. Atrial fibrillation hemodynamic effects on lenticulostriate arteries identified at 7-tesla cerebral magnetic resonance imaging. *Clinical and Translational Medicine*, 13(9), 2023.

[106] Andrea Saglietto, Francesco Tripoli, Jaco Zwanenburg, Geert Jan Biessels, Gaetano Maria De Ferrari, Matteo Anselmino, Luca Ridolfi, and Stefania Scarsoglio. Role of the vessel morphology on the lenticulostriate arteries hemodynamics during atrial fibrillation: A cfd-based multivariate regression analysis. *Computer Methods and Programs in Biomedicine*, 254:108303, 2024.

[107] Fatima Sanchez-Cabo, Xavier Rossello, Valentin Fuster, Fernando Benito, Jose Pedro Manzano, Juan Carlos Silla, Juan Miguel Fernández-Alvira, Belen Oliva, Leticia Fernandez-Friera, Beatriz Lopez-Melgar, et al. Machine learning improves cardiovascular risk definition for young, asymptomatic individuals. *Journal of the American College of Cardiology*, 76(14):1674–1685, 2020.

[108] Damián Sánchez-Quintana, Manuel Doblado-Calatrava, José Angel Cabrera, Yolanda Macías, and Farhood Saremi. Anatomical basis for the cardiac interventional electrophysiologist. *BioMed Research International*, 2015(1):547364, 2015.

[109] Stefania Scarsoglio, Andrea Saglietto, Francesco Tripoli, Jacobus JM Zwanenburg, Geert J Biessels, Gaetano Maria De Ferrari, Matteo Anselmino, and Luca Ridolfi. Cerebral hemodynamics during atrial fibrillation: Computational fluid dynamics analysis of

lenticulostriate arteries using 7 t high-resolution magnetic resonance imaging. *Physics of Fluids*, 34(12), 2022.

[110] Matteo Sclafani, Giulio Falasconi, Giacomo Tini, Beatrice Musumeci, Diego Penela, Andrea Saglietto, Luca Arcari, Chiara Bucciarelli-Ducci, Emanuele Barbato, Antonio Berruezo, et al. Substrates of sudden cardiac death in hypertrophic cardiomyopathy. *Journal of Clinical Medicine*, 14(4):1331, 2025.

[111] Khader Shameer, Kipp W Johnson, Benjamin S Glicksberg, Joel T Dudley, and Partho P Sengupta. Machine learning in cardiovascular medicine: are we there yet? *Heart*, 104(14):1156–1164, 2018.

[112] Konstantinos C Siontis, Peter A Noseworthy, Zachi I Attia, and Paul A Friedman. Artificial intelligence-enhanced electrocardiography in cardiovascular disease management. *Nature Reviews Cardiology*, 18(7):465–478, 2021.

[113] Nils Strodthoff, Patrick Wagner, Tobias Schaeffter, and Wojciech Samek. Deep learning for ecg analysis: Benchmarks and insights from ptb-xl. *IEEE journal of biomedical and health informatics*, 25(5):1519–1528, 2020.

[114] Stefano Valcher, Alessandro Villaschi, Giulio Falasconi, Mauro Chiarito, Filippo Giunti, Laura Novelli, Lucio Addeo, Antonio Taormina, Cristina Panico, Pietro Francia, et al. Low-voltage area ablation in addition to pulmonary vein isolation in patients with atrial fibrillation: A systematic review and meta-analysis. *Journal of Clinical Medicine*, 13(15):4541, 2024.

[115] Joske van der Zande, Marc Strik, Rémi Dubois, Sylvain Ploux, Saer Abu Alrub, Théo Caillol, Mathieu Nasarre, Dirk W Donker, Eline Oppersma, and Pierre Bordachar. Using a smartwatch to record precordial electrocardiograms: a validation study. *Sensors*, 23(5):2555, 2023.

[116] Isabelle C Van Gelder, Michiel Rienstra, Karina V Bunting, Ruben Casado-Arroyo, Valeria Caso, Harry JGM Crijns, Tom JR De Potter, Jeremy Dwight, Luigina Guasti, Thorsten Hanke, et al. 2024 esc guidelines for the management of atrial fibrillation developed in collaboration with the european association for cardio-thoracic surgery (eacts) developed by the task force for the management of atrial fibrillation of the european society of cardiology (esc), with the special contribution of the european heart rhythm association (ehra) of the esc. endorsed by the european stroke organisation (eso). *European Heart Journal*, page ehae176, 2024.

[117] Pasquale Vergara, Wendy S Tzou, Roderick Tung, Chiara Brombin, Alessandro Nonis, Marmar Vaseghi, David S Frankel, Luigi Di Biase, Usha Tedrow, Nilesh Mathuria, et al. Predictive score for identifying survival and recurrence risk profiles in patients undergoing ventricular tachycardia ablation: the i-vt score. *Circulation: Arrhythmia and Electrophysiology*, 11(12):e006730, 2018.

[118] P Wagner, N Strodthoff, R Bousseljot, W Samek, and T Schaeffter. Ptb-xl, a large publicly available electrocardiography dataset. physionet, 2020.

[119] Karolina Weinmann, Deniz Aktolga, Alexander Pott, Carlo Bothner, Manuel Rattka, Tilman Stephan, Wolfgang Rottbauer, and Tillman Dahme. Impact of re-definition of paroxysmal and persistent atrial fibrillation in the 2012 and 2016 european society of cardiology atrial fibrillation guidelines on outcomes after pulmonary vein isolation. *Journal of Interventional Cardiac Electrophysiology*, 60:115–123, 2021.

[120] Florian A Wenzl, Simon Kraler, Gareth Ambler, Clive Weston, Sereina A Herzog, Lorenz Räber, Olivier Muller, Giovanni G Camici, Marco Roffi, Hans Rickli, et al. Sex-specific evaluation and redevelopment of the grace score in non-st-segment elevation acute coronary syndromes in populations from the uk and switzerland: a multinational analysis with external cohort validation. *The Lancet*, 400(10354):744–756, 2022.

[121] Michelle C Williams, Aakash D Shanbhag, Jianhang Zhou, Anna M Michalowska, Mark Lemley, Robert JH Miller, Aditya Killekar, Parker Waechter, Heidi Gransar, Serge D Van Kriekinge, et al. Automated vessel-specific coronary artery calcification quantification with deep learning in a large multi-centre registry. *European Heart Journal-Cardiovascular Imaging*, page jeae045, 2024.

[122] Roger A Winkle, R Hardwin Mead, Gregory Engel, Melissa H Kong, and Rob A Patrawala. Atrial arrhythmia burden on long-term monitoring in asymptomatic patients late after atrial fibrillation ablation. *The American journal of cardiology*, 110(6):840–844, 2012.

[123] Jianwei Zheng, Guohua Fu, Kyle Anderson, Huimin Chu, and Cyril Rakovski. A 12-lead ecg database to identify origins of idiopathic ventricular arrhythmia containing 334 patients. *Scientific data*, 7(1):98, 2020.